UNIVERSITAT POLITÈCNICA
DE CATALUNYA
BARCELONATECH

A reactive barrier to enhance the removal of emerging organic compounds during artificial recharge of aquifers through infiltration basins

Cristina Valhondo

A REACTIVE BARRIER TO ENHANCE THE REMOVAL OF EMERGING ORGANIC COMPOUNDS DURING ARTIFICIAL RECHARGE OF AQUIFERS THROUGH INFILTRATION BASINS

PhD Thesis

Hydrogeology Group (GHS)

Dept. Geotechnical Engineering and Geosciences,

Universitat Politecnica de Catalunya, UPC-Barcelona Tech

Institute of Environmental Assesment and Water Research (IDAEA), Spanish Research Council (CSIC)

Cristina Valhondo

Supervisors: Dr. Jesús Carrera Dr. Carlos Ayora

November, 2016

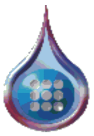

HYDROGEOLOGY GROUP

TECHNICAL UNIVERSITY OF CATALONIA

This thesis was funded by Spanish Research Council (CSIC) with a JAE-Predoc grant and was developed in the framework of the LIFE08 ENV/E/117 ENSAT (Enhancement of Soil Aquifer Treatment to Improve the Quality of Recharge Water in the Llobregat River Delta Aquifer) project, *ENSAT*, contract XXX1-XX-2000-00034. Final portions were performed with funding from EU project ACWAPUR (PCIN-2015-245).

Dedicatoria.

Abstract

Artificial recharge of aquifers through infiltration basins (AR) improves water quality and increases groundwater resources, which make of it an appropriate technique for the renaturalization of waters affected directly or indirectly by wastewater effluents. Emerging organic compounds (EOCs), typically present in such waters, are mainly reduced during AR by sorption and biotransformation.

We installed a reactive barrier in an infiltration basin (5000 m^2) to enhance the removal of EOCs in the recharge water. The barrier consisted of sand, vegetable compost, iron oxide and clay. Vegetable compost was aimed at: 1) release organic carbon to be used as a carbon source by the microbial community thus promoting the generation of diverse redox conditions, and 2) to adsorb neutral EOCs. Clay and iron oxides were aimed at increasing sorption sites for cationic and anionic EOCs, respectively.

Field application of such a design was tested by comparing the redox indicators and behavior of EOCs prior and after the installation of the reactive barrier. Residence time distributions of the recharge water at the monitoring points were obtained by a pulse tracer test. These distributions were used for calibrating a conservative transport and flow model of the aquifer. Finally, first order rates and retardation factors of several EOCs were estimated by fitting model outputs to observed concentrations. The estimation of the first order decay rates and retardation factors of several EOCs allowed the comparison of such values with values reported from other field sites

and column experiments.

The reactive barrier succeed in releasing organic carbon and achieving diverse redox conditions. The transformation of most EOCs was enhanced after the installation of the reactive barrier. In fact, first order rates and retardation factors were higher in the reactive barrier than in the rest of the aquifer and similar or higher than those from literature.

In summary, addition of proposed reactive barrier significantly enhanced the performance of artificial recharge via infiltration basins, thus contributing to the renaturalization of recharged waters.

Resumen

La recarga artificial de acuíferos a través de balsas de infiltración (AR) mejora la calidad del agua y aumenta recursos de aguas subterráneas, convirtiendola en una técnica apropiada para la renaturalización de las aguas afectadas directa o indirectamente por los efluentes de aguas residuales. En este tipo de aguas la presencia de compuestos orgánicos emergentes (EOCs) es más que frecuente. Durante la recarga artificial este tipo de compuestos es eliminado principalmente debido a la adsorción y a la biotransformación.

Para mejorar la eliminación de los EOCs durante la infiltración del agua de recarga se instaló una barrera reactiva en una balsa de infiltración. La barrera consistía en arena, compost vegetal, óxidos de hierro y arcilla. La finalidad del compost vegetal era por un lado la de aportar carbono orgánico disuelto para ser utilizado como principal fuente de carbono por la comunidad microbiana promoviendo así la generación de diversas condiciones redox, y por otro lado la de adsorber EOCs neutros. La Arcilla y los óxidos de hierro se pusieron con la intención de aumentar los sitios de adsorción para los EOCs catiónicos y aniónicos, respectivamente.

La efectividad de la barrera en el campo se estudió comparando el comportamiento de los indicadores redox y de los EOCs antes y después de la instalación de la barrera. Mediante un ensayo de trazadores tipo pulso se obtuvieron las distribuciones de los tiempos de residencia del agua de recarga a los puntos de observación. Estas distribuciones se utilizaron para calibrar un modelo de flujo y transporte conservativo del acuífero. Por último, las tasas de degradación de

primer orden y los factores de retardo de varios EOCs se estimaron mediante el ajuste de los resultados del modelo con las concentraciones observadas. Las tasas de degradación y los factores de retardo estimados se compararon con valores encontrados en la bibliografía.

La barrera reactiva cumple su función aportando carbono orgánico y generando diversas condiciones redox. Muchos de los EOCs estudiados mostraron una mejor transformación cuando la recarga se realizó con la barrera reactiva. Las tasas de degradación y factores de retardo estimados en la barrera son mayores que los estimados para el resto del acuífero, y del mismo orden o superiores a los encontrados en la bibliografía.

En resumen, la barrera reactiva propuesta mejora significativamente el rendimiento de la recarga artificial a través de balsas de infiltración, contribuyendo así a la renaturalización de las aguas recargadas.

Table of Contents

List of Figures

List of Tables

Chapter 1

Introduction

Water scarcity is an acute concern in many parts of the world, specially in arid and semiarid regions. Population growth has increased water demand and led to generalized aquifer over-exploitation (*Konikow and Kendy*, 2005; *Wada et al.*, 2010) and to the need of reclaiming effluents from municipal wastewater treatment plants and effluent-receiving water bodies (*Levine and Asano*, 2004). Under this frame, managed aquifer recharge has been frequently proposed as a technique to replenish and/or enhance the quality of groundwater resources, thus renaturalizing the reclaimed water. Artificial recharge from infiltration basin (AR) is a type of managed aquifer recharge that facilitates the removal of organic matter (*Vanderzalm et al.*, 2006; *Bekele et al.*, 2011), nutrient (*Bekele et al.*, 2011), metals (*Dillon et al.*, 2006; *Hoppe-Jones et al.*, 2010; *Patterson et al.*, 2011) and pathogen (*Dillon et al.*, 2006) from the recharged water passing through the unsaturated zone before reaching the underlying aquifer. Appropriate management of AR systems requires understanding the fate of potential contaminants, which depends on hydraulics and biogeochemistry.

Common sources of water for AR include wastewater effluents (after different stages of treatment) and effluent-receiving rivers (*Díaz-Cruz and Barceló*, 2008; *Drewes*, 2009; *Maeng et al.*,

2011b) in which the presence of emerging organic compounds (EOCs) is frequent (*Heberer*, 2002; *Heberer et al.*, 2004). EOCs are contaminants that have only recently become an issue of concern, so that their health effects are largely unknown and there are not standards for most of them. They comprise a broad rande of anthropogenic organic compounds and their transformation products (such as pharmaceuticals, pesticides, personal care products, industrial additives, water and wastewater treatment by-products, or flame retardants) and are detected in surface, groundwater and drinking water at trace levels ranging from nanograms per liter to micrograms per liter (*Lapworth et al.*, 2012; *Nödler et al.*, 2013; *Tran et al.*, 2013). Many EOCs are not completely removed by conventional treatment technologies (*Carballa et al.*, 2004; *Chefetz et al.*, 2008; *Díaz-Cruz and Barceló*, 2008; *Reemtsma et al.*, 2010; *Radke et al.*, 2009; *Kasprzyk-Hordern et al.*, 2008). Therefore effluents from municipal sewage treatment plants constitute a main source of EOCs into aquatic environment (*Heberer*, 2002; *Bound and Voulvoulis*, 2004).

Several studies reported the efficiency of the AR to remove some EOCs from the recharged water mainly due to biological degradation or transformation and sorption mainly to organic matter and clay minerals (*Dillon et al.*, 2006; *Maeng et al.*, 2010; *Hoppe-Jones et al.*, 2010; *Patterson et al.*, 2011; *Maeng et al.*, 2011b; *Liu et al.*, 2013; *Schaffer et al.*, 2015). The low concentrations exhibited by EOCs in the possible water sources suggest that they are biotransformed by co-metabolism, that is, the presence of a primary carbon source, such dissolved organic carbon (DOC) is needed to support microbial growth (*Tran et al.*, 2013). In consequence, the amount and kind of DOC affects EOCs biotransformation (*Rauch-Williams et al.*, 2010; *Li et al.*, 2013; *Alidina et al.*, 2014a,b; *Regnery et al.*, 2015). EOCs, like most organic compounds, manifest a redox-dependent biotransformation (*Greskowiak et al.*, 2005, 2006; *Massmann et al.*, 2008a; *Maeng et al.*, 2010; *Barbieri et al.*, 2011; *Maeng et al.*, 2011b; *Storck et al.*, 2012; *Liu et al.*, 2013). Therefore, the passage of infiltrated water though diverse redox conditions should increase the number of compounds susceptible to biotransformation. Other factors such as temperature and residence time also affect the removal of EOCs during subsurface passage (*Massmann et al.*, 2006, 2008b).

We designed a reactive barrier with the objective to test the above conjecture, namely that the removal of EOCs can be enhanced by favoring diverse redox conditions and sorption sites during AR. The barrier comprised vegetable compost, to release DOC into the water so as to promote microbial growth and generate diverse redox states and to provide sorption surfaces for neutral compounds. Small amounts of clay and iron oxide were added to the barrier in order to provide sorption sites for cationic and anionic compounds, respectively. To test such design we installed the reactive barrier in an infiltration basin located at Sant Vicenç dels Horts (Barcelona, Spain) in April 2011. The effectiveness of the reactive barrier to promote diverse redox conditions and enhance EOCs degradation was qualitatively verified by comparing DOC, redox indicators, and several EOCs concentrations along the infiltration path prior to and after the installation.

A quantitative evaluation of biotransformation and sorption (in terms of first order degradation rate, λ and retardation factor, R) is required to compare to values from the literature. To estimate the λ and R values, the residence time distribution (RTDs) of the recharge water in the aquifer has to be determined. The RTDs were obtained from a tracer test. They were extended to other flow conditions by means of a multilayer numerical model calibrated against head and tracer test data. The model was then used to estimate λ and R of ten of the studied EOCs. To assess the effectiveness of the reactive barrier enhancing the removal of EOCs, the estimated λ and R were compared to values from literature.

The thesis is structured as four articles that have been published or are in the publication process:

Chapter 2 (based on Valhondo *et al.,* 2014) describes qualitatively the effectiveness of the reactive barrier to promote diverse redox conditions beneath the infiltration basin, using DOC and redox indicators concentrations, and suggests the possible presence of preferential flow path through the reactive barrier. The behavior of four EOCs is also described in this chapter.

Chapter 3 (based on Valhondo *et al.,* 2015) focus on the behavior of nine EOCs during the AR

through the reactive barrier. The EOCs were selected based on their high frequency of detection in treatment plant effluents and their valence at experimental pH ranges.

Chapter 4 (based on Valhondo *et al.,* 2016) describes the multilayer numerical model of the infiltration system, its boundary and initial conditions, parameterization, assumptions and calibration. Flow and conservative transport parameters were calibrated using hydraulic head and concentration data from the tracer test and than validated by blind prediction of electrical conductivity and 1,1,2-Trichloroethane. The model was used to estimate the portion of infiltration water that uses the preferential flow paths to flow through the reactive barrier.

Chapter 5 (based on Valhondo *et al.,* 2016b) contains the estimation of reactive transport parameters for ten EOCs using the multilayer numerical model described in Chapter 4. These parameters are compared to those reported in literature for column and field experiments.

Because of this structure, a good deal of information is repeated, especially site description. I leave it to the discretion of the reader to skip repeated information. On the other hand, the advantage of this structure is that chapters can be read independently.

Chapter 2

Characterizing redox conditions and monitoring attenuation of selected pharmaceuticals during artificial recharge through a reactive layer[†]

2.1 Introduction

Demand for water increases in response to population growth, which leads to widespread aquifer over-exploitation and other detrimental effects (*Konikow and Kendy*, 2005; *Wada et al.*, 2010). Artificial recharge of aquifers (AR) through infiltration basins may alleviate some of these effects because this technology contributes to water resources and enhances water quality during soil passage (*Bouwer*, 2002; *Greskowiak et al.*, 2005). Numerous studies have demonstrated that

[†]the present chapter is based on the paper Characterizing redox conditions and monitoring attenuation of selected pharmaceuticals during artificial recharge through a reactive layer, by Cristina Valhondo, Jesús Carrera, Carlos Ayora, Isabel Tubau, Lurdes Martinez-Landa, Karsten Nödler, and Tobias Licha *Science of the Total Environment*., Doi:10.1016/j.scitotenv.2015.01.030

AR reduces the concentration of organic matter (*Vanderzalm et al.*, 2006; *Bekele et al.*, 2011), nutrients (*Bekele et al.*, 2011), metals (*Dillon et al.*, 2006; *Bekele et al.*, 2011), pathogens (*Dillon et al.*, 2006), and organic contaminants (*Dillon et al.*, 2006; *Hoppe-Jones et al.*, 2010; *Patterson et al.*, 2011). The performance of AR, however, varies among pharmaceutically active compounds (PhACs), with some PhACs exhibiting site-specific removal efficiency. PhACs, which, by definition, are designed to have specific biologic effects, are reported to be present in the water cycle (*Heberer et al.*, 2004; *Drewes*, 2009; *Kosonen and Kronberg*, 2009; *Onesios et al.*, 2009; *Maeng et al.*, 2010; *Rauch-Williams et al.*, 2010). "Many PhACs, such as carbamazepine, display recalcitrant behavior during conventional wastewater treatment (*Carballa et al.*, 2004; *Chefetz et al.*, 2008; *Díaz-Cruz and Barceló*, 2008; *Maeng et al.*, 2011b; *Jelic et al.*, 2012) and in the aquatic environment" (*Lim et al.*, 2008; *Arye et al.*, 2011). Consequently, they are frequently detected in surface and ground waters and, in some cases, in drinking water (*Heberer*, 2002; *Jones et al.*, 2004; *Hoppe-Jones et al.*, 2010; *Maeng et al.*, 2011b; *Dickenson et al.*, 2011; *Lapworth et al.*, 2012).

Typical sources of water for AR include wastewater effluents (after different stages of treatment) and effluent-receiving rivers (*Drewes*, 2009; *Maeng et al.*, 2011b). Consequently, AR water often contains PhACs (*Heberer*, 2002; *Heberer et al.*, 2004). The concentration of organic micro-contaminants is decreased during AR through infiltration basins due to various attenuation processes, such as biodegradation and adsorption (*Maeng et al.*, 2011b; *Schaffer et al.*, 2012b). The type and bio-availability of organic matter affect PhACs degradation because the organic matter serves as a co-substrate in microbiologically-facilitated transformations (*Rauch-Williams et al.*, 2010; *Tran et al.*, 2013; *Li et al.*, 2013; *Alidina et al.*, 2014b). The enzymes responsible for the biotransformation of different PhACs are produced by a range of microorganisms that are differentially affected by the composition and amount of organic matter (*Li et al.*, 2013; *Alidina et al.*, 2014b). Electron acceptors are consumed during organic matter oxidation according to the energy released to the mediator microorganisms, which naturally leads to a sequence of redox states and different metabolic pathways. This is a well-established sequence described most recently by

Farnsworth and Hering (2011). For bank filtration, reducing conditions occur near the bank and aerobic conditions occur near the production well. Nevertheless, *Alewell et al.* (2008) hypothesized that the theory of the sequential reduction chain does not always hold true under field conditions; they observed that sites with high dissolved organic carbon (DOC) concentrations may not follow the pattern of the sequential reduction chain because high electron donor availability does not trigger competition between processes attributed to different redox potentials. Some PhACs are preferentially removed under specific redox conditions (*Patterson et al.*, 2011; *Rauch-Williams et al.*, 2010; *Barbieri et al.*, 2011; *Maeng et al.*, 2011b; *Storck et al.*, 2012; *Valhondo et al.*, 2014). Therefore, the passage of water through several redox environments should enhance the number and proportion of eliminated PhACs.

Adsorption depends on both the surface type and the pollutant type. Neutral compounds tend to sorb onto solid organic matter, and cations and anions tend to sorb onto negatively- (e.g., clay) and positively- (e.g., iron oxide) charged surfaces, respectively (*Schaffer et al.*, 2012b). Adsorption of PhACs is enhanced and hence the residence time prolonged, by increasing the diversity of sorption sites through the flow path. Thus, ideally, artificially recharged water should encounter neutral, positively-, and negatively-charged surfaces during infiltration.

We designed a layer acting as a reactive barrier to provide a broad range of redox states and a diverse set of sorption surfaces. We installed the layer in March 2011 in an infiltration basin that had been operating intermittently since 2009. The reactive barrier comprised 1) vegetable compost to release degradable organic matter, to promote microbial growth and generate diverse redox states, and to provide sorption surfaces for neutral organic compounds; 2) clay to increase sorption of cationic compounds; and 3) iron oxide to facilitate sorption of anionic compounds.

The aim of this paper is to report the practical application of this newly designed reactive layer and the field response. The effectiveness of the reactive layer to promote diverse redox conditions was verified by comparing DOC and redox indicators along the infiltration path prior to and after installation of the reactive layer. The behavior of four PhACs: atenolol, cetirizine,

gemfibrozil and carbamazepine, was also studied during AR with the system operating prior to and after installation of the reactive barrier. The four PhACs were selected because of their respective charges (cation, zwitter-ion, anion, and neutral, respectively) at the experiment pH range (6.3–8.4), their different degradation behaviors and sorption properties, and their frequent detection in aquatic environments (*Heberer*, 2002; *Schaffer et al.*, 2012b; *Bahlmann et al.*, 2012; *Grenni et al.*, 2013).

2.2 Materials and methods

2.2.1 Site description

The infiltration site is located in the Llobregat Lower Valley aquifer, 15 km inland from the Mediterranean coast. The aquifer beneath the basin comprises Quaternary alluvial sediments, mainly gravel and sand with a small fraction of clay (*Barbieri et al.*, 2011). The minerals include quartz, calcite, dolomite, and the solid phase fraction of organic carbon is less than 0.002 (g_{OC}/g_{Soil}). The regional groundwater flow direction is from NNW to SSE (*Iribar et al.*, 1997) with a natural hydraulic gradient of 2.3 ‰ (Fig. 3.1B). Infiltration water is brought from the Llobregat River, which is impacted by numerous treatment plant effluents (**?**), to a settlement pond ($\approx$ 5000 m^2), with a residence time of 2 to 4 days. Thereafter, the water is transferred to the infiltration pond ($\approx$ 5000 m^2). This system has operated intermittently since February 2009 with a mean infiltration rate of 1 m/d.

The monitoring network comprised seven piezometers to sample aquifer water, and two suction cups to sample the vadose zone underneath the basin (Fig. 3.1A). The two suction cups, labeled cc1 and cc2, were installed at 1 and 2 m below the surface, respectively. One piezometer (P-1) was located upstream from the infiltration basin to monitor background concentrations of local groundwater, hereafter referred to as "Amb-GW" (ambient-groundwater). Three piezome-

ters (P-8.3, P-8.2, and P-8.1) were located in the middle of the infiltration pond and screened at different depths (7–9 m, 10–12 m, and 13–15 m, respectively). Their placement allowed us to evaluate changes in the water quality at various depths within the saturated zone immediately upon entrance of the recharge water into the aquifer. Four completely screened piezometers (P-2, P-5, P-9, and P-10) were placed downstream along the flow path to assess the quality of the infiltrated water at increasing residence times. Most of the piezometers were equipped with CTD-Diver (Schlumberger water services, Delft, The Netherlands) sensors for continuous recording of electrical conductivity (EC), temperature, and water level.

2.2.2 Experimental procedure

To assess the effectiveness of the barrier, we performed three different infiltration tests: one prior to and two after installation of the reactive barrier. Infiltration rates were similar during the three tests (Fig. 2.2). The infiltration system was run continuously with occasional stops for maintenance operations or due to high turbidity levels in the source water. The sampling concentrated on three campaigns. The first campaign, referred to as the 'pre-L' test, lasted 29 days in early 2011 (Jan. 12th to Feb. 10th). Samples were collected from monitoring points and the infiltration pond after 20 days of continuous infiltration. The second campaign, referred to as the 'L-2011' test, was performed for 46 days in late 2011 (Sep. 8th to Oct. 24th), 4 months after installation of the reactive layer. The system operated intermittently during the previous 4 months (May - August), but was stopped whenever turbidity at the entrance of the infiltration basin was higher than 25 turbidity unit to avoid clogging the system. During this second campaign, monitoring points were sampled in six weekly events starting on Sep. 23rd. Water from the infiltration pond was sampled 14 times (at least twice a week). The third campaign, referred to as the 'L-2012' test, was performed for 50 days in the summer 2012 (Jun. 13th to Aug. 2nd), beginning 14 months after installation of the reactive layer. Water from the infiltration basin was sampled six times, suction cup CC2 was sampled once, and the monitoring points were sampled from two to six times. The

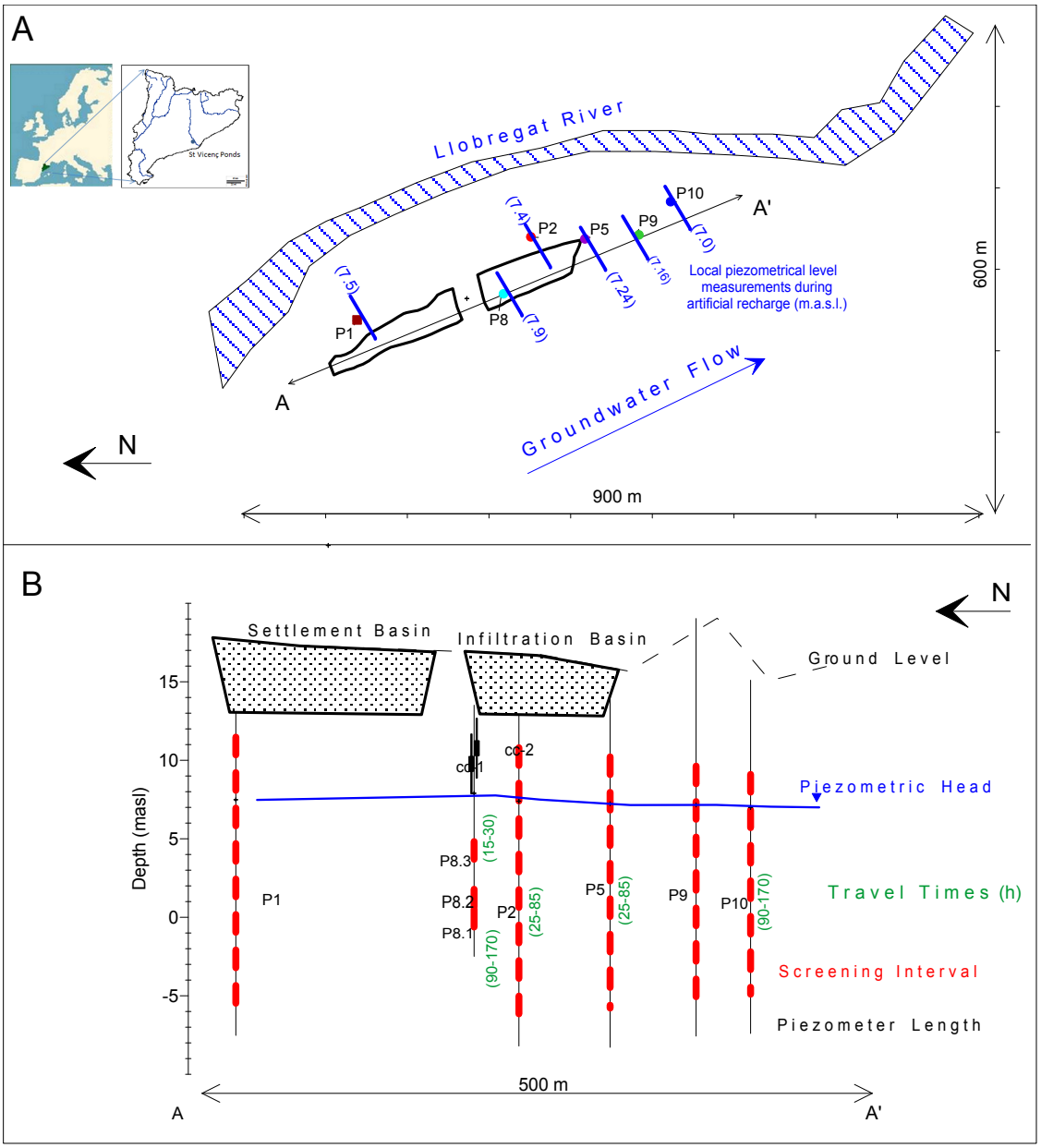

Figure 2.1: Schematic A) location and plan view, and B) cross-section of the field site. In the figure m.a.s.l. = meters above sea level.

first sample was collected 3 weeks after started the infiltration. Mean infiltration rates were 1 m/d during the three tests. Fig. 2.2 shows the sampling times and the recharge rate (m^3/h) for the three tests. For each test time, time zero is defined as the first day when the system worked continuously

for long enough to assure that the monitoring points were flooded with infiltration water. The pre-L test (Fig. 2.2 A) was terminated after 30 days due to high turbidity in the river, which might have clogged the infiltration basin. Only the samples collected when monitoring points were flooded by infiltration water (blue circles) were used to evaluate the behavior of redox-sensitive species and PhACs. During the L-2011 test, four additional samples were collected from the monitoring points to assess how long the system took to reach the composition of the Amb-GW once the infiltration stopped (grey circles in Fig. 2.2 B). During the same period, several samples were collected but not considered for further interpretation due to discontinuous functioning of the system (black circles in Fig. 2.2 B).

Two additional sets of samples from several monitoring points (including the suction cups) were collected in February and May 2009. Bulk chemistry was analyzed in these samples although no PhACs analysis were performed.

Prior to sample collection, piezometers were purged until the field parameters were stable and a volume of at least three times the borehole volume was extracted. Field parameters were measured using a flow-through cell (Eijkelkamp, Giesbeek, The Netherlands) and specific sensors for temperature and pH (Hanna Instruments, Woonsocket, RI, USA), EC (Knick Elektronische Messgeräte, Berlin, Germany), and dissolved oxygen (YSI, Yellow Springs, OH, USA). The suction cups were sampled with a vacuum pump without purging. Collected samples were transported to the laboratory on ice and stored at 4 °C until analysis.

2.2.3 Reactive layer

The reactive barrier, approximately 65 cm-thick, comprised equal volumetric proportions of coarse sand and gravel (to ensure structural integrity and permeability) and vegetable compost from gardens and wood (to provide organic sorption sites and to yield easily degradable organic carbon), supplemented with clay ($\leq 1\%$ in volume). The layer covered the entire surface of the infiltration

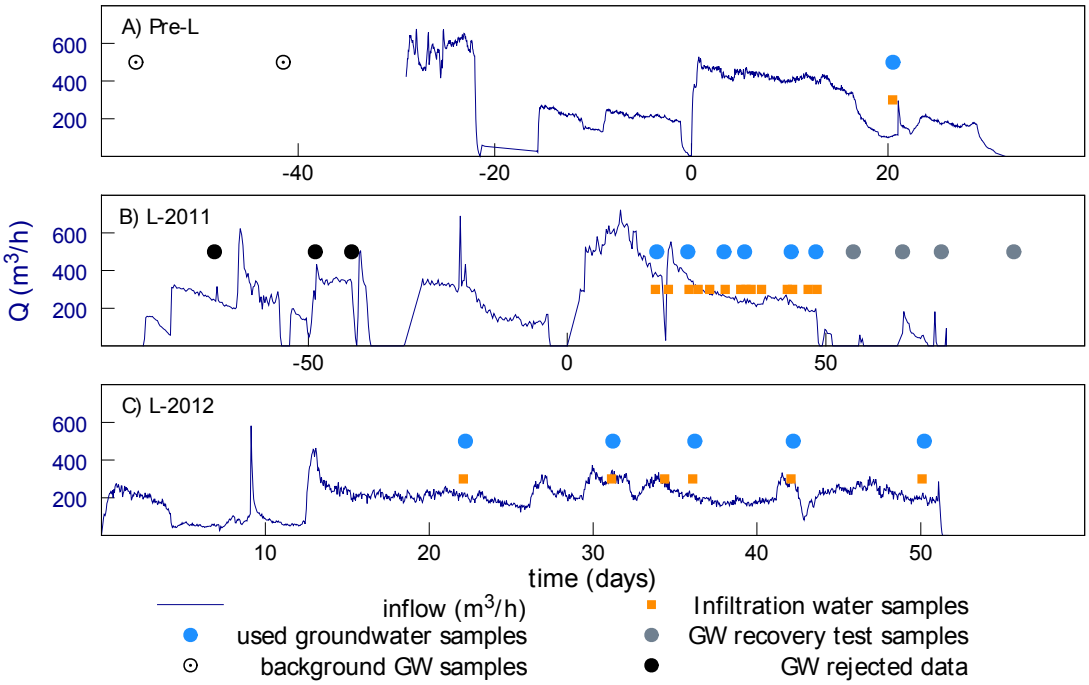

Figure 2.2: Inflow (m^3/h) for A) pre-L, B) L-2011, and C) L-2012 tests, and sample frequency for each test (Orange squares = infiltration basin water, empty circles = background data collected when no AR was taking place, blue circles = samples collected with the system operating continuously and used for further interpretation, black circles = samples collected with a discontinuous functioning of the system and therefore not considered for further interpretation, and grey circles = samples collected after the L-2011 termination and used to assess the recovery of the aquifer).

pond. The thickness of the reactive layer was constrained by the excavation depth of the basin and the stability of its walls. The components were blended on site with an excavator until homogenization was visually evident. This layer was covered with approximately 5 cm of sand to prevent the woody material from floating away. Iron oxides in the form of goethite ($\leq 0.1\%$ in volume) was scattered on top to minimize iron reduction. The added clay, (comprising mainly illite, 33 wt%, smectite, 16 wt%, and chlorite, 9 wt%) and fine grained iron oxide (goethite) provided extra sorption capacity for cationic and anionic contaminants, respectively. This reactive barrier was installed from March to April 2011. Because the layer contained a high proportion of aquifer material ($> 49\%$ in volume), the infiltration rates, considered as the volume per hour poured in the infiltration basin, indicated no relevant differences between tests (Figure 2.2).

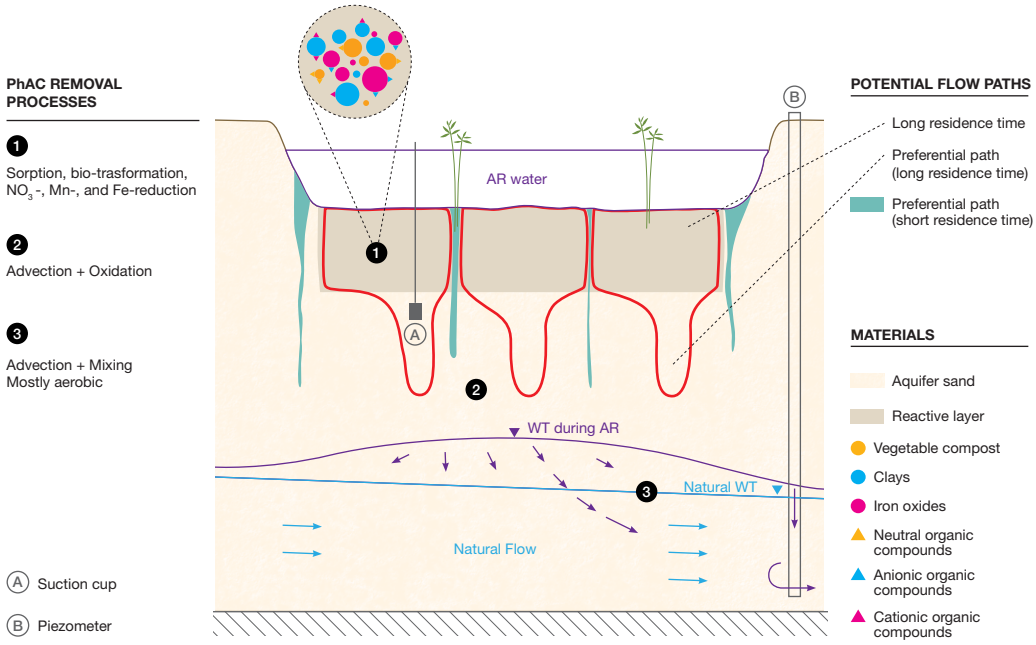

Figure 2.3: Schematic cross-section of the infiltration basin and the assumed preferential flow paths through the reactive layer. The water table (WT) and flow lines are shown for the natural flow and recharge periods. Processes affecting the removal of PhACs in the reactive barrier (1), vadose zone (2), and aquifer (3) are listed on the left. The potential flow paths of the recharged water and materials that comprise the basin are listed on the right.

A leaching test, using 0.5 L of compost and 1 L ultra-pure water, was performed before installation of the reactive layer to assess whether the reactive layer was a source of PhACs in the infiltrated water. The concentrations of the four studied PhACs in the leachate were negligible. Therefore, we did not consider the reactive layer as a source of PhACs.

2.2.4 Flow through the reactive layer and chemical processes: proposed model

The natural water table (without AR) displayed a 2.3‰ gradient from NNW to SSE (pale blue in Fig. 2.3). AR generated a dome below the infiltration basin and changed the flow lines leading to

a flow with a vertical component (violet in Fig. 2.3).

Flow through the vadose zone was expected to occur along the fast preferential flow paths for two reasons. First, the medium comprised relatively clean sand that was more permeable than the reactive layer. Under these conditions, flow occurred along fingers that travel a velocity equal to the hydraulic conductivity (*Hill and Parlange*, 1972; *Selker et al.*, 1996; *Cueto-Felgueroso and Juanes*, 2008). Second, the barrier was expected to be heterogeneous, partly because of plant growth and partly because the edges of the basin were not covered with reactive material (green flow paths in Fig. 2.3).

The infiltration water traveling through these preferential paths reached the aquifer without an intense interaction with the reactive barrier and therefore without being exposed to conditions as reducing as water with a longer residence time in the barrier. These preferential paths were named "short residence time flow paths".

The main processes affecting the PhACs during infiltration are expected to change along the flow path. In the first stage, water infiltrated through the reactive barrier where sorption (to the different materials) and bio-transformation (mediated by communities developed under the reducing conditions) took place. Afterwards, water infiltrated through the unsaturated zone. The variability in residence time at the reactive layer should lead to variability in DOC enrichment and the achievement of reducing conditions. This, together with the presence of O_2 supplied throughout unsaturated zone surronding the infiltration basin, should favor the oxidation of PhACs, either at the unsaturated zone or when mixing occurs at the aquifer under saturated conditions.

2.2.5 Analytical methods

Samples for analysis of PhACs were collected in amber-glass bottles. The samples were allowed to settle at 4 °C overnight and only the supernatant was used for extraction and analysis. To ensure analyte stability, the sample was extracted by solid phase extraction within 24 h after sampling and

the dried cartridges were stored at -18 °C before resuming analysis (*Nödler et al.*, 2010; *Hillebrand et al.*, 2013). In the case of groundwater, 500 mL of the sample was spiked with 10 μL of an internal standard (IS)-mix containing 100 ng atenolol-D7 (IS for atenolol), 100 ng carbamazepine-D10 (IS for carbamazepine and cetirizine), and 200 ng ibuprofen-D3 (IS for gemfibrozil) and 5 mL of a phosphate buffer concentrate (neutral pH). OASIS HLB (6 mL, 500 mg; Waters, Eschborn, Germany) was used for the solid phase extraction, applying an extraction speed of 15 mL/min. The cartridges were pre-conditioned with 4 mL methanol and 3x4 mL ultrapure water. For surface water and water from the vadose zone (river, pond, and suction cups) 250 mL of the sample was diluted to 500 mL with ultrapure water and extracted in the same way as the groundwater samples. The analytes were eluted with methanol and ethyl acetate. The extract was evaporated to dryness at 40 °C using a stream of nitrogen. The extract was then re-dissolved in 1 mL aqueous 5-mM ammonium acetate solution containing 4% methanol. Before the analysis, the extract was centrifuged for 10 min (4000 rpm) after it was transferred to an auto sampler vial. The samples were analyzed by HPLC-MS/MS according to *Nödler et al.* (2010). The quantitation limits of the method were 3.5 ng/L for atenolol, 2 ng/L for gemfibrozil, 2.2 ng/L for cetirizine, and 2.2 ng/L for carbamazepine in groundwater (500 ml samples), and double those for surface water and water collected from the vadose zone (250 ml samples). The relative standard deviations of the analytes were $\leq 5.0\%$.

Samples for the analysis of Cl^-, $SO_4{}^{-2}$, NO_3^-, and HCO_3^- were filtered through 0.45-μm PALL (New York, USA) Acrodisc© sterile syringe filters with a Supor© membrane. They were analyzed by ion chromatography using a Dionex (California, USA) DX-120 with ionPack AS18 4x250mm column and KOH as the eluent within 72 h and stored at 4 °C. The analytical error was estimated to be 13%.

Glass bottles were used to collect samples for the DOC analyses. The samples were filtered through 0.45 μm membrane filters, acidified and stored at 4 °C. DOC was analyzed using a total organic carbon analyzer Shimadzu (Kyoto, Japan) TOC-VCSH with an infrared detector using the

non-purgeable organic carbon method.

Samples collected for Fe, Mn, Ca, Na, Mg, and K analysis were filtered through 0.45-μm membrane filters, acidified, and stored at 4 °C. The samples were analyzed by inductively-coupled plasma optical emission spectometry using a Perkin Elmer (Massachusetts, USA) Optima 3200DV. The estimated analytical error was below 15%. Lower limits of calibration were 6 μg/L for Fe, 15 μg/L for Mn, 4.5 mg/L for Ca, 6.1 mg/L for Na, 0.2 mg/L for Mg, and 0.8 mg/L for K.

1,1,2-Trichloroethane (TCA) was analyzed in samples collected in amber-glass bottles, and stored at 4 °C. The analysis was performed using a head-space–GC-MS instrument, Agilent Technologies (California, USA) 6890N-5973MSD, with a DB-624 column (60m x 0.32mm, 1.80μm). The detection limit was 8 μg/L with an estimated analytical error below 25%.

2.3 Results and discussion

2.3.1 Artificial recharge water characterization

The four selected PhACs were measured in river and infiltration basin samples over 9 sequential days to characterize their time variability. The infiltration basin samples were collected 3 days later than the river samples to account for the residence time of the settlement basin. Fig. 2.4 displays the concentration in river (green) and infiltration basin (orange) water during the 9 days (December 8th through 16th 2010 for river water and December 11th through 19th 2010 for infiltration basin water) of A) atenolol, B) cetirizine, C) gemfibrozil, and D) carbamazepine. The concentration of the four selected PhACs at the infiltration basin had similar medians but smaller dispersion than in the river, which was expected due to homogenization during the residence time in the settlement pond (2–4 days). The concentration medians were slightly lower in the infiltration basin water than in river water, with the exception of gemfibrozil.

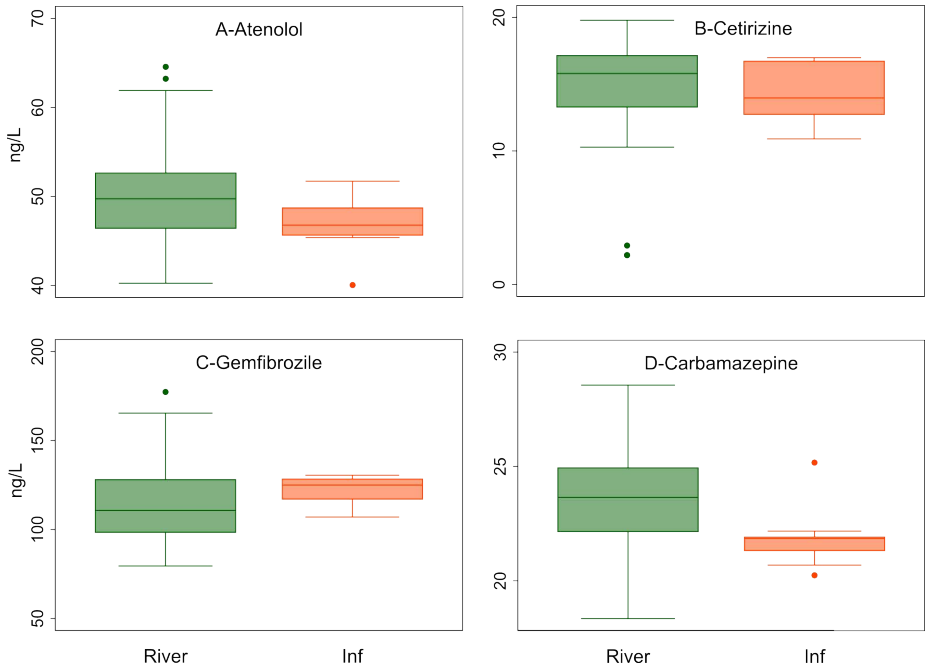

Figure 2.4: Concentration of A) atenolol, B) cetirizine, C) gemfibrozil, and D) carbamazepine in 9 river and infiltration samples collected daily in December 2010. Box represents the 25th (lower hinge) and the 75th (upper hinge) percentiles. The whiskers of the box represent the lower (10th percentile) and the upper (90th percentile) adjacent values and the dots represent the outside values.

2.3.2 Travel times and mixing ratios

Field parameters, major solutes, DOC, TCA and selected PhAC concentrations at end-member waters (infiltration-, ambient-groundwater, and water collected at the vadose zone) are summarized in Table 3.1. The infiltration water was mainly Ca-Na-Cl type and mean pH was 8.2. TCA was present in Amb-GW at the hundreds of μg/L level because of historical contamination. It can be considered conservative for the time ranges of the tests (several weeks) and was used as an indicator of Amb-GW.

EC was used as a tracer to assess the presence of infiltrated water at monitoring points by analyzing the differences between the infiltration water and the Amb-GW (P-1). EC was also used to evaluate travel times by observing the delay in response to fluctuations in infiltration water at the

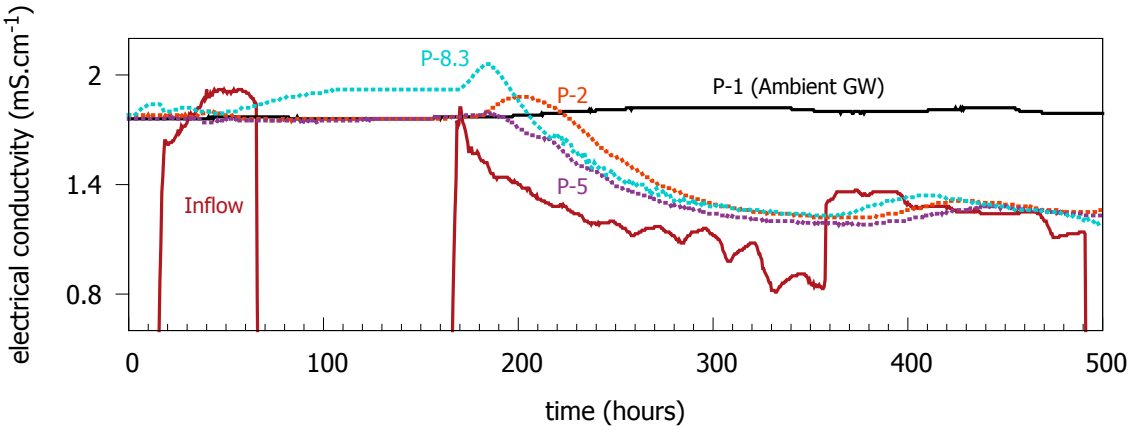

Figure 2.5: Time evolution of the EC at inflow water (infiltration basin) and groundwater both upstream (P-1) and downstream (P-8.3, P-2 and P-5).

monitoring points. This analysis was restricted to piezometers equipped with CTD-Diver sensors. Fig. 2.5 displays the change in EC at P-1, P-2, P-5, P-8.3, and in the recharge water for 500 h of the L-2011 test when the EC of the recharge water varied sharply. The EC at P-1 remained constant and averaged 1.8 mS/cm for the 500 h. The EC of recharge water decreased slowly (hour 170–360) and then rose sharply, which facilitated interpretation. The jump of the EC occurred several days after the onset of infiltration with the result that a quasi-steady state could be assumed for the flow. The change in EC at the piezometers was smoother, with shorter delays than that measured in the recharge water. The fact that the EC at the piezometers approached the EC of the recharge water strongly suggests that the samples collected at these piezometers came mainly from infiltrated water. The delays provided the approximate travel time from the infiltration pond to the piezometers. The smooth response suggests dispersion and mixing to be important processes. The jump in EC of the infiltration water at hour 360 caused a response at P-8.3 within 15 hours, which required 30 additional hours to stabilize. Similarly, the EC response took between 30 and 70 hours at P-2 and between 25 and 85 hours at P-5. The fast initial response at P-8.3 indicated that at least some of the infiltration occurred along the fast pathways. A conceptual sketch of the flow paths is represented in Fig. 2.3.

Samples collected from piezometers (except P-1) were expected to be a mixture of infiltrated-

and Amb-GW. The concentrations of TCA, together with the EC, was used to determine 1) whether infiltrated water reached monitoring points, and 2) the mixing ratios between Amb-GW and infiltrated-GW. The concentration of TCA was below the detection limit in all samples collected at monitoring points P-2, P-5, P-8.3, and P-10, indicating that they comprised primarily infiltrated water. Monitoring points P-8.2, P-8.1, and P-9 displayed a mixture of infiltrated-GW and Amb-GW, although the concentrations were closer to the infiltration water composition (Table 2.2). Table 2.2 summarizes the number of samples collected from each monitoring point for the three tests, screen interval depths (m), travel times (h) computed from EC records, and mixing ratios (Amb/Inf) computed from TCA concentrations at the monitoring points.

2.3.3 Redox sensitive species and DOC

The concentration of dissolved oxygen and DOC in the inflow ranged from 8.9 to 11.7 mg/L (0.25–0.33 mmol/L), and from 3.1 to 4.1 mg/L (0.26–0.34 mmol/L), respectively (Table 3.1). Therefore, the amount of DOC present in the inflow would be barely enough to consume the dissolved oxygen considering the stoichiometry of aerobic respiration. Thus, the reactive barrier was needed to establish other than aerobic redox conditions.

The success of the reactive layer in promoting reducing conditions that were not reached without such a layer was demonstrated by the behavior of redox-sensitive species (NO_3^-, Mn, and Fe). Figs. 2.6 A and 2.6 B display the evolution of normalized NO_3^- and Mn(II) vs. travel times (monitoring points) in the primary y axis (note the log scale for Mn). The concentrations were normalized to those measured in the inflow for each test, shown in the secondary axis. At the vadose zone (cc1 and cc2), installation of the reactive barrier caused a complete depletion of NO_3^- (Fig. 2.6 A and Table 3.1), an order of magnitude increase in the dissolved Fe concentration (Table 3.1), and an increase in the dissolved Mn concentration (Fig. 2.6 B). The variation in the redox-sensitive species after installation of the reactive barrier observed in the aquifer was smoother than that described for the vadose zone. The redox-sensitive species indicate no reducing conditions in

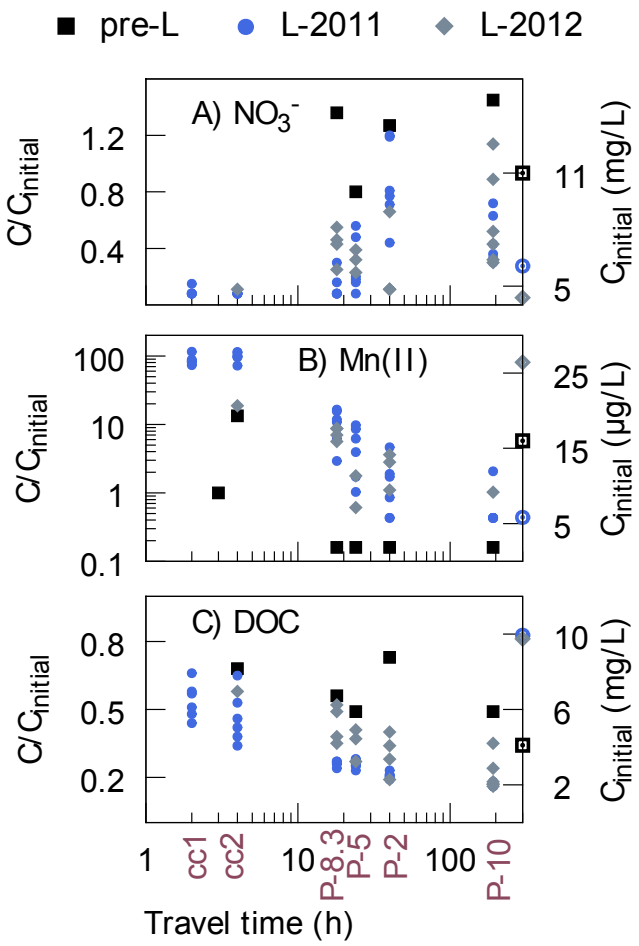

Figure 2.6: Normalized concentrations of A)NO_3^-, B)Mn(II) and C) DOC vs. travel time during pre-L (black square), L-2011 (blue circles), and L-2012 (grey diamonds). Initial mean concentrations for pre-L (black square), L-2011 (blue circle), and L-2012 (grey diamond) are shown in the secondary y axis.

the samples collected during February 2009 and May 2009 (Table 2.3). During the L-2011 and L-2012 tests, the high concentration of NO_3^- in the aquifer, compared to the vadose zone, implies preferential flow paths that allow part of the inflow to reach the aquifer without an intense interaction with the reactive layer (Fig. 2.3). This variation in the concentration of the redox-sensitive species along the infiltrated water flow path was negligible during the pre-L test. Therefore, installation of the reactive layer succeeded in leading to well-defined reducing conditions.

The amount of DOC released by the reactive layer during the L-2011 test can be estimated from the concentration of redox-sensitive species in cc1. The DOC values at cc1 during the L-2011 test averaged 5.4 mg/L (0.45 mmol/L), which was 2.3 mg/L more than in the inflow water (Table 3.1). Actually, the DOC supplied by the reactive layer was larger than that because some DOC had already been consumed in reducing dissolved oxygen, NO_3^-, Mn(IV), and Fe(III) by the time the infiltrated water reached cc1. The redox reactions considered for the estimation of released DOC by the reactive layer include:

Aerobic respiration:

$$CH_2O + O_2(g) \Longrightarrow CO_2 + H_2O$$

Denitrification:

$$CH_2O + 0.8\ NO_3^- \Longrightarrow HCO_3^- + 0.4\ N_2(g) + 0.2\ H^+ + 0.4\ H_2O$$

Manganese-reduction:

$$CH_2O + 2\ MnO_2(s) + 3\ H^+ \Longrightarrow HCO_3^- + 2\ Mn^{+2} + H_2O$$

Iron-reduction:

$$CH_2O + 4\ FeOOH(s) + 7\ H^+ \Longrightarrow HCO_3^- + 4\ Fe^{+2} + 10\ H_2O$$

Therefore, the total amount of DOC released by the reactive layer was computed as the measured increase of DOC (cc1 minus inflow), 2.3 mg/L (0.19 mmol/L), plus the DOC required to: (1) consume 8.9 mg/L (0.25 mmol/L) of dissolved oxygen assuming no dissolved oxygen in cc1 (0.25 mmol/L of DOC), (2) consume 6 mg/L (0.097 mmol/L) of NO_3^- present in the inflow and depleted in cc1 (0.12 mmol/L of DOC), (3) reduce 0.5 mg/L (0.009 mmol/L) of Mn-oxide absent in the inflow and present in cc1 (0.005 mmol/L of DOC), and (4) reduce 1.14 mg/L (0.02 mmol/L) of Fe-oxide absent in the inflow and present in cc1 (0.005 mmol/L of DOC). Some DOC was also invested in building biomass (not considered here). Therefore, the estimated total DOC released

by the reactive layer during the L-2011 test was at least 6.8 mg/L (0.6 mmol/L). In the same way, the DOC released by the reactive layer during the L-2012 test was at least (without including the DOC invested in building biomass) 6 mg/L.

Fig. 2.6 C displays the DOC concentration (mg/L) in the inflow (secondary axis) and DOC concentration normalized with the inflow (input to the unsaturated zone) vs. travel times (monitoring points) (primary axis). During the pre-L test, DOC concentration decreased to 56% of the input by the time the infiltrated water arrived to P-8.3 (travel time $\approx$ 20 h). The drop in DOC was faster during the L-2011 and L-2012 tests, as DOC at P-8.3 was 26% and 44% of the estimated input DOC, respectively. DOC measured from samples collected during 2009 displayed similar behavior as DOC measured during the pre-L test (Table 2.3), with a decrease of 62% of the input by the time the infiltrated water arrived at P-5 (travel time $\approx$ 30 h). A faster degradation rate during the L (-2011 and -2012) tests could reflect the fact that organic carbon released by the barrier was easily degradable. Taking into account the amount of DOC released by the barrier during the L-2011 and L-2012 tests, the higher degradation rate during L-2011 compared to L-2012 could indicate a change in the released DOC composition. The DOC released during the L-2011 was probably easily degradable, and with increasing time the remaining DOC became more refractory to degradation.

In summary, the reactive barrier successfully generated reducing conditions. Part of the infiltration, however, might occur through preferential flow paths with little impact from redox processes. Fingering is driven both by heterogeneity and gravity (the basin lies largely on clean sand). Therefore, it is unavoidable and not wholly undesirable (return to oxidizing conditions is facilitated by oxygen transport in the unsaturated zone). Still, we feel that, in addition to residence time considerations, future designs would benefit from a thicker layer and extension the reactive barrier over the basin walls. The results of the L-2012 test indicate that 14 months after installation of the reactive barrier, the release of organic matter decreased, although it was still sufficient to produce other than aerobic redox conditions. The simultaneously occurring redox processes are consistent

with the suggestion by *Alewell et al.* (2008) that in high DOC concentration environments, the sequential reduction chain is not a suitable concept, and because organic matter as the electron donor is freely available, redox processes attributed to low potential are not out-competed by processes attributed to high redox potential and processes differing in redox potentials occur simultaneously.

2.3.4 Behavior of the four selected PhACs

Fig. 2.7 displays the evolution along the flow path of the four selected PhACs normalized by their respective inflow concentrations. Clear differences can be identified in the PhAC behavior between the three tests. These differences can be attributed to changes in boundary conditions, such as redox and sorption conditions caused by the reactive barrier. The effect of temperature appears to be small. *Storck et al.* (2012) suggested lower temperatures could favor the removal of compounds under aerobic conditions during riverbank filtration because of higher oxygen saturation. In a study comparing occurrence, removal, and discharge of contaminants of emerging concern by diverse on-site treatment systems and potential seasonal patterns (two sampling seasons with variation of average temperature of 7.5 °C) *Du et al.* (2014) reported, however, that differences in the removal of total concentrations of all detected compounds between the two sampling seasons were not significant ($p < 0.05$).

Inflow concentrations of cetirizine and carbamazepine were similar during the three tests, while atenolol and gemfibrozil concentrations during the pre-L were double those of the L-2011 and L-2012 tests. *Storck et al.* (2012) summarized the results obtained during riverbank filtration experiments under changing boundary conditions. They found that for substances that are relatively easy to remove, decreasing concentrations in river water do not affect their removal efficiencies, while removal efficiencies of less degradable substances tend to be lower when their inflow concentrations decrease. Therefore, the impact of variations in the inflow concentrations should be small and, if any, would favor the removal efficiency of the pre-L test. We argue that most differences in observed PhAC behavior should be attributed to the presence of the reactive

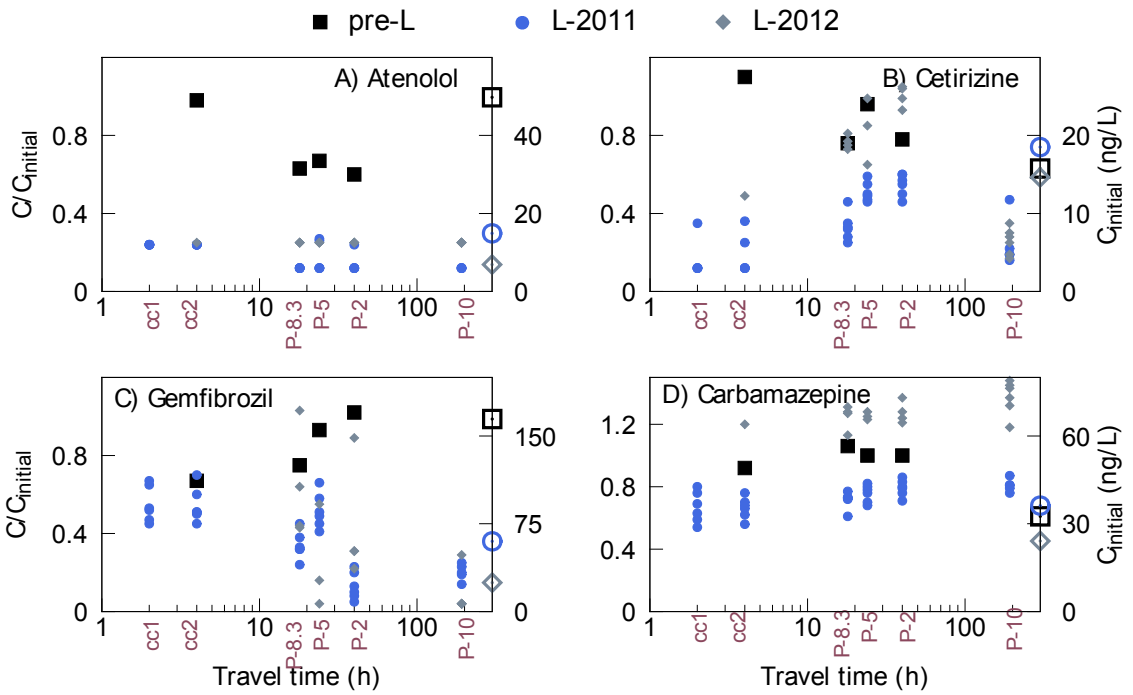

Figure 2.7: $C/C_{initial}$ of A) Atenolol, B) Cetirizine, C) Gemfibrozil, and D) Carbamazepine vs. travel time (h) during the pre-L (black squares), the L-2011 (blue circles), and the L-2012 (grey diamonds) tests on principal y axis, and their inflow average concentrations (ng/L) during the pre-L (black square),the L-2011 (blue circle), and the L-2012 (grey diamond) in the secondary y axis.

barrier.

Atenolol is a cationic beta-blocker at the experiment pH range (pK_a = 9.2 ± 0.4; $logK_{OW}$ = 0.34) (*Barbieri et al.*, 2011; *Schaffer et al.*, 2012a), and is reported to degrade under aerobic conditions (*Radjenović et al.*, 2008) and anoxic conditions. *Storck et al.* (2012) summarizing the results of bank filtration systems, placed atenolol in the list of compounds that are not impacted by redox conditions. We observed higher removal of atenolol during the tests performed after installation of the reactive layer. During the pre-L test, the concentration of atenolol decreased from the unsaturated zone (cc2), where the concentration was the 98% that of the inflow, to the saturated zone (P-8.3, P-5, and P-2) where it remained constant and averaged 63% that of the inflow concentration (Fig. 2.7 A) indicating a partial attenuation under aerobic conditions. *Laws*

et al. (2011) reported the removal of 96% after a travel time of 3 days in a field-scale infiltration system with variable redox conditions. After installation of the reactive barrier, atenolol exceeded the detection limit in 18 of 19 samples from the infiltration water (mean = 15 ± 3 ng/L during the L-2011 test and 7 ± 1.2 ng/L during the L-2012 test). Atenolol was detected only in 4 of 36 groundwater samples collected during the L-2011 test and below the detection limits in all 17 samples collected in the L-2012 test. In fact, during the L-2011 and L-2012 tests, atenolol was virtually removed by the time the water reached the first monitoring point (cc1 $\approx$ 2h). This rapid removal of atenolol during the tests performed after installation of the reactive barrier is consistent with the findings of *Barbieri et al.* (2011), who performed microcosm batch experiments in the absence of oxygen and found that increased reducing conditions led to faster removal of atenolol. *Du et al.* (2014) in study of a diverse on-site treatment system, including subsurface flow constructed wetlands, reported negligible differences regarding atenolol removal between two seasonal campaigns with 7.5 °C temperature variation. This would support the small effect of temperature indicate out that the reactive barrier increased the removal of atenolol.

Cetirizine, a zwitter-ionic antihistamine (two basic groups with pK_a of 2.2 and 8.8, respectively and one acidic group with pK_a of 2.9, $\log K_{OW} = 2.1$), is relatively stable in aquatic environments (*Kosonen and Kronberg*, 2009; *Schaffer et al.*, 2012b). Cetirizine concentrations exceeded the detection limit in all samples from the infiltration water and had a very similar mean concentration in all three tests (14 ± 2 ng/L in the pre-L, 18 ± 4 ng/L in the L-2011, and 14 ± 1 ng/L in the L-2012 tests) (Fig. 2.7B). *Kosonen and Kronberg* (2009) reported cetirizine to be inefficiently eliminated during wastewater treatment and relatively stable in the aquatic environment. Consistent with their report, scant removal of cetirizine was observed during the pre-L test when the concentration measured in the aquifer was the 83% that of the inflow. Nevertheless, during the L-2011 test, the mean cetirizine concentration was 33% that of the inflow concentration after only 18–24 hours travel time (P-8.3) and it was even lower in samples collected in the unsaturated zone (17% that of the inflow). This increase in the cetirizine concentration in the aquifer compared to that in the vadose zone could indicate a bypassing of the barrier through preferential flow paths.

For travel times close to 200 hours (P-10), the concentration of cetirizine was reduced to 26% that of the inflow. During the L-2012 test, the behavior of cetirizine was similar to that observed during the pre-L test. The redox conditions below the infiltration basin, the temperature, and the inflow concentration were comparable during the two tests performed after the barrier installation. This diverse behavior might be a consequence of the different degradation rates of DOC observed between the two tests. To the best of our knowledge, this is the first report of the behavior of cetirizine during AR through an infiltration basin.

Gemfibrozil, a blood lipid regulator, is recalcitrant and frequently detected in aquatic environments, including drinking water (*Jelic et al.*, 2012; *Grenni et al.*, 2013). It is anionic in the pH range of the experiment, (pK_a = 4.8; $logK_{OW}$ = 4.3) (*Kröger*, 2014). We observed two different trends in the behavior of gemfibrozil during the experiment. The first trend was observed during the pre-L test, when gemfibrozil concentrations at the monitoring points with travel times between 18 and 72 hours (P-8.3, P-5, and P-2) decreased to 90% that of the inflow (Fig. 2.7C), with the lowest concentration measured in the unsaturated zone (67% that of the inflow). This removal (10%) was small compared to that reported by *Laws et al.* (2011), who reported complete removal of 92% for travel times of 3 days in a field-scale infiltration system with variable redox conditions. The second behavior trend was observed during the L-2011 and L-2012 tests. In these cases, the gemfibrozil concentration was depleted to 34% (during L-2011) and 64% (during L-2012) that of the inflow concentration after travel times of 18–24 (P-8.3). For travel times longer than 100 hours (P-10), the concentrations of gemfibrozil were reduced to 25% and 8% that of the inflow during the L-2011 and L-2012 tests, respectively. *Kröger* (2014) performed column experiments simulating AR and, using the same compost contained in the reactive barrier, observed that the degradation of gemfibrozil increased with the amount of DOC. Consistently, *Lim et al.* (2008), in microcosm experiments, observed that for a given type of DOC, the biodegradation rate of gemfibrozil increased with the amount of DOC. *Rauch-Williams et al.* (2010) who performed column experiments simulating AR, speculated that the biodegradation of gemfibrozil is limited by the concentration of biodegradable organic carbon. *Maeng et al.* (2012) suggested that the type of DOC also affects the

degradation of gemfibrozil after observing better removal in columns fed with low biodegradable fractions of DOC, such as humic substances, compared to columns fed with more biodegradable DOC. Thus, the increased concentration of DOC in the infiltrated water and/or the reducing conditions achieved after installation of the reactive barrier, L-2011 and L-2012 tests, might be the reason for the increased removal compared to the pre-L test.

Among PhACs, carbamazepine, an anticonvulsant drug, is one of the most extensively reported recalcitrant water pollutants, and it is neutral at the experiment pH range (pK_a = -0.5 ± 0.2; $logK_{OW}$ = 1.9) (*Drewes et al.*, 2003a; *Clara et al.*, 2004; *Arye et al.*, 2011; *Borisover et al.*, 2011; *Dickenson et al.*, 2011; *Du et al.*, 2014; *Kröger*, 2014). *Clara et al.* (2004) and *Bekele et al.* (2011) observed that neither sorption nor degradation are meaningful attenuation processes for carbamazepine in AR systems. Consistently, *Heberer* (2002), reviewed a number of field studies and reported that carbamazepine is consistently not attenuated during bank filtration. In fact, little removal has been found in column experiments under different redox conditions and different bulk organic carbon matrices (*Rauch-Williams et al.*, 2010) or during groundwater recharge (*Drewes et al.*, 2003a; *Laws et al.*, 2011). On the other hand, *Chefetz et al.* (2008) and *Maoz and Chefetz* (2010) reported that adsorption of carbamazepine by soil organic matter could be expected. Indeed, *Arye et al.* (2011) observed a correlation between the soil organic matter and the carbamazepine content in the profiles of soil samples taken from an infiltration basin. *Maeng et al.* (2010), compared bank filtration to AR via infiltration basins, and observed that the attenuation of carbamazepine was higher when the residence time was increased under reducing conditions. Accordingly, *Storck et al.* (2012) investigated the factors controlling micropollutant removal during riverbank filtration and reported higher carbamazepine removal under anaerobic/anoxic conditions. We found quite constant concentrations in the inflow water throughout the experiment (Fig. 2.7D). No carbamazepine attenuation was observed during the pre-L test. During the L-2011 test, the carbamazepine concentration at the monitoring points was decreased compared to the inflow concentration. The removal occurred within the infiltration basin and the first monitoring point (cc1), where we found the highest removal, 67% that of the inflow. No further removal was

observed; in fact, the removal at P-8.3 was 71% that of the inflow, and it was 73% that of the inflow at P-10. Therefore, the removal occurred in the vadose zone, where the most reducing conditions were achieved and where, as a result of the installation of the reactive barrier, the soil organic matter content was highest. This same removal was expected during the L-2012 test, but on the contrary the carbamazepine concentration was higher in the aquifer than in the infiltration water, 125% and 137% that of the inflow in P-8.3 and P-10, respectively. *Bekele et al.* (2011), studying water quality changes due to infiltration through the vadose zone, also found higher concentrations of carbamazepine in the infiltrated water than in the inflow water. During AR via an infiltration basin, *Arye et al.* (2011) found that carbamazepine might accumulate in soil layers with a higher organic matter content during the flooding/drainage cycle and be released during subsequent flooding of the basin, resulting in higher concentrations of carbamazepine in the infiltrated water. This is a plausible explanation for the differences in the behavior of carbamazepine observed between the L-2011 and L-2012 tests. Thus, we found carbamazepine to be highly recalcitrant during AR through infiltration basin under different redox conditions and with a high content of soil organic matter.

2.3.5 Conclusions

The reactive barrier succeeded in releasing DOC as demonstrated by the two tests performed 5 (L-2011) and 16 (L-2012) months after its installation. The released DOC concentration was similar during both tests, although the degradation rate of DOC was higher in the earlier test. Despite these differences, nitrate-, manganese-, and iron-reducing conditions were achieved beneath the reactive barrier in both tests.

The reactive barrier was successful in enhancing removal of three of the four selected PhACs during AR. The removal of atenolol and gemfibrozil increased within short travel times when the recharge occurred through the reactive barrier. Thus, atenolol was already depleted below detection limits in all samples collected in the vadose zone. After 18–24 hours of residence time in

the vadose zone and aquifer (P-8.3), gemfibrozil concentrations decreased to 34% and 64% that of the inflow in the L-2011 and L-2012 tests, respectively. In contrast, the gemfibrozil concentration was only reduced to 75% that of the inflow in the tests perforned prior to installation of the reactive barrier.

The concentration of cetirizine measured after 18–24 hours of travel time (P-8.3) during the pre-L test was 83% that of the inflow concentration, whereas during the L-2011 test cetirizine was removed to 33% that of the inflow. The attenuation of cetirizine during the L-2012 test, however, was poor, with a concentration of 77% that of the inflow at the monitoring point P-8.3.

The increase in the removal of these three PhACs after installation of the reactive layer may be partially due to sorption or biodegradation under the different redox conditions promoted by the released DOC. No clear criteria regarding could be determined in the field experiment described here.

Carbamazepine concentrations exhibited little variation along the travel times in all three tests, confirming its well-known recalcitrant behavior in the aquatic environment.

Table 2.1: Mean values (standard deviations, indicative of variability, not measurement errors) of field parameters, main anions and cations, DOC, TCA and four selected PhACs in P-1 (Amb GW), infiltration water (Inf), and vadose zone (cc1, cc2) during the pre-L, L-2011, and L-2012 tests.

Parameters (Units)	Amb-GW Pre-L	Inf Pre-L	cc2 Pre-L	Amb-GW L-2011	Inf L-2011	cc1 L-2011	Amb-GW L-2012	Inf L-2012	cc2 L-2012
pH	6.9	8.2	7.9	6.8(0.18)	8.2(0.12)	7.5(0.27)	6.9(0.14)	8.9(0.12)	-
T (°C)	20	8	-	17.6(1.2)	19.7(1.5)	-	16.5(0.5)	26.7(1.3)	-
O_2 (mg/L)	1.76	11.7	-	3.7(0.3)	8.9	-	6.5(0.9)	12.7(3.4)	-
EC (mS/cm)	1.4	1.0	-	1.6(0.03)	1.5(0.09)	-	1.5(0.08)	1.4(0.06)	-
Cl^- (mg/L)	228	253	-	220(3)	281(26)	285(15)	211.8(20.4)	281.5(11.2)	288
NO_3^- (mg/L)	11	14.1	-	17.2(2.6)	6(0.7)	0.25*	8.38(4.1)	4.9(2.9)	0.5*
SO_4^{-2} (mg/L)	183	166	-	24.8(10)	140(9)	134(5)	178.8(47.3)	171.5(42.7)	146
HCO_3^- (mg/L)	334	228	183	406(39)	230(7)	269(27)	339(44)	210(22)	206
Fe (II)(μg/L)	3.5	3.5	104	4.8(2)	5.6(4.4)	1139(395)	8.3(8.4)	31.5(32.6)	1710
Mn (II)(μg/L)	5	16	16	4.2(4.2)	5.8(7)	511(83)	2.5(0)	26.4(28.2)	497
Na (mg/L)	117	128	119	132(2.4)	156(9)	156(9)	130.4(7.2)	152.3(6.3)	157
K (mg/L)	24.5	27	26	24.8(0.4)	31.8(1.3)	32.3(1)	20.6(0.54)	35(1.5)	35
Mg (mg/L)	33.1	31	30.2	42.5(1.5)	26.3(0.8)	26.6(0.5)	35.4(2.8)	28.1(1.1)	28.1
Ca (mg/L)	132	97.2	100	180(5.3)	105(1.9)	110(3.5)	143(9.6)	98.7(8.1)	91.8
DOC (mg/L)	1	4.1	2.8	1.4(0.6)	3.1(0.25)	5.4(0.8)	1.5(0.2)	3.7(0.9)	5.7
TCA (μg/L)	647	4*	4*	502(251)	4*	4*	110(78)	4*(0)	4
Atenolol (ng/L)	1.8*	49.8	48.8	1.8*	14.8(3.7)	3.5*	5.9(9.4)	6.9(1.2)	1.7*
Cetirizine (ng/L)	2.8	15.7	17.4	1.1*	18.5(4.8)	2.9(1.7)	1.1*(0)	14.6(1.0)	7.3
Gemfibrozil (ng/L)	5.1	164.5	111	1*	60(13.2)	32.9(5.5)	1*(0)	24.8(2.7)	32
Carbamazepine (ng/L)	35.7	32.5	30	22.5(1.5)	36.2(11.8)	24.2(3.6)	31.1(4.9)	24(0.7)	29

Note: - not measured, * Quantitation limit/2

Table 2.2: Number of samples collected ifrom each monitoring point for the three infiltration tests, screening interval, calculated travel times, and mixing ratios (cthe one with higher proportion of Amb-GW was selected when there were differences between the three tests), and TCA range (pre-L/L-2011/L-2012) for the monitoring points

Monitoring point	Number of samples pre-L	L-2011	L-2012	Screening interval (m from surface)	Travel time (h)	Mixing ratio (Amb/Inf)	TCA (μg/L)
INF	1	14	6	-	0	0/1	4*/4*/4*
cc1	-	6	1	-	1–3	0/1	4*/4*/4*
cc2	1	6	1	-	3–6	0/1	4*/4*/4*
P-8.3	1	6	4	7–9	15–30	0/1	4*/4*/4*
P-5	1	6	3	5–21	25–85	0/1	4*/4*/4*
P-2	1	6	4	6–24	30–70	0/1	4*/4*/15.5
P-8.2	1	6	2	10–12	30–90	0.01/0.99	8.3/5/11.5
P-9	1	5	6	9–29	170–560	0.01/0.99	53/12.3/72
P-8.1	1	6	2	13–15	90–170	0.2/0.8	132/119/342
P-10	1	6	6	6–20	90–170	0/1	4*/4*/9.1
P-1	1	6	5	6–24	-	1/0	647/502/110

Note: - data not available, * Quantitation limit/2

Table 2.3: Values of DOC (mg/L), NO_3^- (mg/L), Mn (II) (μg/L), and Fe (II) (μg/L) in samples collected in 2009.

Monitoring point	Feb-2009 DOC(mg/L)	Feb-2009 NO_3^-(mg/L)	Feb-2009 Mn(II)(μg/L)	Feb-2009 Fe(II)(μg/L)	May-2009 DOC(mg/L)	May-2009 NO_3^-(mg/L)	May-2009 Mn(II)(μg/L)	May-2009 Fe(II)(μg/L)
Inf	4.5	17.4	69	20	4.8	7.9	25*	25*
cc1	-	-	-	-	4.7	8.4	25*	25*
cc2	-	-	-	-	4.3	7.8	25*	25*
P-2	1.3	11.7	9	2	3.6	9.0	25*	25*
P-5	3.2	9.2	6	2	2.5	9.4	25*	25*

Note: - not measured, * Quantitation limit/2.

Chapter 3

Behavior of nine selected emerging trace organic contaminants in an artificial recharge system supplemented with a reactive barrier[‡]

3.1 Introduction

Water shortages are a serious concern in many parts of the world, which promotes the recycling of effluents from municipal wastewater treatment plants and effluent-receiving water bodies (*Levine and Asano*, 2004; *Liu et al.*, 2013). Artificial recharge of aquifers is a technology that expedites the restoration and reuse of treated effluents or receiving rivers. In addition to contributing to water resources, artificial recharge of aquifers through infiltration basins enhances water quality

[‡]the present chapter is based on the paper Behavior of nine selected emerging trace organic contaminants in an artificial recharge system supplemented with a reactive barrier by Cristina Valhondo, Jesús Carrera, Carlos Ayora, Manuela Barbieri, Karsten Nödler, Tobias Licha, and Maria Huerta *Environ Science and Pollution Research*., Doi:10.1007/s11356-014-2834-7

during its passage through the soil (*Greskowiak et al.*, 2005) by decreasing the concentration of suspended solids, pathogens, nitrogen, phosphates, metals, and dissolved organic carbon (DOC) (*Bouwer*, 2002).

Many emerging trace organic contaminants (EOCs), such as endocrine-disrupting chemicals, pharmaceuticals, and personal care products, are detected in wastewater, surface water, groundwater, and drinking water, at trace levels ranging from ng/L to μg/L (*Tran et al.*, 2013; *Lapworth et al.*, 2012; *Nödler et al.*, 2013). Attention to EOCs is escalating due to their potential undesirable health effects on humans and ecosystems (*Jones et al.*, 2004; *Bound and Voulvoulis*, 2004; *Tran et al.*, 2013). Several EOCs are released into aquatic environments, mostly by effluents from municipal sewage treatment plants (*Heberer*, 2002; *Bound and Voulvoulis*, 2004) because they are not completely removed by conventional treatment technologies (*Carballa et al.*, 2004; *Díaz-Cruz and Barceló*, 2008; *Reemtsma et al.*, 2010; *Radke et al.*, 2009; *Kasprzyk-Hordern et al.*, 2008). Landfill leachates or manufacturing residues constitute other possible sources of groundwater EOCs contamination (*Heberer*, 2002; *Jones et al.*, 2004; *Pedersen et al.*, 2005).

The water used for artificial recharge of aquifers often comprises wastewater effluents or effluent-receiving rivers containing EOCs (*Drewes*, 2009; *Maeng et al.*, 2011b; *Díaz-Cruz and Barceló*, 2008). Biodegradation (*Maeng et al.*, 2011b) and sorption (*Burke et al.*, 2013; *Schaffer et al.*, 2012a,b) are essential processes for organic contaminant attenuation during subsurface flow. These two processes remove some EOCs from the infiltrated water during soil-passage in artificial recharge systems (*Maeng et al.*, 2011b; *Liu et al.*, 2013). In addition, some EOCs are preferentially removed under specific redox conditions (*Barbieri et al.*, 2011; *Liu et al.*, 2013; *Maeng et al.*, 2010). Therefore, the passage of infiltrated water through diverse redox environments should enhance the number of contaminants removed. In the same way, increasing the diversity of sorption sites (neutral, cationic, and anionic) along the flow path should enhance the sorption of EOCs.

In the present study, we aimed at enhancing the removal of EOCs by installing a reactive barrier at the bottom of an infiltration basin to promote variable redox conditions below the basin

and increase the diversity and number of sorption sites. To promote variable redox conditions, the reactive barrier comprised vegetable compost, which releases DOC into the infiltrating water, thus leading to reducing conditions that should become oxidizing again after transport through the aquifer. The compost further acts as a sorbent for neutral EOCs. To provide positively- and negatively-charged sorption sites, the reactive barrier was supplemented with small amounts of iron oxide and clay. We studied the behavior of nine selected EOCs during artificial recharge before and after installing the reactive barrier.

Compounds selection was based on the respective charges of the EOCs at experimental pH ranges (6.61 to 9.17) and on the frequency of their detection in the aquatic environment. We selected two cationic (citalopram and trimethoprim), five neutral (paracetamol, 1H-benzotriazole, tolyltriazole, caffeine, and benzoylecgonine), and two anionic (ibuprofen and sulfamethoxazole) compounds.

3.2 Materials and methods

3.2.1 Local hydrogeology

The infiltration system was placed over the Llobregat Lower Valley aquifer, 15 km inland from the Mediterranean coast (Figure 3.1). The aquifer comprises of Quaternary alluvial sediments, mainly coarse gravel and sand with small clay lenses (*Iribar et al.*, 1997). The minerals include mainly silicates, calcite, and dolomite, and the solid phase contains a small portion of organic matter (f_{OC} less than 0.2%) (*Barbieri et al.*, 2011). At this site, the aquifer extends to a depth of 23 to 27 m below ground, underlain by Pliocene marls. The regional groundwater flow direction is from NNW to SSE (*Iribar et al.*, 1997) with a natural hydraulic gradient of 2.3‰. The Llobregat River is not expected to be a major recharge source st the site because, although the water table is below the river, they are not locally connected. The depth to the water table varied between 5 and 7 m

below the infiltration basin during the test, which ensures that recharged water flows through a rather thick unsaturated zone. Contamination of the aquifer by chlorinated solvents was detected in 1994 (*Samper et al.*, 1999). Currently trichloroethane (TCA) levels measured in groundwater samples collected near the infiltration system average 324 μg/L.

3.2.2 The facility and water source

The artificial recharge system comprises a settlement basin (≈5000 m^2 and ≈4 m depth, although the depth below the spill level is 2 m) and an infiltration basin (≈5000 m^2 and ≈3 m depth, but the water rarely exceeded 0.7 m deep). The two basins were excavated in alluvial terrace deposits, so that their bases comprised mainly sand with some silty lenses. The system has been intermittently operational since February 2009. Residence time in the settlement basin was from 2 to 4 days. The settlement basin was clogged shortly after the beginning of the operations and virtually no water has infiltrated from it. Infiltration rates in the infiltration basin ranged between 0.5 and 2 m/d. The recharge water runs through a pipe from the Llobregat River upstream of Sant Vicenç dels Horts. By the time the river reaches the capture point, it has received effluent from more than 50 waste water treatment plants, explaining the presence of a broad range of contaminants well above detectable concentrations (*Köck-Schulmeyer et al.*, 2011).

3.2.3 Description of monitoring points

A network of monitoring points was installed around the recharge system to assess the quality of the background and artificially infiltrated groundwater (Figure 3.1). Piezometer P1, located upstream of the settlement basin and screened over the full aquifer thickness (6 – 24 m depth interval), remained unaffected by infiltration water (INF). Therefore, field parameters (electrical conductivity [EC], temperature) and samples collected at this point are assumed to represent the background concentrations of the aquifer, named hereafter background-groundwater (BGW).

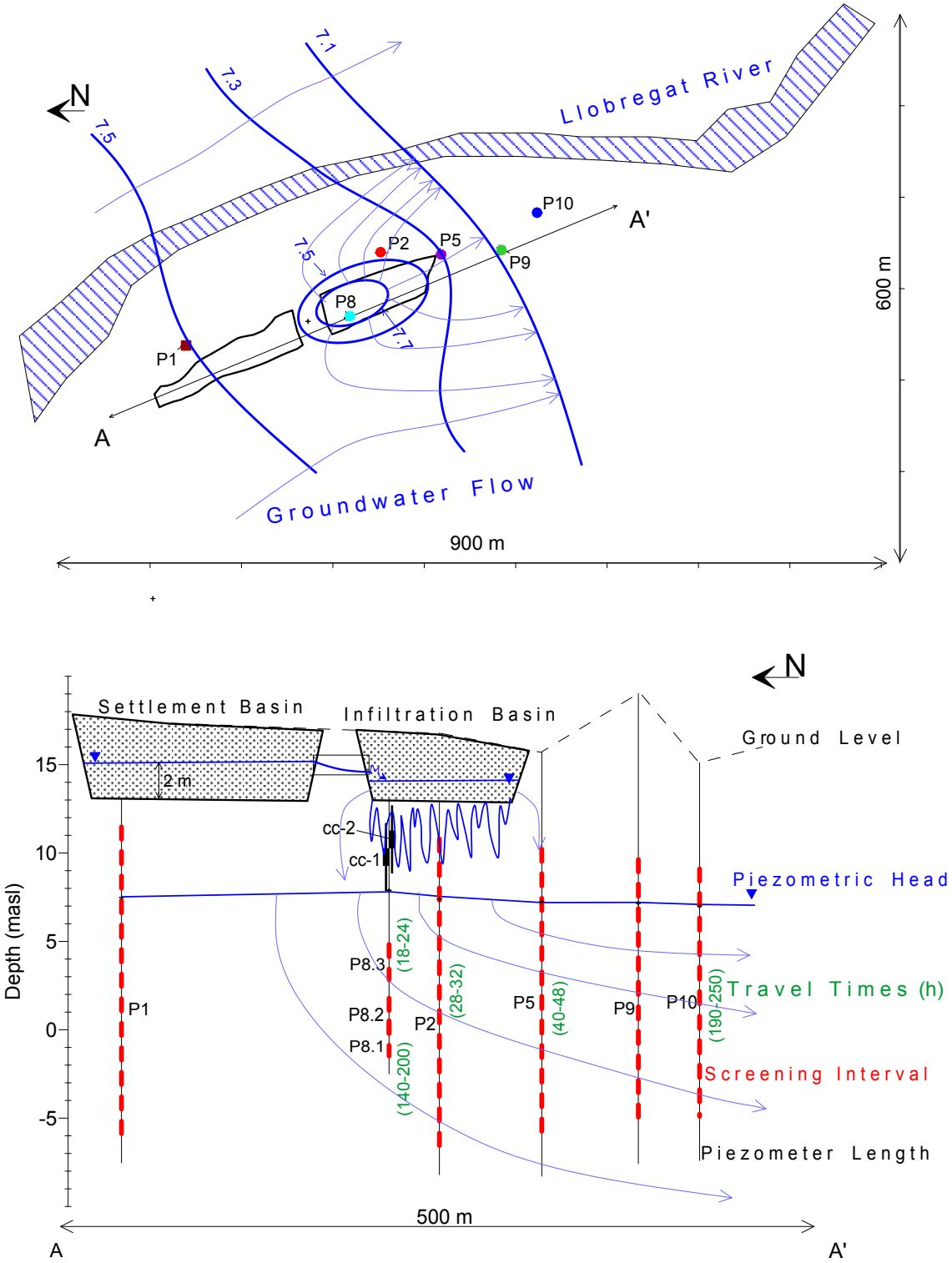

Figure 3.1: Schematic plant view and cross-section of the field site and monitoring points

Piezometer P8, located in the middle of the infiltration basin, is a nest of three sampling points screened at depths of 7 to 9 m (P8.3), 10 to 12 (P8.2), and 13 to 15 m (P8.1). Monitoring point P8.3 was used to assess changes in water quality of the infiltrated water through the vadose zone and capillary fringe, whereas P8.1 was used to monitor longer residence times. Two piezometers were drilled close to the infiltration basin (P5 and P2). Piezometer P5, fully screened (5.5 – 21.5 m), is located 3 meters downstream of the infiltration basin. Piezometer P2, completely screened (6 – 24 m), is located adjacent to the basin and was also expected to receive infiltration water during recharge periods. Two additional fully-screened piezometers were installed 70 m and 127 m downstream of the infiltration basin and named P9 and P10, respectively (screened from 9.4 – 24.4 m and from 6 – 20 m). Most piezometers were completed with 5-cm diameter PVC pipes with the exception of P1, which was completed with an 11-cm diameter PVC pipe. Additionally, two suction cups were installed in the vadose zone at a depth of 1 m (named cc1) and 2 m (named cc2) and at the same location of P8.

Travel times of the infiltrated water to the different monitoring points was determined from the transmission of EC fluctuations in the infiltration water during the infiltration tests. These data indicated a travel time of around 18 to 24 h from the infiltration basin to the piezometer located in the middle of the infiltration basin (P8.3). The travel time to the most distant piezometer (P10) was between 8 to 10 days.

3.2.4 The reactive barrier

A reactive barrier (65 cm thick) that completely covered the infiltration basin (5000 m^2) was installed in March 2010 to enhance natural processes involved in the removal of the EOCs during soil aquifer treatment. Specifically, we aimed at enhancing both, adsorption by providing a range of sorption site types and biodegradation by adding organic matter to promote a broad range of redox conditions and thus the growth of microorganisms with diverse metabolic pathways. Therefore, the barrier consisted of aquifer sand (49.5% in volume), vegetable compost from gardens and

woods (49.5% in volume), clay (≤ 1% in volume), and iron oxide dust (≤0.1% in volume). The role of the sand was to provide structural integrity to the barrier and to ensure high hydraulic conductivity. The role of the vegetable compost was to provide sorption sites for neutral contaminants and to release DOC into the infiltrating water. The total volume of compost used in the reactive barrier was 1500 m^3. The role of the clay (consisting mainly of quartz 42 wt%, illite 33 wt%, smectite 16 wt%, and chlorite 9 wt%) and the iron oxide (goethite) was to provide sorption sites for cationic and anionic contaminants.

Aquifer material, vegetable compost, and clays were blended in an approximately 60-cm thick layer that was installed at the base of the infiltration basin using an excavator. The excavator avoided passing over the barrier. To prevent material from floating, the layer was covered with approximately 5 cm of aquifer sands. Iron oxide was spread over the barrier's surface in order to minimize its reduction and mobilization.

To determine whether the reactive barrier could act as a source of EOCs, a 0.5-L sample of vegetable compost was leached with 1 L ultra-pure water for 12 h. Caffeine (19 ng/L), 1H-benzotriazole (17 ng/L), and tolytriazole (30 ng/L) were the only EOCs detected with concentrations above the limit of quantitation in the leachate sample, and all were an order of magnitude lower than their concentration in the infiltration water. Therefore, we assumed that the barrier did not act as a source of EOCs. The leachate had a pH of 8.4, and the concentrations of nitrate, phosphate and DOC were 2.8, 0.57, and 7.9 mg/L, respectively. Additionally, column experiments were performed to assess the amount of organic carbon released by the compost and its durability over time prior to beginning the field experiments.

3.2.5 Procedure and collection of water samples

Three infiltration tests were performed for assessing the effect of the barrier on contaminant removal; one before and two after the reactive barrier installation. The first test, referred to as the

"NB" test below, was performed in February 2011. The second test, referred to as "B-2011", took place in September-October 2011, 5 months after installation of the reactive barrier. The last test, referred to hereafter as "B-2012", was performed in July 2012. Infiltration rates averaged 1 m/d (200 m^3/h) during all tests. The infiltration periods lasted 3 weeks (NB) and 7 weeks (B-2011 and B-2012).

Piezometer sampling was conducted by pumping while monitoring field parameters (T, pH, EC, and Eh) in a flow cell. To ensure that samples were representative for groundwater, they were collected when field parameters had stabilized and after pumping a volume of water equal to at least three times the borehole volume. Physicochemical field parameters of the infiltration water (pH, Eh, T and EC) were determined using electrodes in the water flowing from the settlement to the infiltration basin.

Samples from the river were collected daily for 3 weeks in December 2010, to assess variations in EOCs in the inflow water. In addition, 9 daily samples were collected from the infiltration basin to observe changes in the EOCs concentrations between the river and the infiltration basin (i.e., due to mixing and removal processes during transport and retention in the settlement basin). The variability in the EOCs concentrations was compared between these 9 samples from the infiltration basin (collected daily), and the corresponding 9 river water samples. Results are shown in Figure 3.2. The average concentrations of most of the selected EOCs were lower in the infiltration basin than in the river indicating that some removal occurs. The residence time in the settlement basin homogenized the water used for recharge which displayed less variability than river water. For these two reasons, the quality of the infiltration water was characterized using exclusively the infiltration basin samples.

The infiltration basin was sampled once during the NB test, 14 times during the B-2011 test, and 6 times during the B-2012 test. Samples from piezometers were collected during the three infiltration tests. One single sample was collected from each monitoring point during the NB test. The NB test had to be terminated because high levels of turbidity in the infiltration water occurred

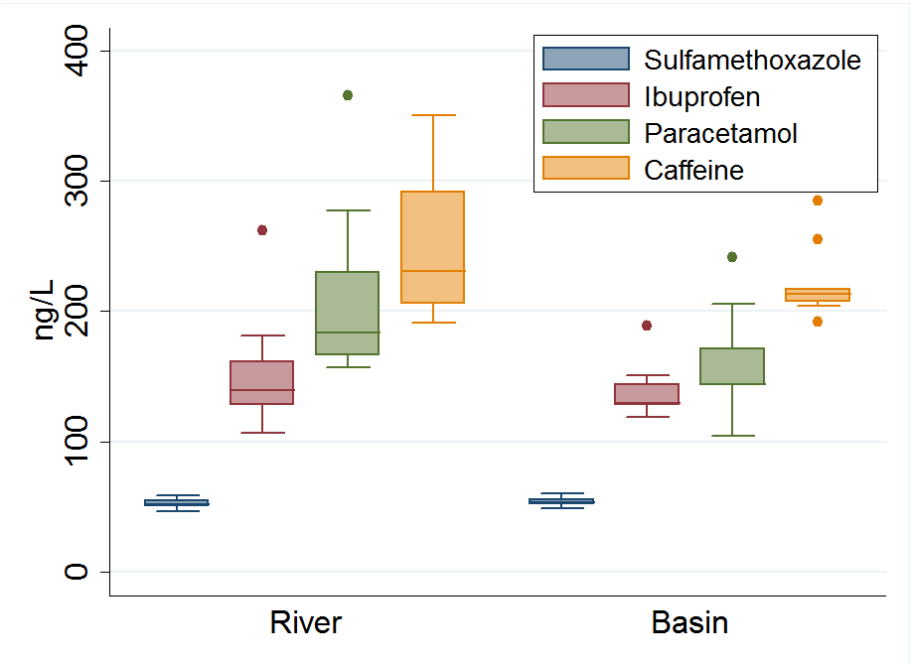

Figure 3.2: Boxplot of the concenrtations of four selected EOCs in river and infiltration basin samples collected for 9 consecutive days

and clogging of the infiltration basin was feared. Theses samples were gathered 20 days after infiltration had started. During the B-2011 and B-2012 tests, samples were collected for 6 and 4 weeks, respectively. Infiltration began 15 and 14 days before the first samples were collected during the B2011 and B-20122 tests.

3.2.6 Analysis of water samples

Water samples were analyzed for major ions, nutrients, metals, DOC and EOCs.

Samples collected for Cl^-, SO_4^-, NO_3^-, and HCO_3^- analysis were filtered through 0.45-μm PALL Acrodisc© sterile Syringe filters with a Supor© membrane, stored at 4°C, and analyzed within 72 h by ion chromatography using a Dionex DX-120 with a ionPac AS18 4x250mm column and KOH as the eluent. The analytical error was estimated to be 13%.

Samples for the analysis of Fe, Mn, Ca, K, Na, Mg, and B were also filtered through 0.45-

μm membrane filters, acidified immediately after filtration, and stored at 4°C until analysis. The samples were analyzed within 72 h by inductively coupled plasma optical emission spectroscopy using a Perkin Elmer Optima 3200DV. The analytical error was estimated to be below 15% for Ca, Na, Mn and B, and below 12% for Mg, K, and Fe. Lower limits of calibration were 6.1 mg/L for Na, 4.5 mg/L for Ca, 0.2 mg/L for Mg, 0.8 mg/L for K, 15 μg/L for B, 6 μg/L for Fe, and 15 μg/L for Mn.

Samples for the analysis of DOC were collected in glass bottles, filtered through 0.45 μm, acidified immediately after filtration, and stored at 4°C. DOC was analyzed using a total organic carbon analyzer (Shimatzu TOC-Vcsh) with an infrared detector using the NPOC method.

Samples for the analysis of TCA were collected in amber glass, stored at 4°C, and analyzed within 72 h by headspace (Gester Inc) coupled with a GC-MS instrument (Agilent Technologies 6890N-5973MSD) using a DB-624 column (60m x 0.32mm, 1.80μm). The analytical error was estimated to be below 25%, and the detection limit was 8 μg/L. Amber-glass bottles were used to collect samples for EOC analysis. In accordance with *Nödler et al.* (2010), the samples were allowed to settle at 4°C for 24 h before extraction and only the supernatants were used for analysis. For groundwater extraction, 500 mL of the sample was spiked with 10 μL of an internal standard (IS)-mix using a 10-μL syringe and with 5 mL phosphate buffer concentrate (neutral pH). The internal standard contained 200 ng of paraxanthine-D_6 (IS for 1H-benzotriazole, tolytriazole, caffeine and paracetamol, 100 ng of diazepam-D_6 (IS for citalopram), 100 ng of sulfamethoxazole-^{13}C6 (IS for sulfamethoxazole), 100 ng of carbamazepine-D_{10} (IS for benzoylecgonine and trimethoprim), and 200 ng of ibuprofen-D_3 (IS for ibuprofen). For surface (river and basin) and vadose zone water, 250 mL of the sample was diluted to 500 mL with ultrapure water and processed as described for the groundwater samples. The sample was extracted by solid-phase extraction. OASIS HLB (6 mL, 500 mg; Waters, Eschborn, Germany) was used for the solid-phase extraction and an extraction speed of 15 mL/min was applied. Prior to extraction, the sorbent was conditioned with 4 mL methanol and rinsed twice with 4 mL ultra-pure water. After extraction, the sorbent was

rinsed twice with 1.5 mL ultra-pure water to remove the inorganic salt matrix. The sorbent was then dried and stored at -18°C before resuming analysis. This method proved to be an adequate approach regarding analyte stability (*Hillebrand et al.*, 2013). The analytes were eluted with 2x2 mL methanol, followed by 2x2 mL ethyl acetate. The extract was evaporated to dryness at 40°C with a gentle stream of nitrogen and re-dissolved in 1 mL aqueous 5-mM ammonium acetate solution containing 4% of methanol. The extract was transferred to an auto sampler vial and centrifuged for 10 min (4000 rpm) before analysis. The extracts were analyzed by HPLC-MS/MS according to *Nödler et al.* (2010). The method quantitation limits (MQLs) ranged from 2.3 to 4.9 ng/L in groundwater and 4.6 to 9.8 ng/L in surface water, respectively. Relative standard deviations of the analytes were ≤5.0%.

3.3 Results and discussion

3.3.1 Characterization of end-members and mixing rates in monitoring points

Field parameters and concentrations of major ions and selected EOCs in the two end-member waters (BGW: background-groundwater; INF: infiltration water) and in P8.3 are displayed in Table3.1. Most of the analyzed parameters exhibited relatively constant values in background-groundwater samples (P1) during all experiments. Infiltration water displayed a higher variability than background-groundwater, especially in temperature, caffeine, 1H-benzotriazole, ibuprofen, paracetamol, and trimethoprim. Infiltration water temperature during the NB test was lower than that during the B-2011 and B-2012 tests. Caffeine, ibuprofen, and paracetamol concentrations were higher, whereas the 1H-benzotriazole concentration was lower during the NB test. Major ions, temperature, and TCA values measured in P8.3 were closer to the values measured in the infiltration water than to the values measured in the background-groundwater, with the exception of sulfate and potassium in the NB test. Measured values of Eh were lower in P8.3 in all three tests than those measured in the infiltration water.

The high TCA values measured in background-groundwater (P1), resulting from a historical contamination in the aquifer (*Samper et al.*, 1999) together with the recalcitrant behavior of TCA, allowed us to use it as indicator of background-groundwater in our tests. Figure 3.3 shows TCA versus boron concentrations measured in samples of background-groundwater, infiltration water, and monitoring points to establish the origin of the sampled water and to determine the mixing ratios of infiltration water and background-groundwater in each sample. Samples from P8.3, P5, P2, and P10 consisted essentially of infiltration water, with the exception of two samples collected during the B-2012 test. On the other hand, monitoring points P9, P8.2, and P8.1 (the two deepest piezometers located in the middle of the infiltration basin) were partially affected by infiltration water. Most of the samples collected from these piezometers represented a mixture of infiltration water and background-groundwater in varying proportions. Given their variability, these three points were not considered when evaluating the efficiency of the barrier.

Table 3.1: Mean values (standard deviations) of field parameters, major ions and selected EOCs in infiltration water (INF), background-groundwater (BGW) and monitoring point P8.3 during the three tests

Parameters (Units of measure)	No Barrier			B-2011			B-2012		
	INF	P8.3	GW (P1)	INF	P8.3	GW (P1)	INF	P8.3	GW (P1)
EC (mS/cm)	1.03	1.04	1.4	1.46 (0.09)	1.52 (0.07)	1.57 (0.03)	1.49 (0.06)	1.52 (0.02)	1.54 (0.08)
T (C)	8.0	8.2	20.0	19.7 (1.5)	21.4 (1.6)	17.6 (1.2)	26.7 (1.4)	26.5 (0.5)	16.5 (0.5)
pH	8.2	7.45	6.9	8.2 (0.12)	7.2 (0.1)	6.8 (0.18)	8.9 (0.1)	7.2 (0.1)	7 (0.1)
Eh	188	71	164	36 (29)	8 (29.4)	76 (33)	187 (18)	143 (68)	156 (68)
DOC (mg/L)	4.1	2.3	1.7	3.1 (0.25)	2.6 (0.1)	1.4 (0.6)	3.7 (0.8)	4.2 (0.8)	1.6 (0.2)
Cl^- (mg/L)	253	295	229	281 (26)	283 (13)	220 (3)	281 (11)	284 (3)	219 (13)
SO_4^- (mg/L)	166	196	183	140 (9)	142 (3)	242 (10)	171 (43)	146 (3)	179 (47)
NO_3^- (mg/L)	11	15	11	6.1 (0.7)	0.8 (0.5)	17.2 (2.6)	4.4 (2.3)	1.8 (0.5)	9.7 (3.3)
HCO_3^- (mg/L)	228	247	334	230 (7)	243 (23)	408 (35)	211 (22)	222 (14)	340 (44)
Ca (mg/L)	97	107	132	105 (2)	106 (3)	180 (5)	99 (8)	99 (3)	143 (10)
K (mg/L)	27	25	25	32 (1)	30 (1)	25 (1)	35 (2)	35 (1)	21 (1)
Na (mg/L)	128	146	117	156 (9)	156 (2)	132 (2)	152 (6)	155 (3)	130 (7)
Mg (mg/L)	31	34	33	26 (1)	27 (1)	42 (1)	28 (1)	28 (1)	35 (3)
B (μg/L)	163	173	135	128 (11)	118 (13)	190 (12)	151 (20)	142 (13)	171 (18)
TCA (μg/L)	4*	4*	647	4* (0)	4* (0)	474 (271)	4* (0)	4* (0)	178 (88)
1H-benzotriazole (ng/L)	179	158	79.0	324 (96)	235 (34)	9 (4)	279 (37)	335 (99)	48 (34)
Tolyltriazole (ng/L)	501	444	223	600 (136)	377 (21)	165 (15)	576 (36)	688 (191)	295 (38)
Citalopram (ng/L)	11.1	1.6*	1.6*	13.1 (4.5)	1.6* (0)	1.6* (0)	12.5 (1.3)	1.6* (0)	1.6* (0)
Caffeine (ng/L)	329	70.6	6.1	125 (41.9)	10.2 (9.7)	2.6 (1)	100 (23.1)	3.8 (3.3)	6.6 (3.5)
Sulfamethoxazole (ng/L)	68.4	176	7.4	50.5 (8.1)	32.9 (1.6)	4.1 (0.9)	44.5 (3.6)	6.7 (1.6)	5.5 (0.9)
Benzoylecgonine (ng/L)	28.4	36.2	2.6	16.8 (3.1)	3.3 (3.1)	12* (0)	26.6 (5)	4.9 (0.8)	1.1* (0)
Ibuprofen (ng/L)	259	1.8	68.5	56.5 (20.4)	5.7 (3.6)	1.8* (0)	40.1 (14)	8.4 (12.1)	1.8* (0)
Paracetamol (ng/L)	366	8.3	1.9	109 (28)	47.7 (16.8)	1.9* (0)	33 (7.3)	29.1 (11.5)	9.7 (3.3)
Trimethoprim (ng/L)	48.8	3.3	1.3	3.3 (1.4)	1.25* (0)	1.3* (0)	5.9 (4.7)	1.25* (0)	1.2* (0)

Note: * Quantitation limit/2

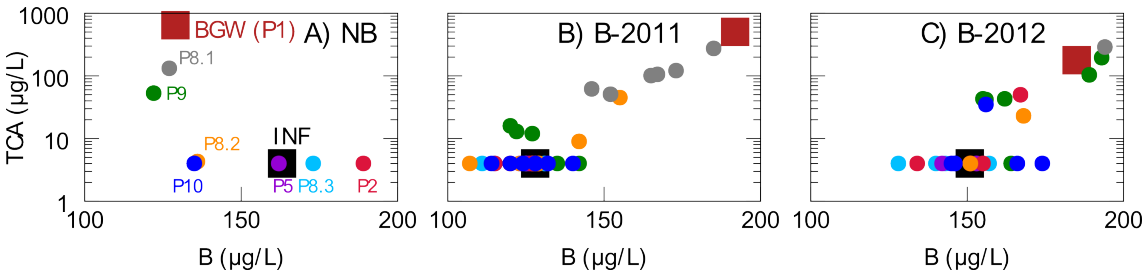

Figure 3.3: Concentrations of TCA versus boron in samples collected during the A) NB, B) B-2011, and C) B-2012 tests. Dots represent sample concentrations at monitoring wells identified in the NB graph and squares identify end-members; background-groundwater (BGW) and infiltration water (INF). Notice the log scale on the TCA axis.

3.3.2 Travel times of infiltration water

Electrical conductivity in the infiltration water was too variable for mixing analyses (Figure 3.3). Electrical conductivity, however, was recorded continuously at several points and this allowed us to estimate the travel times from the infiltration basin to the different monitoring points.

Figure 3.4 shows the evolution of EC at infiltration water (INF), background-groundwater (BGW), and monitoring points P8.3, P5, P2, P10, and P8.1 for 33 days starting in May 2012. Infiltration water EC varied sharply, while EC at P1 (background-groundwater) remained constant at around 1.8 mS/cm. Electrical conductivity of infiltration water was measured using a CTD instrument installed in a structure located in the middle of the infiltration basin. Therefore, when infiltration stopped, the EC values dropped to zero because the instrument was measuring the EC of the air. Infiltration water EC decreased from 1.8 mS/cm at t≈175 h to 0.8 mS/cm at t≈320 h, and then increased abruptly to 1.5 mS/cm in less than 20 h (Figure 3.4). The EC at monitoring points was delayed and smoother when compared to that of infiltration water. The fact that the EC at piezometers P8.3, P5, and P2 equalized the infiltration water EC strongly suggests that samples collected at these piezometers come mainly from infiltration water which is consistent with TCA observations. The delays yield approximate travel times from the infiltration basin to the piezometers.

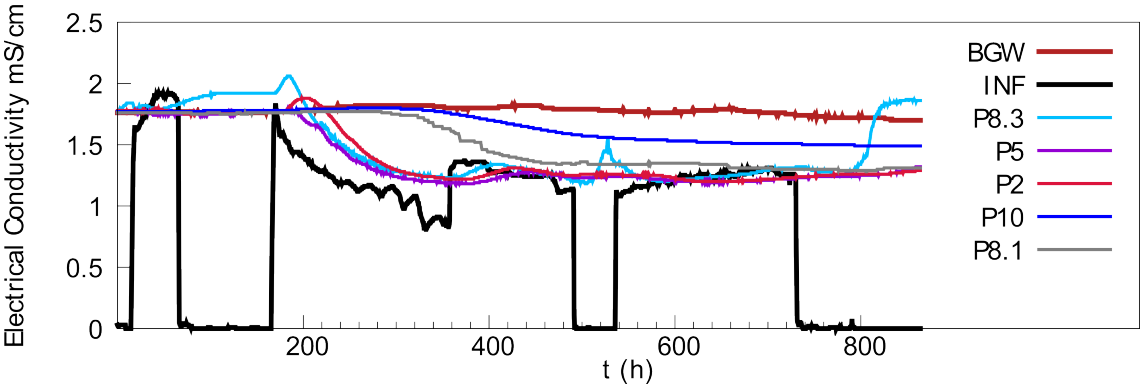

Figure 3.4: Electrical conductivity measured in the infiltration water (INF), the background-groundwater (BGW) and in the monitoring points P8.3, P5, P2, P10, and P8.1.

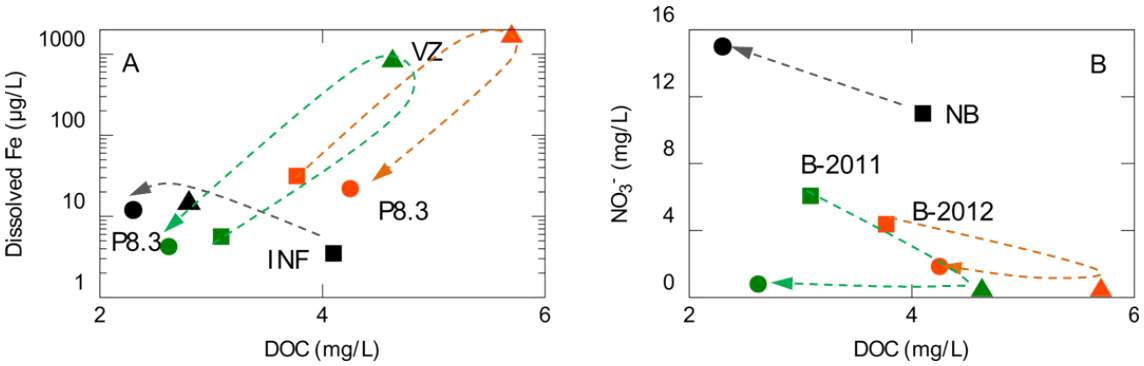

Figure 3.5: Average concentrations of dissolved Fe and NO_3^- versus DOC in infiltration water (INF, squares), vadose zone (VZ, triangles), and P8.3 (GW, dots) during NB (black), B-2011 (green), and B-2012 (orange) tests.

Travel times are expected to be inversely proportional to the infiltration rate, which did not change significantly after installation of the reactive barrier. The inflow rate was maintained at around 200 m^3/h during all three tests. This means that large differences in travel times were not expected.

3.3.3 Changes in DOC and in redox indicators after barrier installation

The evolution of DOC and redox indicators was analyzed during the three tests in order to assess the effectiveness of the barrier toward promoting variable redox conditions. Redox indicators

(dissolved Fe and NO_3^-) and DOC in infiltrating water during its passage through the vadose zone are shown in Figure 3.5. Dissolved oxygen data had to be omitted as redox indicators because they are not meaningful from suction cup samples. DOC concentrations in the infiltration water were 3 to 4 mg/L in all three tests. The DOC concentration decreased along the flow path during the NB test. By the time infiltration water reached the aquifer (P8.3), the DOC concentrations had halved. After installing the barrier (B-2011 and B-2012 tests), DOC concentrations in the vadose zone increased by 2 mg/L relative to the infiltration water. This indicates that the DOC release rate from the barrier was higher than its DOC oxidation rate. Further downstream, DOC concentrations began to decrease and, by the time the infiltration water reached P8.3, DOC concentrations were approximately 2 mg/L lower than that in the vadose zone (i. e., similar to infiltration water).

During the NB test, NO_3^- and dissolved Fe concentrations increased slightly with the decrease in DOC. The low dissolved Fe and the lack of NO_3^- depletion suggest aerobic conditions below the basin. This is consistent with the low DOC of the infiltration water (0.34 mmol/L), which is not sufficient to consume the dissolved oxygen contained in this water, assuming that weter was initially in equilibrium with the atmosphere (0.36 mmol/L). Therefore, in the hypothetical case in which the complete amount of DOC had been degraded, the only electron acceptor consumed would have been dissolved oxygen, so that no further biochemical redox reactions should be expected. In contrast, during the B-2011 and B-2012 tests, the DOC concentration in the vadose zone averaged 0.47 mmol/L. This DOC concentration, however, was not the total DOC released by the barrier, as part of it was already degraded, which can be concluded from the depletion of nitrate and the presence of Fe. After installing the barrier, the higher DOC concentrations in the vadose zone were accompanied by a two-order of magnitude increase in dissolved Fe, and the complete depletion of NO_3^-. This implies denitrification and the presence of iron-reducing conditions. Concentrations of dissolved Fe had dropped by the time the infiltration water reached the aquifer (P8.3), indicating that reduced iron must have oxidized again. The slight increase in NO_3^- suggests that part of the infiltration occurred through preferential flow, such as fingers (Figure 3.1), which have been expected because of the high permeability along the vadose zone.

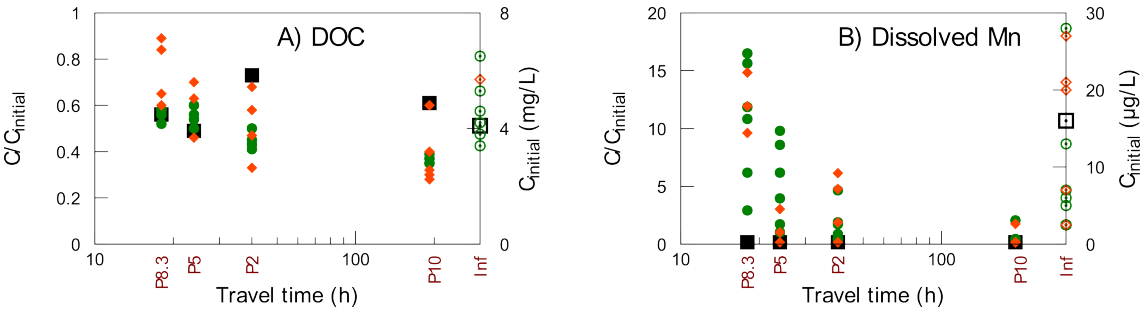

Figure 3.6: Evolution of DOC/DOC$_{initial}$ and dissolved Mn/dissolved Mn$_{initial}$ at observation points along the flow path (placed in the axis according to their travel time) during NB (black squares), B-2011 (green dots) and B-2012 (orange rhombus) tests. DOC$_{initial}$ (mg/L) and dissolved Mn$_{initial}$ (μg/L) plotted over the right axis.

Further oxidation continued in the aquifer. Figure 3.6 shows the evolution of A) DOC and B) dissolved Mn along the aquifer. Concentrations were normalized by the initial concentrations (plotted over the left axis) during each test. The initial dissolved manganese concentrations were assumed to be the average concentrations in the infiltration water for each test. As initial concentration of DOC during the NB test we adopted the concentration of the infiltration water. Because the reactive barrier released DOC, the initial DOC concentration during the B-2011 and B-2012 tests were assumed to be the average DOC concentrations at the vadose zone during each test. During the NB test, the DOC concentration decreased to half of the initial concentration after approximately 18 to 24 h travel time and no further degradation was observed, indicating that most of the degradation took place in the vadose zone and within the first few meters of the saturated zone. No dissolved Mn was detected in the groundwater samples during the NB test, indicating that Mn-reducing conditions were never reached during this test.

DOC concentrations after 18 to 24 h travel times (P8.3) were also half of the initial concentration during the B-2011. The DOC concentration decreased slightly further downstream, so that remaining DOC was 30% of the initial value for travel times close to 200 h. The DOC decrease during the B-2012 test was somewhat slower, and travel times close to 40 h were needed to attenuate the DOC to half the initial values. In all three tests, most DOC degradation occurred in the vadose zone and within the first meters of the saturated zone. Dissolved manganese val-

ues confirmed that the reactive barrier promoted manganese reduction in the vadose zone and in monitoring points located close to the infiltration basin.

DOC values in the vadose zone suggest that the amount of DOC released during B-2012 was similar to that in B-2011. According to the column experiment conducted to assess the DOC release from the barrier, we expected a DOC increase in the infiltrated water during B-2011, but not during B-2012. We attribute the continuing release of DOC to the decay of plants that grew extremely well at the infiltration basin floor, probably favored by the barrier material. As a consequence of the DOC release by the reactive barrier, variable redox conditions were achieved along the flow path during the B-2011 and B-2012 tests.

3.3.4 Changes in EOCs behavior after the barrier installation

As shown in Figure 3.7, the nine selected EOCs showed a broad range of behaviors during the three tests, from almost complete removal in all three tests (citalopram, ibuprofen and trimethoprim) to only slight removal (tolyltriazole, 1H-benzotriazole and sulfamethoxazole). Five of the EOCs showed different behavior during the three tests (ibuprofen, paracetamol, caffeine, sulfamethoxazole and benzoylecgonine) whereas four others (citalopram, 1H-benzotriazole, tolyltriazole and trimethoprim) exhibited similar behavior.

Infiltration water had the highest concentration of 1H-benzotriazole during the B-2011 test and the lowest concentration during the NB test (Figure 3.7 A). The initial concentration of 1H-benzotriazole ranged from 0.18 to 0.32 μg/L. *Liu et al.* (2013) reported a high resistance of benzotriazole to microbial degradation in microcosm experiments and observed faster biodegradation under aerobic than under anaerobic conditions (the fastest calculated half-life for this contaminant was 43 days). *Reemtsma et al.* (2010) found a correlation between 1H-benzotriazole and DOC concentrations versus travel time during bank filtration, suggesting that this compound was degraded via cometabolism. In our experimental site, 1H-benzotriazole was not completely elimi-

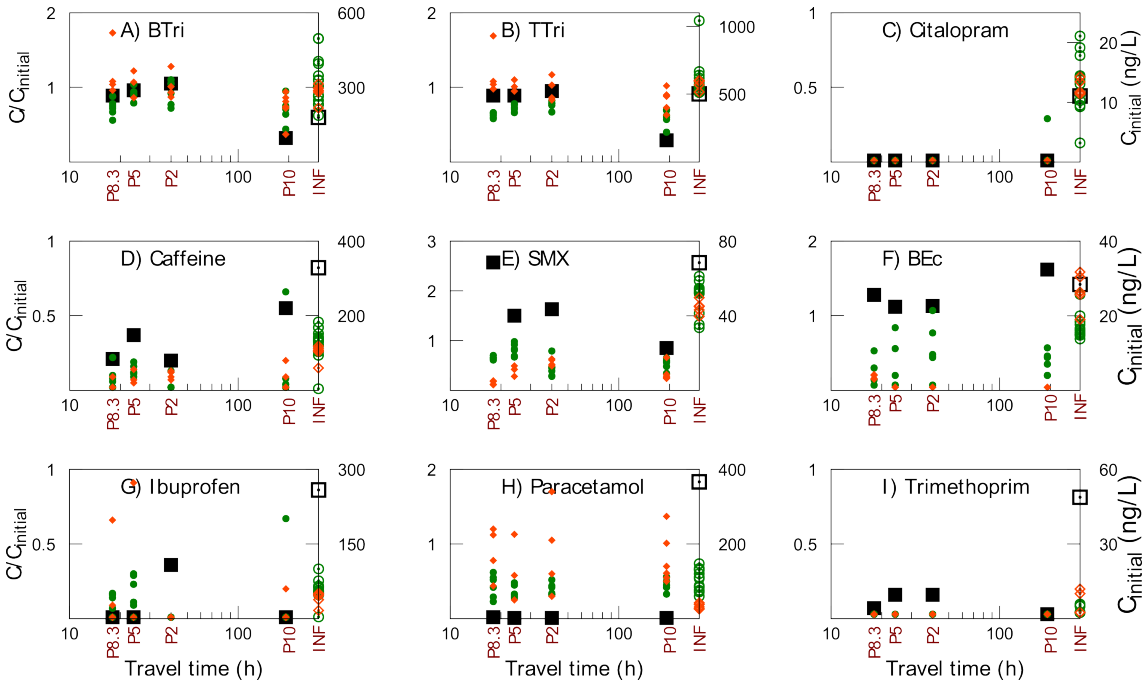

Figure 3.7: Evolution of concentration/ concentration$_{initial}$ of A) 1H-benzotriazole (BTri), B) tolyltriazole (TTri), C) citalopram, D) caffeine, E) sulfamethoxazole (SMX), F) benzoylecgonine (BEc), G) ibuprofen, H) paracetamol and I) trimethoprim versus travel times (h) during the NB (black squares), B-2011 (green dots) and B-2012 (orange rhombus) tests and EOC$_{initial}$ concentrations (ng/L) in the infiltration water plotted over the right axis.

nated. This finding is not unexpected as the longest monitored travel time (200 h) was shorter than the half-life calculated by *Liu et al.* (2013). Our results are consistent with literature observations, with some removal at the points with longest travel time, but negligible at the others, where the slight attenuation at the B-2011 and B-2012 tests may reflect improved sorption.

Tolyltriazole is a mixture of the 4- and 5- methyl isomer containing only trace amounts of the 6 and 7-methyl isomers (*Hart et al.*, 2004). The two isomers are reported to behave quite differently in the environment (*Reemtsma et al.*, 2010). The initial concentrations of tolyltriazole were quite similar during all three infiltration tests in our experiment, averaging 0.55 μg/L. During the NB test, marked removal was observed for travel times close to 200 h (P10). Similar to 1H-benzotriazole, changes in the tolyltriazole levels were very slight or nonexistent for travel times shorter than 48 h. For travel times shorter than 48 h the highest level of removal occurred during

the B-2011 test and the lowest level of removal occurred during the B-2012 test (Figure 3.7 B). The slight removal of 1H-benzotriazole and tolytriazole for travel times of 8 to 10 days is consistent with *Reemtsma et al.* (2010), who found that neither benzotriazole nor 4-tolytriazole were completely eliminated during bank filtration after travel times of 120 days under variable redox conditions.

Low concentrations of citalopram were present in the infiltration water during all three tests (Figure 3.7 C). With the exception of one sample collected at P10 during B-2011, citalopram was below quantitation limits in all samples of groundwater, suggesting efficient removal of this antidepressant for travel times shorter than 18 to 24 h, regardless of the redox condition. *Silva et al.* (2012) reported log K_{OC} of 5.63 calculated with five different soils and sediment. This high adsorption coefficient accounts for the rapid complete depletion of this compound in all of the three tests. To the best of our knowledge, this is the first report of the behavior of citalopram during artificial recharge through an infiltration basin.

Caffeine concentrations were highly variable within the three tests (Figure 3.7 D). The highest concentration of caffeine in the infiltration water was measured during the NB test: approximately double that during the B-2011 and B-2012 tests. Caffeine is known to be readily degradable in groundwater, even in fast flowing karst aquifers (*Hillebrand et al.*, 2012). Caffeine removal was high for travel times shorter than 48 h. Removal increased after installation of the reactive barrier. These findings suggest that most of the caffeine removal occurred in the vadose zone and within the first few meters of the saturated zone. *Karnjanapiboonwong et al.* (2010) reported a very low sorption of caffeine onto organic matter (log K_{OW} = -0.07). The DOC supply by the reactive barrier potentially increased the biological activity, which led to a higher removal of caffeine during the B-2011 and B-2012 tests.

Concentrations of sulfamethoxazole in the infiltration water ranged from 33 to 70 ng/L, with the highest concentrations detected during the NB test (Figure 3.7 E). Unexpectedly, higher concentrations of sulfamethoxazole were measured in the piezometers than in the infiltration water

during this test. This could be due to acetyl-sulfamethoxazole. Indeed, this compound is one of the major human metabolites of sulfamethoxazole, and can be present in waste water treatment plant effluents at concentrations similar to those of sulfamethoxazole (*Göbel et al.*, 2004). *Radke et al.* (2009) reported that acetyl-sulfamethoxazole is a potential in-stream source of sulfamethoxazole as they observed a rapid retransformation into sulfamethoxazole. We observed an improvement in the removal of sulfamethoxazole (Figure 3.7 E) during the tests performed after installation of the reactive barrier, and removal was significantly enhanced during the B-2012 test. Sulfamethoxazole concentration decreased and rebounded during the B-2011 and B-2012 tests, but not during the NB test. This rebound was also reported by *Barbieri et al.* (2012) and *Nödler et al.* (2012), who attributed it to the formation of sulfamethoxazole-nitro products in the presence of nitrite and to the return of the parent compounds when the concentration of nitrite dropped. This would be consistent with the lower concentrations of NO_3^- measured at P8.3 during the B-2011 and B-2012 tests (Figure 3.5). However, the 4-nitro-sulfamethoxazole was not detected. *Lin and Gan* (2011) and *Srinivasan et al.* (2014) found sorption of sulfamethoxazole to be negligible onto two different soils. *Srinivasan et al.* (2014), however, also reported that sorption increased with the organic carbon content of the soils. *Lin and Gan* (2011) reported half-life values of 9 to 11.4 days under aerobic conditions and 15.3 to 18.3 days under anaerobic conditions. *Mohatt et al.* (2011), however, reported that the fastest rate of sulfamethoxazole loss in soil microcosms occurred under iron-reducing conditions. They found that sulfamethoxazole concentration decreased by >95% in <1 day. We observed rapid decrease in this compound during the B-2011 and B-2012 tests in P5 and P2 (to 30% in 32 – 48 h) and then the concentration was maintained, which could be explained by faster degradation below the basin where iron-reducing conditions were achieved.

The lowest concentrations of benzoylecgonine in the infiltration water were measured during the B-2011 test, ranging from 13 to 20 ng/L (Figure 3.7 F). During the NB and the B-2012 tests the concentration of benzoylecgonine in the infiltration water ranged from 25 to 31 ng/L. No changes on the levels of this metabolite were observed during the NB test. In fact, similar to sulfamethoxazole observations, higher concentrations of benzoylecgonine were measured in the piezometers

than in the infiltration water. Benzoylecgonine conjugates are reported to (re-)transform to benzoylecgonine (*Dean et al.*, 1992). In contrast to the NB test, complete removal of benzoylecgonine occurred for travel times shorter than 48 h during the B-2012 test. Removal was also significant, though incomplete during the B-2011 test.

Input concentrations of ibuprofen were significantly higher during the NB test (258 ng/L) than during the B-2011 (average 56 ng/L) and B-2012 (average 40 ng/L) tests (Figure 3.7 G). During the NB test, concentrations of ibuprofen were below the detection limits in all samples except one, and complete removal was observed after travel times of less than 18 to 24 h. During the two tests performed after installation of the reactive barrier, travel times longer than 48 h were necessary to decrease the ibuprofen concentration below the detection limits. These results are consistent with the better removal of ibuprofen under aerobic conditions described by *Banzhaf et al.* (2012). Similarly, *Lin and Gan* (2011) reported lower half-live values of ibuprofen under aerobic conditions (10.4 – 15.2 d) than under anaerobic conditions (49.9 d) and found negligible sorption onto the two studied soils.

Paracetamol levels exhibited wide variability within the three different tests, with the highest concentration in the infiltration water during the NB test (Figure 3.7 H). Paracetamol removal was complete after 18 to 24 h of residence time during the NB test, while its complete removal was not observed during the tests performed after installation of the reactive barrier, even for travel times close to 200 h. Paracetamol removal averaged 60% during the B-2011 test, and degradation occurred during the first 18 to 24 h of travel time. No further removal was observed after 24 h. During the B-2012 test, paracetamol concentrations were more variable than in the other two tests, and here were higher concentrations in the piezometers than in the infiltration water. This is consistent with *Ranieri et al.* (2011), who reported higher removal efficiency for paracetamol in constructed wetlands under more aerobic conditions.

Trimethoprim was completely removed during all three tests (Figure 3.7 I). Removal rates were faster during the tests performed after installing the reactive barrier. During the B-2011 and

B-2012 tests, trimethoprim was completely removed after 18 to 24 h of travel times, while travel times around 200 h were required for complete removal during the NB test. *Lin and Gan* (2011) reported strong sorption of trimethoprim onto two different soils and reported log K_{OC} of 3.66. These authors reported that biodegradation occurs only under aerobic conditions with a half-life of 26 days. The rapid depletion observed during the B-2011 and B-2012 tests strongly suggests that sorption is the most probable mechanism of trimethoprim removal.

3.4 Conclusion

The reactive layer installed at the infiltration basin bottom fulfills its objective of releasing enough DOC to achieve reducing conditions below the basin. Dissolved organic carbon release has not slowed after 17 months of operations, which we attribute to the addition of organic matter from plants that grew in the basin after installation of the barrier.

The addition of the reactive barrier slowed down the removal of contaminants that are degraded under aerobic conditions (ibuprofen and paracetamol). This is not a concern, because aerobic conditions will eventually prevail in the aquifer, which ensures elimination of these. Removal rates of other EOCs were either unaffected (1H-benzotriazole and tolyltriazole) or significantly increased (sulfamethoxazole, caffeine and benzoylecgonine). Therefore, we conclude that the addition of the reactive layer improves water quality during artificial recharge operations.

Chapter 4

Tracer test modeling for characterizing heterogeneity and local scale residence time distribution in an artificial recharge site[§]

4.1 introduction

The need to satisfy the increasing demand for water is the main driver behind managed aquifer recharge, which is becoming a standard technique for replenishing and/or enhancing groundwater resources. One of the goals of managed aquifer recharge is to provide aquifers with good water quality, even when lesser quality water is used to recharge the aquifer (e.g., treatment plant effluents or runoff water).

[§]The present chapter is based on the paper Tracer test modeling for characterizing heterogeneity and local scale residence time distribution in an artificial recharge site, by Cristina Valhondo, Lurdes Martínez-Landa, Jesús Carrera, Juan J. Hidalgo, Isabel Tubau, Katrien De Pourcq, Alba Grau-Martínez , and Carlos Ayora *Hydrology and Earth System Sciences*., Doi:10.5194/hess-2016-197

Water quality is enhanced during passage through soil (*Bouwer*, 2002; *Greskowiak et al.*, 2005) because the passage causes reduction not only in turbidity and suspended matter, but also in the concentrations of dissolved organic matter (*Vanderzalm et al.*, 2006), nutrients (*Bekele et al.*, 2011), pathogens (*Dillon et al.*, 2006), and some trace organic contaminants (*Dillon et al.*, 2006; *Hoppe-Jones et al.*, 2010; *Valhondo et al.*, 2014, 2015). The appropriate management of artificial recharge systems requires an understanding of the fate of the potential contaminants. This is especially relevant for recharge through infiltration basins or river bank filtration, which typically involve larger volumes of poorer quality water than typically used for injection wells.

The fate of contaminants depends on hydraulics, which is the focus of this work, and biochemistry. Hydraulics control the residence time distribution (RTD) of the recharged water reaching pumping wells, which is required to (1) ascertain the removal of potential contaminants, (2) interpret removal observations to obtain parameters describing field reaction rates and transport, and (3) foresee (and eventually correct) future changes in groundwater quality.

Understanding hydraulics entails an understanding of the spatial and temporal distributions of water fluxes around the recharge system and the relationship between the recharge system and the aquifer (i.e., recharge affected area, mixing of recharged and native groundwater, travel times) (*Clark et al.*, 2004, 2014; *Massmann et al.*, 2008b; *Bekele et al.*, 2014). The flux distribution is affected by the complexity and heterogeneity of natural systems. Sedimentary deposits frequently consist of layers with varying grain size distributions that may cause the aquifer to behave locally as a multilayer system, where the actual flux distribution is not controlled as much by the hydraulic conductivity within the layers as by their continuity and inter-connectivity, particularly in the vertical dimension (*Fogg*, 1986; *Martin and Frind*, 1998). Characterizing heterogeneity in such systems at the recharge basin scale is required for proper representation of RTDs because heterogeneity causes uncertainty (*Park et al.*, 2006) and promotes a broad range of residence time distributions (*Tompson et al.*, 1999). But it is hard because the head differences are small and detailed hydraulic testing difficult to perform. Even when sophisticated characterization techniques

(e.g., direct push, *Butler et al.* (2002); *Dietrich et al.* (2008)) are adopted, it is unfeasible to characterize the small scale variations of hydraulic properties.

A reasonable and easy way to address heterogeneity and RTDs is to perform tracer tests. Ironically, few tracer tests have been performed in the context of artificial recharge. Notable exceptions are the studies in Berlin, Germany (*Massmann et al.*, 2008b), which were restricted to environmental tracers due to the proximity to the water supply, and California (*Clark et al.*, 2004; *Becker et al.*, 2014), which used environmental and deliberate (SF_6) tracers. In both cases, the goal was to monitor the recharge water plume. Both studies found a strong variation of groundwater age with depth. To the best of our knowledge, however, no test has been performed for site scale characterization. To this end, we performed a pulse injection test at the Sant Vicenç site (Barcelona, Spain) (*Valhondo et al.*, 2014, 2015) to obtain the RTDs by monitoring breakthrough curves.

The objective of this paper is to describe the tracer test and its interpretation using both heterogeneous and homogeneous models to assess the need for model complexity, which may be required to reproduce RTDs and thus, mixing, spreading and water quality improvement during artificial recharge.

4.2 Materials and methods

4.2.1 Site description and instrumentation

The work was performed at the recharge basin owned by the Catalan Water Agency, located at Sant Vicenç dels Horts, approximately 15 km inland from the Mediterranean shore (Fig. 5.1 A) along the Llobregat Lower Valley aquifer (Barcelona, Spain). Recharge water is taken from the Llobregat River, which is impacted by numerous treatment plant effluents (*Köck-Schulmeyer et al.*, 2011). River water was diverted to a settlement basin ($\approx 5000\,m^2$), where it remained for 2 to 4

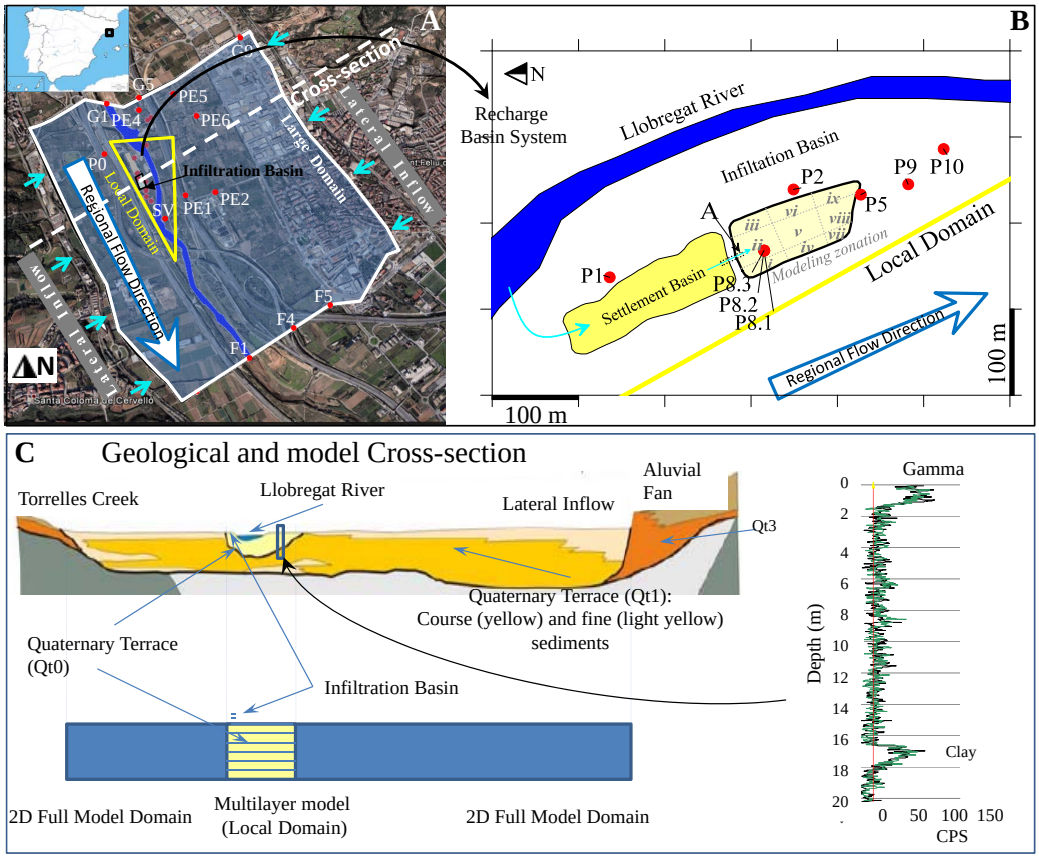

Figure 4.1: General (A) and local (B) plan views of the infiltration system, monitoring points, and model dimensions. (C) Geologic cross-section of the site and the conceptualization used in the numerical model, and natural gamma measurements from the site. The area identified with the yellow triangle in A was modeled as a multilayer aquifer (see C).

days. Thereafter, the water flowed to the infiltration basin ($\approx 5000\,m^2$), Fig. 5.1 B. A flowmeter (Teledyne Isco Inc, Lincoln, Nebraska, United States) installed in the pipe connecting the two basins recorded hourly the flow rate to the infiltration basin. The infiltration rate averaged 1 m/d. The system has been operational since February 2009.

A 65 cm-thick reactive barrier was installed at the bottom of the infiltration basin in March 2011. The barrier comprises vegetable compost and aquifer sand in equal volumetric proportions and a very small fraction of clay and iron oxides. The vegetable compost aimed to release dissolved organic carbon into the infiltrating water to favor a broad range of redox conditions below

the basin, thus increasing the diversity of microbial metabolic paths to enhance removal of organic contaminants (*Li et al.*, 2013; *Alidina et al.*, 2014b; *Valhondo et al.*, 2014, 2015). Clay and iron oxide were added to provide sorption sites for cationic and anionic organic compounds, respectively. Details on the barrier are provided by *Valhondo et al.* (2014, 2015).

The aquifer beneath the basin comprises Quaternary alluvial sediments with a predominant portion of gravel and sand, and a small fraction of clay (*Barbieri et al.*, 2011). The aquifer extends to a depth of 20 to 23 m below the ground at the site and is underlain by Pliocene marls that are assumed impervious. The saturated thickness during 2010–2014 ranged from 12 to 14 m. The groundwater flows from NNW to SSE with a natural gradient of 2.3‰ (*Iribar et al.*, 1997). Fig. 5.1 C shows a simplified cross-section of the site. The Llobregat River deposits are intertwined with colluvial deposits from lateral alluvial fans of local creeks, forming complex alternating layers of different compositions. The varying fractions of gravel, sand, and clay causes a significant heterogeneity in the vertical dimension (*Gámez et al.*, 2009). This layering was represented in the numerical model as a multilayered local domain.

Eight piezometers were used for monitoring (Fig. 5.1). Piezometer P1, located upstream from the infiltration basin, monitored the background regional groundwater flowing under the basin. Piezometers P8.3, P8.2, and P8.1, located in the middle of the infiltration basin at depths of 7 to 9 m, 10 to 12 m and 13 to 15 m, (below the infiltration basin surface) respectively monitored the depth-related changes of the recharged water. Piezometers P2, P5, P9, and P10, fully screened and located downstream along the flow path at increasing distances from the infiltration basin, monitored the recharged water at increasing travel times. Most of the piezometers were equipped with CTD-Diver (Schlumberger water services, Delft, The Netherlands) sensors for continuous recording of electrical conductivity (EC), temperature, and water level (as pressure). The CTD-Divers were installed prior to artificial recharge. An additional CTD-Diver was placed in the middle of the infiltration basin (beside P8 nest) to measure EC, temperature, and level of the infiltration water. Samples from monitoring points and infiltration basin were collected for analysis

during several campaigns (*Valhondo et al.*, 2014, 2015).

4.2.2 Tracer test

A natural flow tracer test experiment was performed between 9 July and 14 September, 2012. Amino-G acid was selected as the tracer because it can be detected at very low concentrations, is stable in the experimental pH range (*Flury and Wai*, 2003), and has relatively low sorption onto organic matter and clay (*Trudgill*, 1987; *Smart and Smith*, 1976). It is, however, photo-degradable.

The recharge system was operating for three weeks before adding the tracer, while trying to maintain a 1 m column in the infiltration basin to sustain steady-state flow. On 9 July, "day 0", 8 kg of amino-G acid diluted in 0.9 m^3 of water from the settlement basin was poured into the entrance of the infiltration basin over approximately 15 minutes (point A in Fig. 5.1B) in the late afternoon to minimize photo-degradation. Breakthrough curves were measured in situ with 3 portable GGUN-FL fluorometers (Albillia Co, Neuchâtel, Switzerland) at six downstream monitoring points (P8.3, P2, P5, P8.1, P9, and P10) (Fig 5.1B). The fluorometers were calibrated with serial dilutions (1, 10, and 100 μg/L) prepared with the tracer and water from the settlement basin. Three fluorometers were initially installed at the monitoring points with the shortest expected travel times (P8.3, P2, and P5) and programmed to record a measurement every 5 minutes. Mean travel times were obtained from the EC recordings. Once the bulk of the breakthrough curves had been recorded at these three points, the fluorometers were moved to the monitoring points with longer travel times (P9, P10, and P8.1). Thus, one fluorometer was moved from P8.3 to P8.1 at midnight on 13 July, and the others were moved from P2 to P10 and P5 to P9 at 17:20 on 15 July. The recording interval was changed to 15 minutes on 25 July and maintained until the end of the test on 14 September.

4.2.3 Model construction

An integrated regional hydrogeologic model had been built to improve the management of water resources (*Iribar et al.*, 1997; *Abarca et al.*, 2006). The artificial recharge system is nested within the regional model domain. Therefore, to study the aquifer behavior in the proximity of the artificial recharge system, we created a flow and transport model based on the regional one and refined the local scale detail with information from the recharge system.

Boundary conditions and model parameterization

The model structure was defined to accommodate two requirements: (1) the need to account for layering at the local scale and (2) the need to seek appropriate boundary conditions controlling the flow field. The latter was met by choosing a (large scale) model domain bound along the flow direction by two lines of frequently measured piezometers (G1-G5-G9 and F1-F4-F5 in Fig. 5.1 B), ≈3 km away, which were used to prescribe heads at the northern and southern boundaries. The width of the model (≈ 2.5 km) was established by the fluvial deposits (brown color in Fig. 5.1 C). Inflows from the eastern and western local creeks were prescribed using time dependent inflows of the regional model updated with recent weather data. Time dependent pumping rates were prescribed on the drinking water wells with radial galleries (PE1, PE2, PE4, PE5, and PE6 in Fig. 5.1 A) using data from the water utility (AGBAR). Areal recharge was prescribed by updating the regional model time functions for recharge in urban, rural, and irrigated areas. Infiltration from the river bed is small because the Llobregat River is disconnected from the aquifer most of the time (*Vázquez-Suñé et al.*, 2006) and aquifer heads remained below the river bed elevation throughout the model period. River infiltration was taken from the regional model.

The multilayer nature of the system was modeled explicitly only in the area adjacent to the infiltration basin (local domain ≈0.5 x 1.5 km^2, yellow triangle in Fig. 5.1 A), where a high level of detail was needed. The rest (large domain) was modeled as two-dimensional using linear

triangular elements. Therefore, the 14 m-thick aquifer was divided into seven 2 m-thick layers in the local scale domain to emulate the material differences of the alluvial deposits. Two additional 0.3 m-thick layers were implemented in the infiltration basin surface to represent retention time at the reactive barrier. The nine layers (Ly1 to Ly9 starting from the bottom) that overlapped in the local domain were linked by one-dimensional elements. The number of layers was chosen to obtain a sufficient precision in the vertical discretization while maintaining a reasonable numerical burden. Each layer was homogeneous in the horizontal direction, which is a simplification. The local and larger domains are fully coupled and were solved together in every model run. The element size increased from 5 m at the infiltration basin to ≈185 m at the edges of the model.

The calibration and modeling strategy consisted of three steps. First, starting from the parameterization of the regional model by Abarca et al. (2006), we used updated meteorological and piezometric head data. The large scale domain was re-calibrated using the newly collected four years head data and the original transmissivity values as prior estimates. Second, we calibrate the porosity and hydraulic conductivities of the local scale domain, and the preferential flow through the reactive barrier using the piezometric heads and amino-G acid concentrations measured during the tracer test. We performed the calibration under homogeneous and heterogeneous scenarios. Dispersivity was kept constant at 50 m in the large scale domain and 5 m (longitudinal) and 1.3 m (transverse) in the local scale domain. Third, we validate the model by reproducing observed values of 1,1,2-trichloroethane (TCA) and EC collected under different flow conditions from those used for the calibration.

The model was built using the inversion capabilities of Transdens (*Medina and Carrera*, 1996, 2003; *Hidalgo et al.*, 2004), a code that solves linear flow and transport equations for porous media, using the finite elements method in space and a weighted finite difference scheme in time, and that allows automatically estimate aquifer parameters.

Estimation of flow parameters at the large scale domain

Hydraulic parameters (hydraulic conductivity and storativity) of the local and large domain models were calibrated against the head data at the piezometers shown in Fig. 5.1 from January 2010 through December 2013. Several infiltration episodes took place during these four years, which were discretized into daily time steps. Prior estimates of model parameters were obtained from the regional flow model (*Abarca et al.*, 2006) and completed with local tests (a pumping test and a convergent flow tracer test).

Tracer test and local scale parameters

The estimated flow parameters in the large scale model were used to calibrate transport parameters and recalibrate flow parameters at the local scale domain against the heads and concentrations recorded during the tracer test (from 9 July to 14 September 2012).

A 15 min wide tracer input was added to the inflow at the start of the test. The tracer was poured at the entrance of the infiltration basin (point A in Fig. 5.1 B) and afterwards clean water continued to flow to the basin. Thus, the tracer was not homogeneously diluted in the whole basin water volume. In fact, the maximum concentration measured at P8.3 was 2.75 times higher than the concentration assuming complete dilution of the tracer in the basin volume (1.6 mg/l). Such behavior probably reflects preferential flow through the high permeability sandy sediments below the reactive barrier as well as basin scale variability, which together with the potential photodegradation of the amino-G caused the expected distribution of the amino-G concentration to decrease from north to south in the basin. To address this issue, we divided the basin into nine zones (zones i through ix in Fig. 5.1 B) and estimated the concentration of the tracer at each zone as a multiple of the amino-G acid concentration function. The effect of preferential flow, which was also apparent from the redox sensitive species (*Valhondo et al.*, 2014, 2015), was modeled by distributing the time dependent measured inflow data between the surface of the infiltration basin

in Ly9 and Ly7. Infiltration creates a downwards flux of water. Therefore, samples from the four fully penetrating piezometers should be representative of the highest permeability layer intersected by each piezometer. Since these may vary among piezometers (model layers should be understand as a conceptual abstraction), we did a preliminary screening to find which layer reproduced best observed concentrations in each piezometer.

The time discretization was quite irregular, with the shortest time steps (5 minutes) between the tracer discharge and the arrival of the breakthrough curve at P8.3 and the longest steps (3 days) at the end of the test. The standard deviation assigned to all concentration measurements at each observation point was 1% of the maximum concentration at each point, to ensure that a comparable weight was given to each point during calibration (maximum concentration varied by $\approx$2 orders of magnitude).

The calibration yielded three models: a homogeneous one ("Hom"), where K_x and K_z were constant throughout the model domain, and two heterogeneous ones ("Het-1" and "Het-2") with different hydraulic conductivities for each layer. These last two models represented two different convergence points of the calibration process and both were used to highlight the non-uniqueness of the solution and to assess uncertainty.

4.2.4 Validation

The heterogeneous models have got many degrees of freedom and risk overparameterization. This together with the inherent simplifications of the model might introduce calibration artifacts. We simulated the evolution of TCA and EC during periods of time much longer than those used for calibration to test the validity of the three models. TCA was measured sporadically in both recharge water and piezometers. We found that it was only present in native groundwater. Therefore, it could be used to test how natural groundwater recovered after infiltration periods. TCA simulations covered eight months (from April 2011 to December 2011). Initial concentration and

lateral inflows of TCA concentrations were fixed as the maximum concentration observed at P1 (upstream of the infiltration basin). Artificial recharge concentration was zero. The EC simulations covered four years (2010–2013) when heads fluctuated significantly (Fig. 4.2). Therefore, TCA and EC test the model behavior under different flow conditions. Initial and lateral inflows of EC were fixed at 1200 μS/cm, the mean measured during the period. Recharge water EC was prescribed using a time function based on the measured EC. Both TCA and EC concentrations in the northern border of the local domain were prescribed to be equal to those measured at P1, but shifted in time for the mean travel time from the northern border to P1. Further details on the model structure and reasons behind simplifications can be found in the responses to comments by the reviewers (*Clark*, 2016; *Walther*, 2016; *Anonymous*, 2016; *Valhondo et al.*, 2016a,b).

4.3 Results and discussion

4.3.1 Flow model

Artificial recharge creates a smooth dome below the infiltration basin and modifies the piezometric surface (Fig. 4.2). Figure 4.2 displays head fits at five monitoring piezometers located within the local domain. The fit was good (mean weighted residual of -0.02 ± 0.57 for head observations), which suggests that the size of the multilayer local domain was sufficient to reproduce head variations at the monitoring piezometers close to the basin where the gradient is mainly vertical ($\approx 10\%$) due to the influence of the artificial recharge. The model also reproduces measurements at extraction wells outside of the multilayer local domain (e.g. PE-1 in Fig. 4.2), suggesting that the two-dimensional model was sufficient to create the appropriate head frame for simulating transport.

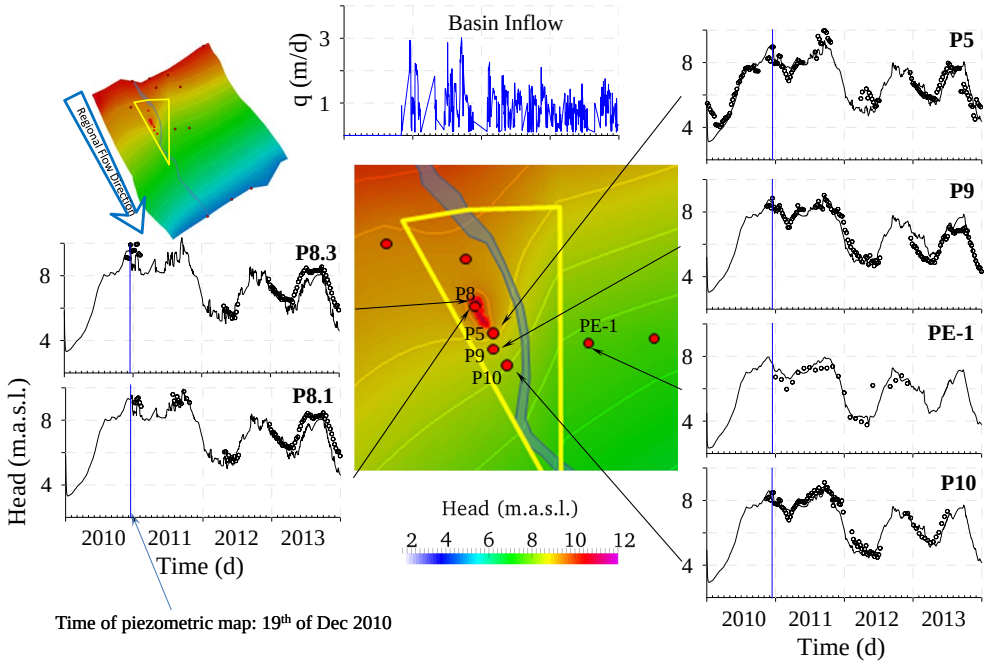

Figure 4.2: Calculated head level surface on 19 of December 2010, when the system was working, and measured (circles) and calculated (line) heads (m.a.s.l.) vs. time (m) at five monitoring piezometers (P8.3, P8.1, P5, P9, and P10) and one extraction well (PE-1).

4.3.2 Tracer test model

Conservative transport parameters were estimated for the nine layers of the local and basin domains using the amino-G acid tracer test data. Flow parameters of the nine layers and the one-dimensional elements linking them were also re-calibrated because concentrations were more sensitive to vertical layering than heads, which are often only mildly sensitive to the degree of hydraulic connection (*Fogg*, 1986). Three sets of parameters (Het-1, Het-2, and Hom) were obtained. Estimated parameters fit, measured by the root mean square-weighted error with prior estimates (RMSWE), and amino-G input mass for these three outcomes are shown in Table 4.1.

Measured and calculated breakthrough curves at monitoring piezometers are displayed in Fig. 4.3, which provides room for some insights. Monitoring piezometers P8.3, P2, and P5 displayed

Table 4.1: Parameters (Hydraulic conductivity, K (m/d), and porosity, ϕ), RMSWE, and input mass in outcomes Het-1, Het-2, and Hom, after calibration.

		K (m/d)			ϕ		
		Het-1	Het-2	Hom	Het-1	Het-2	Hom
Basin Domain (50 x 100 m)	Ly 9 (K_h)	1	1	1.4	0.5	0.5	0.5
	Ly 9 (K_z)	5.0	5.0	3.0	0.0001	0.002	0.0001
	Ly 8 (K_h)	1	1	1.4	0.5	0.5	0.5
Local Domain (1000 x 500 m)	Ly 8 (K_z)	5.0	5.0	3.0	0.0001	0.002	0.0001
	Ly 7 (K_h)	0.2	0.2	1.4	0.17	0.13	0.2
	Ly 7 (K_z)	2.4	3.4	3.0	0.0001	0.01	0.0001
	Ly 6 (K_h)	139.1	158.2	289.9	0.17	0.17	0.2
	Ly 6 (K_z)	2.4	3.4	3.0	0.0001	0.01	0.0001
	Ly 5 (K_h)	1042.1	1187.3	289.9	0.18	0.17	0.2
	Ly 5 (K_z)	93.5	190.5	3.0	0.0001	0.01	0.0001
	Ly 4 (K_h)	203.4	253.9	289.9	0.16	0.20	0.2
	Ly 4 (K_z)	42	210.7	3.0	0.0001	0.01	0.0001
	Ly 3 (K_h)	330.9	479.0	289.9	0.27	0.33	0.2
	Ly 3 (K_z)	0.2	0.2	3.0	0.0001	0.01	0.0001
	Ly 2 (K_h)	131.1	75.5	289.9	0.25	0.22	0.2
	Ly 2 (K_z)	2.1	29.1	3.0	0.0001	0.01	0.0001
	Ly 1 (K_h)	162.3	478.2	289.9	0.10	0.20	0.2
Model Fit (RMSWE)		1979	2000	9358			
Input Mass (g)		6683	6853	7885			

fast responses with maximum concentrations higher than those of piezometers P8.1, P9, and P10, in which dispersion and mixing generated longer tails. The monitoring point P8.3, located below the basin, was the first monitoring point reached by the tracer, and showed the highest observed maximum concentration, more than an order of magnitude higher than the next monitoring point P2. We assume that the early arrival at P8.3 occurred through preferential flow paths. The breakthrough curve at this point was very narrow, as the follow-up water without tracer reached this point equally fast. First arrival at P2 and P5 (1 day) was much faster than at P8.1 (3 days), only 6 m below the phreatic surface, despite the fact that vertical gradient ($\approx$ 10%) was much larger than the horizontal gradient (less than 4%). This observation implies that recharged water spreads laterally faster than vertically and confirms the importance of layering.

Breakthrough curves at P10, P8.1, and P.9 exhibited longer tails than those at P8.3, P2, and P5. The short tails were consistent with the fast arrival. The long tails might suggest the impact of heterogeneity (dispersion) and mixing away from the entrance. The fact that the homogeneous

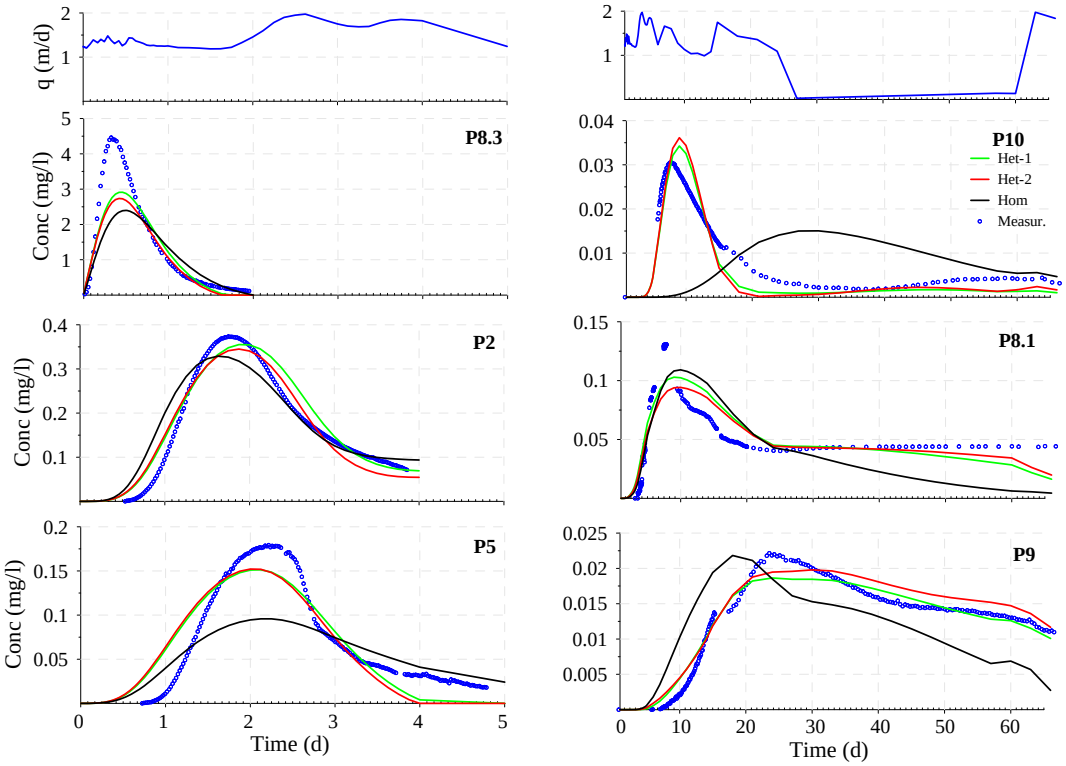

Figure 4.3: Top row, inflow rate to the infiltration basin and lower three rows measured (blue circles) and calculated breakthrough curves from the piezometers monitoring the amino-G acid concentration (mg/l) vs. time (d) using the estimated set of parameters of Het-1 (green line), Het-2 (red line), and Hom (black line). The left row displays only the first five days of the experiment. Note that the vertical scale is different for each monitoring point.

model reproduced tailing quite well (at least for P8.1 and P9), however, implies that broad RTDs are caused not only by heterogeneity but also by the mean flow structure. The "shower" effect of recharge ensures that water flowing initially upstream or falling on the dome top will eventually mix with recently recharged water further downstream. This effect is illustrated by the spatial distribution of the concentration shown in Fig. 4.4.

Several features are apparent from the spatial distribution of the concentrations. First, the distribution was balloon-like. The tracer was distributed along an outer crust that grew by filling with the tracer-less water that kept entering through the basin. Second, the portion of tracer that flowed upstream initially was eventually transported downstream through lateral and downwards flow

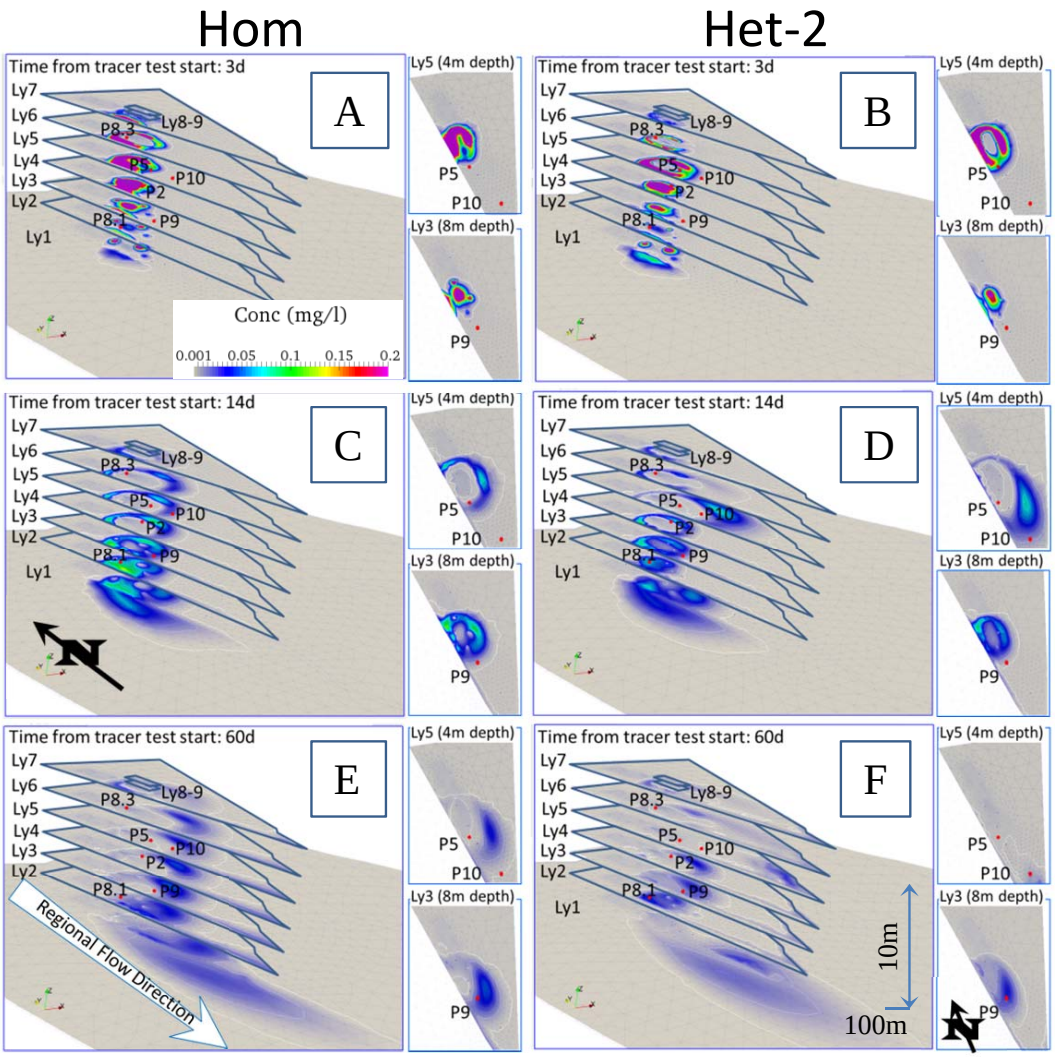

Figure 4.4: Distribution of amino-G acid concentration at three time points (3 d, 14 d, and 60 d) since the test started, calculated with the Hom (A, C, and E) and Het-2 (B, D, and F) models. The concentrations in layers 3 and 5 are shown from below on the side of each frame. Note that the vertical scale is 100 times the horizontal scale.

paths. This promoted shear and lateral mixing. Third, heterogeneous models provided another shear mechanism (Fig. 4.4 B, D and F) by the fluctuations in horizontal hydraulic conductivity (K_x) among the different layers. Note that the plume in layer 5 traveled much faster than in the remaining layers, to the point that it had virtually disappeared from the local domain after 60 days. The plume also almost disappeared in Layers 6 and 7, but in this case the disappearance reflected

vertical, rather than horizontal, displacement.

We contend that these shear mechanisms promoted mixing and that they were more marked in the heterogeneous models than in the homogeneous model. In fact, this observation was confirmed by the plumes shown in Fig. 4.4. Those of the heterogeneous models were much more diluted than those of the homogeneous model.

This kind of shear and mixing promoted broad RTDs and caused recently recharged water (possibly aerobic and loaded with dissolved organic carbon) to mix with more than 60 days old water (possibly anaerobic and depleted of dissolved organic carbon) at monitoring points P8.1, P9, and P10. Such mixing contributes to favoring the presence of a primary substrate to be metabolized by microorganisms, which increases the biotransformation of emerging contaminants, by co-metabolism. It may also explain, at least in part, the excellent performance of the system in eliminating a broad range of emerging contaminants (*Valhondo et al.*, 2014, 2015).

Mixing at the edges of the local domain is unrealistic. As shown in Fig. 5.1, only the local domain was treated as a multilayer. The rest was treated as two-dimensional. This implies that, as the plume left this domain, the outflow of all the layers was mixed. This causes the plume that departs from the western edge of the local domain (plotted as Ly1 in Fig. 4.4) to be artificially smoothed. Whereas this mixing was an artifact of the model structure, it does not affect the computed breakthrough curves because all observation points belong to the local domain.

A final remark on the validity of the models can be drawn from the fact that monitoring point P10 was further away from the basin than monitoring point P9. Nevertheless, P10 was reached by the tracer faster than P9. Breakthrough curves of P10 and P5 were poorly reproduced under the homogeneous medium hypothesis. Both heterogeneous models, Het-1 and Het-2, reproduced the measured concentrations with better accuracy than Hom. The RMSWE values were 1979 and 2000 for Het-1 and Het-2, respectively, and 9358 for Hom. The main difference between Het-1 and Het-2 was the distribution of conductivity and porosity, because the aquifer transmissivity

in the local domain was ultimately the same. Model Het-2 was more consistent with the field observations regarding the materials distribution (Fig. 5.1 C) than model Het-1.

These observations suggest that the Het models were better than the Hom model. But they may be overparameterized (*Poeter and Hill*, 1997; *Carrera et al.*, 2005). It is clear that the heterogeneity assumption is required to reproduce geologic observations, which is valuable information in itself (*D'Agnese et al.*, 1999), and to model mixing (*Le Borgne et al.*, 2010). It is also clear, however, that parameterizing heterogeneity causes non-uniqueness. In fact, the fast arrival at P10, which we reproduced by the high hydraulic conductivity in layer 5, might reflect other causes (e.g., a high-permeability paleochannel within layer 5). Therefore, it would be fair to question the validity of explicitly modeling heterogeneity. We address this question below.

4.3.3 TCA and EC validation

The validity of the models calibrated with the tracer test, as discussed in section 3.2 above, was tested against measurements of TCA and EC. Modeling these simply required changing initial and boundary concentrations (see section 2.4).

Figure 4.5 displays the changes in the measured and calculated concentrations of TCA (μg/L) at the monitoring piezometers. Measured TCA concentrations approached the background concentration of the aquifer (some hundreds of μg/L but varying) when the artificial recharge system was not operating. Concentrations of TCA decreased and fell below the detection limits at most monitoring points when the recharge with TCA-free water was activated. These trends were generally reproduced by the three models and confirmed that the observation points sampled recharge water. The models were far slower in reacting to changes in recharge rate, however, than the actual observations. In particular, they were too slow to reproduce the TCA concentration rebound after the recharge stopped in Nov-Dec. Still, with the exception of P8.3 and P8.1, heterogeneous models dis a better job than the homogeneous one, and Het-2 performed slightly better than Het-1.

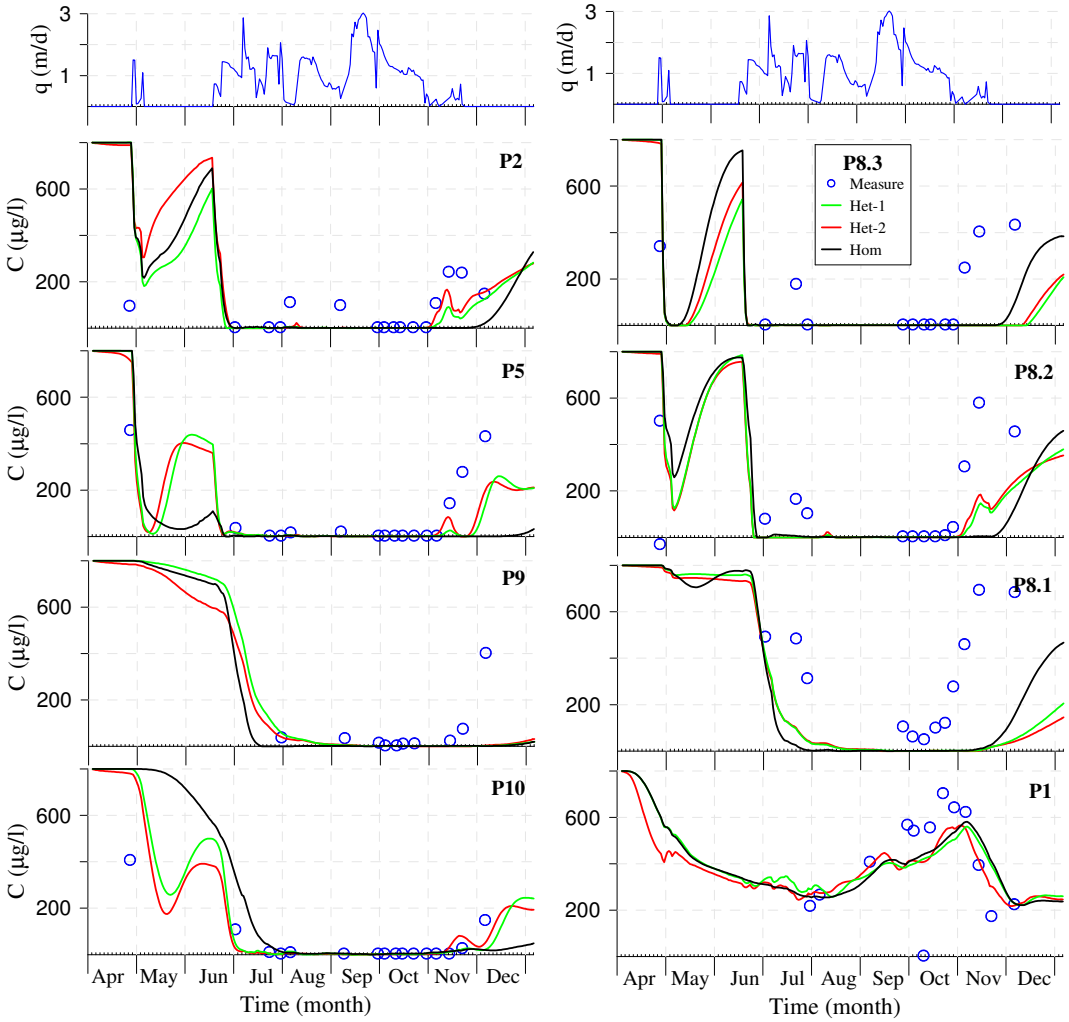

Figure 4.5: Measured (dark blue circles) and calculated TCA concentration (μg/l) changes over time at monitoring piezometers for the Het-1 (green line), Het-2 (red line) and Hom (black line) models. The infiltration rate is also shown (top).

Figure 4.6 displays the changes in measured and calculated EC (μS/cm) during two years. The three models reproduced the observations quite accurately, except during the low recharge period at the end of 2012 and the beginning of 2013. Measured EC at P2, P5, and P10 during this period fell below both the recharge water EC (similar to that of P8.3) and aquifer water EC (similar to P1). Therefore, the error must be attributed to some unaccounted inflow of low EC water rather than to poor model structure.

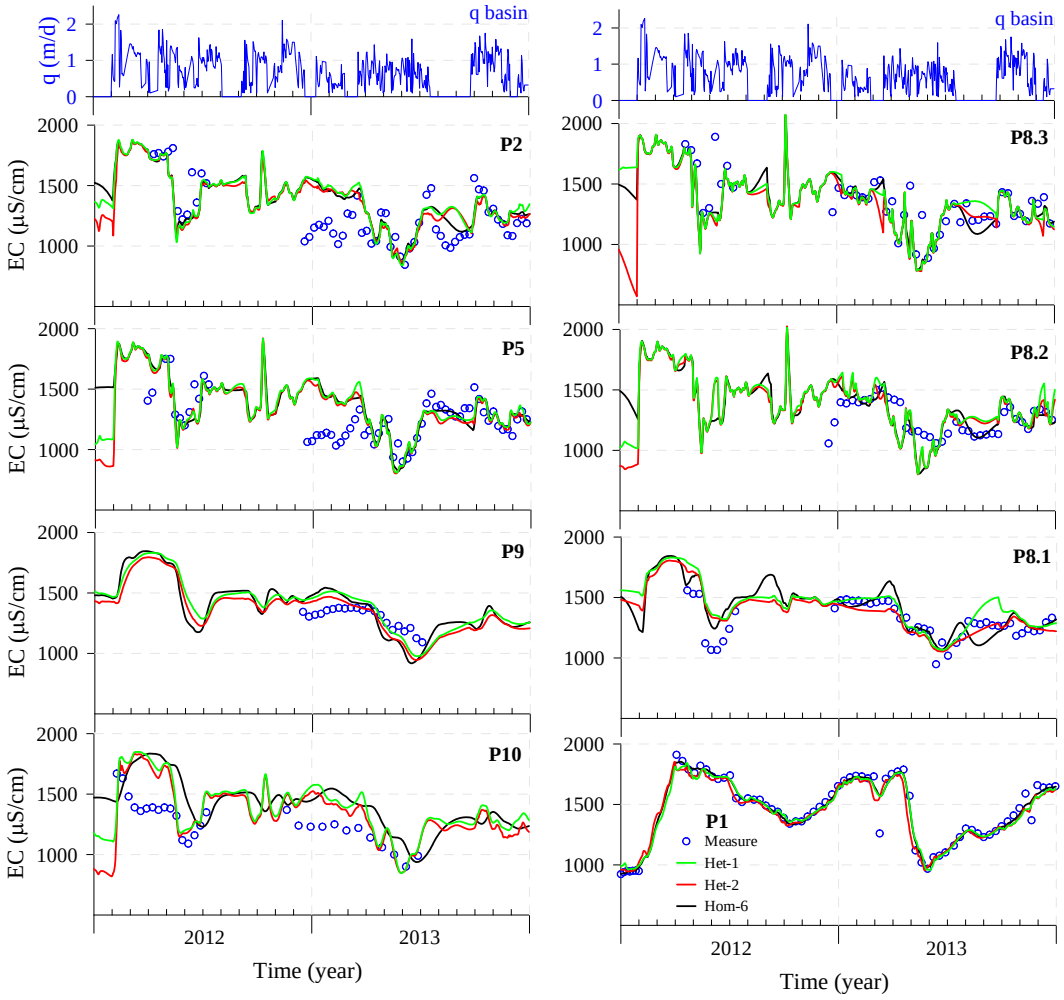

Figure 4.6: Changes in measured (dark blue circles) and calculated EC (μS/cm) at monitoring piezometers for the Het-1 (green line), Het-2 (red line) and Hom (black line) models. The infiltration rate is also shown (top).

In summary, the three models reproduced quite well the change in TCA, which was present in the aquifer but not in the recharge water, and EC, which fluctuates in both. On the one hand, this implies that the velocity field, imposed by recharge and natural aquifer flow, was not overly sensitive to local hydraulic conductivities. On the other hand, it implies that it would be difficult to accurately estimate the layering structure solely based on the concentration breakthrough curves. In fact, the RMSWE for EC with the Hom model (4629) was slightly smaller than that for the Het-1 and Het-2 models (4682 and 4689, respectively), which suggests that the Hom model, having

less uncertain parameters, was more robust than the Het models, at least for EC.

One might be tempted to use multicontinua models (*Haggerty and Gorelick*, 1995), which reproduce the effect of heterogeneity (*Silva et al.*, 2009; *Dentz et al.*, 2011). In fact, such models would probably capture the fast rebound of the TCA concentration when the recharge stopped, as observed in Fig. 4.5. In view of the calibration non-uniqueness of these models, however, would probably worsen identifiability.

4.4 conclusions

This work provides useful insight on both tracer testing for characterization of artificial recharge and on transport modeling.

The tracer test was successful in identifying RTDs at a number of piezometers. These distributions were quite narrow at points immediately adjacent to the basin (P8.3, P2, P5) but were very broad (more than 60 days) at points slightly further away (P8.1, P9, P10). Broad RTDs imply significant mixing of recently recharged water with water recharged some time before. Such mixing, together with the conditions imposed by the reactive layer, promote diverse metabolic paths and helps to explain the effective removal of a wide range of emerging contaminants at this site (*Valhondo et al.*, 2014, 2015).

The model suggests that the broad RTDs are the result of both the flow structure, which is complex, and heterogeneity. Recharged water flows initially upstream and then laterally around and below recently recharged water. This complexity stretches flow tubes and favors mixing (*Dentz et al.*, 2011). This effect is enhanced by temporal fluctuations in recharge and was observed in both the homogeneous and heterogeneous models. Further shear, stretching, and mixing was caused by the variability in the hydraulic conductivity among layers.

Regarding transport modeling, it is clear that the collected breakthrough curves were not suf-

ficient to identify the hydraulic conductivities of the modeled layers or, even less, more complex heterogeneous structures. In fact the simple homogeneous model, which did not perform as well as the two heterogeneous models during the tracer test calibration, yielded similar (if not better) blind predictions of EC under varying flow conditions, and only slightly poorer for TCA.

The introduction of heterogeneity is justified not by the quantitative head or concentration data, but by geologic understanding. Ultimately, the actual RTDs that are required for proper interpretation of pollutant removal, were well reproduced by the heterogeneous models. Therefore, these models should be used for interpreting and predicting the fate of recharge water. Yet, given the importance of artificial recharge and that its clean-up potential can be enhanced by time fluctuations of recharge rate (*de Dreuzy et al.*, 2012), much can be gained by the detailed characterization of recharge sites. To this end, tracer tests are useful, but insufficient. They must be complemented with cross-hole inter-layer testing and other techniques (e.g., geophysics, direct-push tests).

Chapter 5

Evaluation of processes for removing emerging organic compounds during artificial recharge through a reactive barrier[¶]

5.1 Introduction

Artificial recharge of water that is directly or indirectly affected by wastewater effluents is an option for improving the quantitative and qualitative state of groundwater bodies and associated surface water bodies. This option, however, may be limited by the presence of emerging organic compounds (EOCs), which are typically constituents of these effluents, and are detected in the groundwater, surface water, and even drinking water (*Schwarzenbach et al.*, 2006). EOCs, such as

[¶]The present chapter is based on the paper Evaluation of processes for removing emerging organic compounds during artificial recharge through a reactive barrier, by Cristina Valhondo, Lurdes Martínez-Landa, Jesús Carrera, Carlos Ayora, Karsten Nödler, and Tobias Licha. *Submited to Water Research*

pharmaceutical residues, personal care products, and industrial chemicals, are biologically active, but remain unregulated, which has raised concern. Many EOCs are not eliminated by conventional treatment plants, which were not designed to remove them (*Chefetz et al.*, 2008). These contaminants may reach the aquatic environment through treatment plant effluents and, infiltration from livestock, industry, or farming areas (*Lapworth et al.*, 2012; *Rivera-Utrilla et al.*, 2013).

Several active treatment procedures are reported for removing EOCs, such as advanced oxidation, reverse osmosis, and nanofiltration (*Zhang et al.*, 2011; *Rivera-Utrilla et al.*, 2013). These procedures are generally expensive in terms of investment and energy (*Maeng et al.*, 2011b; *Rivera-Utrilla et al.*, 2013). In contrast, passive treatment systems, such as bank filtration and artificial recharge via infiltration basins, may be a low-cost alternative to advanced water treatment procedures (*Drewes et al.*, 2003b; *Shamrukh and Abdel-Wahab*, 2008; *Maeng et al.*, 2010; *Valhondo et al.*, 2014; *Alidina et al.*, 2014a), but their efficiency and robustness have not been fully demonstrated.

The design of natural treatment methods requires an understanding of the processes that influence the fate of EOCs during subsurface flow. The main processes are sorption, generally to organic matter and clay minerals, and biological degradation or transformation (*Lapworth et al.*, 2012). Sorption is generally viewed as a straightforward process, although its actual characterization can be complicated by natural heterogeneity and competition for sorption sites. Biotransformation is difficult to assess because EOC concentrations are typically low (ranging from a few nanograms per liter to a few hundred micrograms per liter). Therefore, it is very unlikely that EOCs would be used as a primary substrate, so it must be assumed that they are biotransformed by co-metabolism (*Tran et al.*, 2013). Co-metabolic degradation implies the presence of a primary substrate, typically dissolved organic carbon (DOC), which provides enough energy to support microbial growth (*Tran et al.*, 2013). The bioavailability of biodegradable DOC as the primary substrate affects the microbial community structure and consequently also affects EOC biotransformation (*Alidina et al.*, 2014a; *Rauch-Williams et al.*, 2010; *Li et al.*, 2013; *Alidina et al.*, 2014b;

Regnery et al., 2015). Biodegradation of the primary source, DOC, produces different enzymes depending on the electron acceptor (metabolic path). These enzymes are involved in the transformation of EOCs, and therefore the redox conditions affect the EOC biotransformation. In fact, several authors have described the redox-dependence of the biotransformation of diverse EOCs (*Maeng et al.*, 2011b, 2010; *Greskowiak et al.*, 2005, 2006; *Massmann et al.*, 2008a; *Barbieri et al.*, 2011; *Storck et al.*, 2012; *Liu et al.*, 2013; *Valhondo et al.*, 2015) and how changing redox conditions might be effective for removing such contaminants (*Maeng et al.*, 2011b). Other factors, such as temperature (*Massmann et al.*, 2006) and residence time (*Massmann et al.*, 2008b), also affect EOC removal during subsurface passage.

Current research is yielding a body of evidence that supports the engineering of artificial recharge with methods to promote varying types of sorption sites and redox conditions. Most research, however, is performed at the laboratory scale, which, while it facilitates process understanding, misses potential synergetic effects associated with the heterogeneous and complex hydrochemical conditions that are inherent in natural systems. To address these conditions, we installed a reactive barrier at the bottom of an infiltration basin in an artificial recharge site to promote the processes involved in the attenuation of EOCs (*Valhondo et al.*, 2014, 2015). The barrier comprised vegetable compost, which releases DOC into the infiltrated water, favoring a broad range of redox conditions underneath. Very small fractions of clay and iron oxide were added to increase the sorption sites for cationic and anionic EOCs, respectively. The qualitative behavior of the system is satisfactory (*Valhondo et al.*, 2014, 2015). Sufficient effort, however, have not been made at this site or elsewhere to quantify the effective sorption and biotransformation parameters associated with such a heterogeneous and complex system and to evaluate how these parameters compare to those obtained under laboratory conditions. Thus, the validity of sorption and biotransformation parameters derived from laboratory tests remains highly uncertain. In fact, geochemical modeling experience suggests that field reaction rates can be orders of magnitude smaller than those derived from laboratory experiments because the transport of reactants to reaction sites limits the reaction rates (*White and Brantley*, 2003; *Moore et al.*, 2012). Therefore, it is important to

determine whether the same discrepancy occurs with the transformation of organic contaminants.

The objective of this work was two-fold: first, to describe a method for evaluating effective sorption and biotransformation parameters in a real-scale complex artificial recharge system; and, second, to evaluate these parameters and compare them to values available in the literature from laboratory and field conditions.

5.2 Materials and Methods

5.2.1 Field Site

The artificial recharge facility is located in Sant Vicenç dels Horts (Barcelona, Spain), close to the Llobregat River and approximately 15 km from the sea (Figure 5.1). The facility comprises a settlement basin and an infiltration basin ($\approx 5000\,m^2$ each) connected by a pipe. Llobregat River water, affected by numerous treatment plant effluents (*Köck-Schulmeyer et al.*, 2011), was carried into the settlement basin (2–4 days residence time) before flowing to the infiltration basin. A CTD-Diver (Schlumberger Water Services, Delft, The Netherlands) and an area velocity flow meter (Teledyne Isco Inc., Lincoln, NE, USA) were installed in the connecting pipe to measure electrical conductivity, temperature, and flow rate of the water entering the infiltration basin. Infiltration rate averaged 1 m/d.

The aquifer beneath the facility, extended to 20–23 m deep with 12–14 m saturated thickness during the experiment time (2010–2014). It contained Quaternary alluvial sediments, mainly gravel and sand with a small fraction of clay (*Barbieri et al.*, 2011), on top of Pliocene marl, which was assumed to be impervious. The varying percentages of gravel, sand, and clay of the sediments caused heterogeneous layering (*Gámez et al.*, 2009). The groundwater flows naturally from NNW to SSE with a mean 2.3 ‰gradient (*Iribar et al.*, 1997), but the flow structure changes during artificial recharge periods when the gradient beneath the infiltration basin becomes nearly vertical

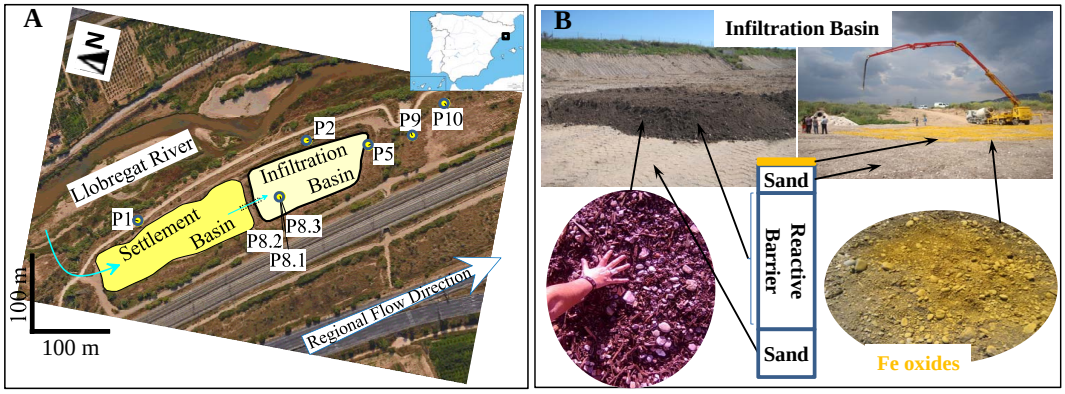

Figure 5.1: Plan view of the infiltration system,and monitoring points (A), and reactive barrier scheme and details (B)

(≈ 10%) (*Valhondo et al.*, 2016c).

Water was sampled at the infiltration basin using eight piezometers and two suction cups (Figure 5.1) to monitor both the evolution of recharged water for increasing travel times, and the native aquifer water (Figure 5.1 A). One piezometer, P1, was located far enough upstream of the infiltration basin to be hardly affected by recharge water and was assumed to be representative of local groundwater (*Valhondo et al.*, 2014, 2015, 2016c). Piezometers P2, P5, P9, and P10 were located downstream and sampled recharge water (*Valhondo et al.*, 2016c). The two suction cups, CC1 and CC2, were located in the middle of the infiltration basin, at depths of 1 and 2 m, respectively, together with piezometers P8.3, P8.2, and P8.1that were located at depths of 7 to 9, 10 to 12, and 13 to 15 m, respectively. A CTD-Diver was installed with each piezometer during most of the infiltration experiments to continuously measure electrical conductivity, temperature, and head values.

The mean temperature of the infiltration water during the experiment was 21.2±2.4° C, very similar to that measured in the groundwater samples, 21.03±2.3° C, and slightly lower than the unsaturated zone samples, 25.2±2.6° C. The pH varied from 8.28±0.15 in the infiltration water to 7.5±0.24 in the unsaturated zone samples and 7.13±0.21 in the groundwater samples.

5.2.2 The reactive barrier

The reactive barrier, installed in April 2011, comprised a 65 cm-thick mixture of coarse sand and vegetable compost, in equal volume proportions, and a small fraction of clay and iron oxide (Figure 5.1B). The sand ensures the structural integrity and permeability, whereas the vegetable compost releases DOC to promote microbial activity and the consumption of electron acceptors that leads to a broad range of redox conditions favoring the biodiversity of the microbial community. In addition, vegetable compost provides sorption sites for neutral EOCs. Clay and iron oxide provide sorption sites for cationic and anionic EOCs, respectively. The barrier covered the entire floor of the infiltration basin. Detailed information about the reactive barrier installation were reported by Valhondo *et al.,* (2014), and the compost characteristics and their effect on the redox conditions in both columns and field experiments were reported by Schaffer *et al.,* (2015) and Valhondo *et al.,* (2014, 2015) (*Valhondo et al.*, 2014, 2015; *Schaffer et al.*, 2015).

5.2.3 Organic micropollutants and analytical methods

In this study, the first-order decay and the retardation coefficient were estimated for 10 EOCs that are typically present in wastewater with different molecular and physico-chemical properties and method quantitation limits (MQL) (Table 5.1).

Analysis of organic micropollutants

Samples were collected in amber-glass bottles, allowed to settle at 4° C overnight and 500 mL, in case of groundwater sample, or 250 mL, in case of surface water and vadose zone water, of the supernatant spiked with 10 μg of internal standard was used for the analysis. Surface and vadose zone water were diluted to 500 mL with ultrapure water to avoid problems with the chromatographic column. The samples were extracted by solid phase extraction using OASIS HLB (6 mL, 500 mg: Waters, Eschborn, Germany) with an applied extraction speed of 15 mL/min. The dried cartridges

were stored at -18° C until resuming analysis. The analytes were eluted with methanol and ethyl acetate, the solvents were evaporated to dryness (40° C and stream of N_2) and the dry residue was dissolved in 1 mL aqueous 5-mM ammonium acetate solution containing 4% methanol. The samples were analyzed by high-performance liquid chromatography coupled with tandem mass spectrometry according to Nödler *et al.,* (2010) (*Nödler et al.*, 2010). The method quantitation limits of each EOC in the groundwater samples are summarized in Table5.1.

Analysis of bulk chemistry

Samples for the analysis of DOC were collected in glass bottles acidified and allowed to settle at 4^oC. Total organic carbon analyzer (Shimatzu TOC-Vcsh, Shimadzu Corporation, Kyoto, Kyoto Prefecture, Japan) with IR detector was used to analyze DOC.

Specific ultraviolet absorbance (SUVA) was measured in water samples by normalizing the absorbance of the sample at 254 nm for the DOC concentration.

Samples for Fe and Mn analysis, were filtered through 0.45 μm PALL Acrodisc© sterile syringe filters with supor© membrane (Sigma-Aldrich, St. Louis, MO, USA), acidified and stored at 4°C. The samples were analyzed by inductively coupled plasma optical emission spectroscopy (ICP-OES) with a Perkin Elmer Optima 3200DV (PerkinElmer, Waltham, MA, USA). The analytical error was estimated to be below 15% for Fe and below 12% for Mn. Detection limits were 50 μg/L for Fe and 20 μg/L for Mn.

Samples for NO_3^- analysis were also filtered through 0.45 μm, stored at 4°C and analyzed within 72 h by ion chromatography using a Dionex DX-120 (Dionex, Sunnyvale, CA, USA) with an ionpack AS18 4x250 mm column and KOH as the eluent. The analytical error was estimated to be 13%.

5.2.4 Fate of EOCs: Estimation of reactive transport parameters

The fate of EOCs is governed by the advection-dispersion reaction equation (ADRE)(eq. 5.1) (*Bear and Bachmat*, 1984)

$$\phi R\frac{\partial C}{\partial t} = -\mathbf{q}\nabla C + \nabla \cdot (\mathbf{D}\nabla C) - \lambda\phi RC \tag{5.1}$$

where ϕ is porosity [-], R is retardation coefficient [-], C [M/L^3] is the concentration of solute, **q** [LT^{-1}] is the water flux, **D** [L^{2}T^{-1}] is the dispersion tensor, and λ [T^{-1}] is a first-order decay constant. Conservative transport is represented by advection (dragging of solutes by water, which moves with a velocity **v**, eq. 5.2) and dispersion (spreading and expansion of solute fronts). Reactions are simplified in terms of linear sorption onto the solid grains, eq. 5.3, where K_d is the distribution coefficient, and first-order degradation, λ.

$$\mathbf{v} = \mathbf{q}\phi \tag{5.2}$$

$$R = 1 + \frac{K_d}{\phi} \tag{5.3}$$

The role of these two parameters is illustrated in Fig. 5.2. Retardation reduces the solute velocity, which becomes $\mathbf{v}_s$=**q**/ϕR, because only the fraction in solution is actually dragged by the water. Retardation may also reduce solute concentrations initially (e.g., for a pulse solute mass input, Fig 5.2A), because part of the input mass is sorbed onto the soils, but not for a continuous input.

To solve the ADRE, one must first solve the flow equation (*Bear and Bachmat*, 1984) to compute **q** and then specify the remaining parameters. We split the latter into two steps. Conservative

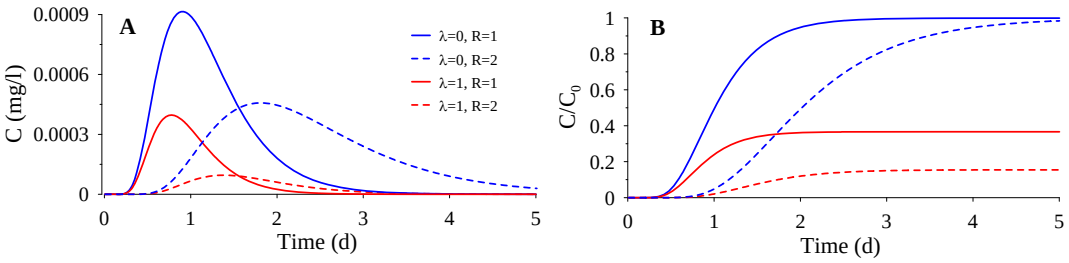

Figure 5.2: ADRE solution for non-reactive (blue line), sorption and no degradation (dashed blue line), degradation and no sorption (red line), and sorption and degradation (dashed red line) for A) solute mass pulse, and B) continuous mass input.

transport parameters (ϕ,**D**) were calibrated against a conservative tracer test using a multilayer model (*Valhondo et al.*, 2016c). The resulting model, which was built using the finite element code Transdens (*Hidalgo et al.*, 2004; *Medina and Carrera*, 1996, 2003), incorporated the complexities associated with heterogeneity and the three-dimensional nature of the flow field, Figure 5.3B. The model yielded not only good calibration fits but also good blind predictions of other tracers (1,1,2-trichloroethane, and electrical conductivity). Therefore, it can be considered a good representation of solute transport at the site and used to estimate reactive parameters.

General reactive transport modeling typically involves solving equations like (Eq. 5.1) for all chemical species because reaction terms depend on the concentrations of all species. Here, two facts allow us to apply some simplifications. First, the EOC concentrations were relatively small compared to the major components, so that their reactions have a minor impact on the overall chemistry. Second, the hydrochemical evolution and, specifically, the redox processes are well known at the site from previous studies (*Valhondo et al.*, 2014, 2015, 2016c), as discussed below.

5.2.5 Redox zonation and parameterization of R and λ

The mean DOC (mg/L), SUVA, NO_3^- (mg/L), and dissolved Fe (μg/L) and Mn (μg/L) values measured at suction cups, monitoring piezometers, and water from the infiltration basin (INF), are summarized in Table 5.2. The concentrations of DOC and SUVA, as indicator of aromaticity, at CC1 and CC2 were higher than in the recharge water, demonstrating the efficiency of the

reactive barrier for releasing DOC. A part of the released DOC was rapidly oxidized, as evidenced by the consumption of electron acceptors. This consumption might take place in a sequential order defined by energy production and referred to as the ecological sequence of terminal electron-accepting processes (*McMahon and Chapelle*, 2008), or simultaneously, as observed in field experiments with high DOC concentrations (*Alewell et al.*, 2008; *Torres et al.*, 2015). NO_3^- concentration decreased from the recharged water to the monitoring points closer to the infiltration basin (CC1, CC2, P8.3, P5) indicating nitrate-reduction. Simultaneously, the concentration of Mn and Fe increased drastically at CC1 and CC2, indicating iron- and manganese-reduction in the reactive barrier and immediately below it. We defined three areas regarding the redox conditions: 1), the reactive barrier, "Dom-1", the conditions of which were assumed to be represented by CC1 with a high DOC concentration and iron- and manganese-reducing conditions, 2) the 2 m-thick layer immediately below the reactive barrier, "Dom-2", the conditions of which were assumed to be represented by CC2 and where part of the DOC has been oxidized and the iron and manganese concentration are lower than in the reactive barrier (probably due to the preferential flow path part of the recharged water arriving faster) and, 3) the rest of the model domain, "Dom-3", the conditions of which are assumed to be an average of the rest of the monitoring points with a DOC concentration that is much lower than that in the reactive barrier and the layer below, and the concentration of NO_3^- is higher and Mn and Fe lower, indicating oxic or suboxic conditions, Figure 5.3.

Schaffer *et al.,* (2015), performed column experiments using the compost from the reactive barrier to fill two columns and observed a similar influence of the DOC released by the compost onn the redox conditions (*Schaffer et al.*, 2015).

Henzler *et al.,* (2014) modeled the reactive transport (R and λ) for 12 EOCs during bank filtration and achieved a proper fit for 8 of them with just 1 first-order rate constant for each contaminant (*Henzler et al.*, 2014). Artificial recharge via river bank filtration typically presents highly varying and dynamic redox conditions and therefore the authors option was to use one λ

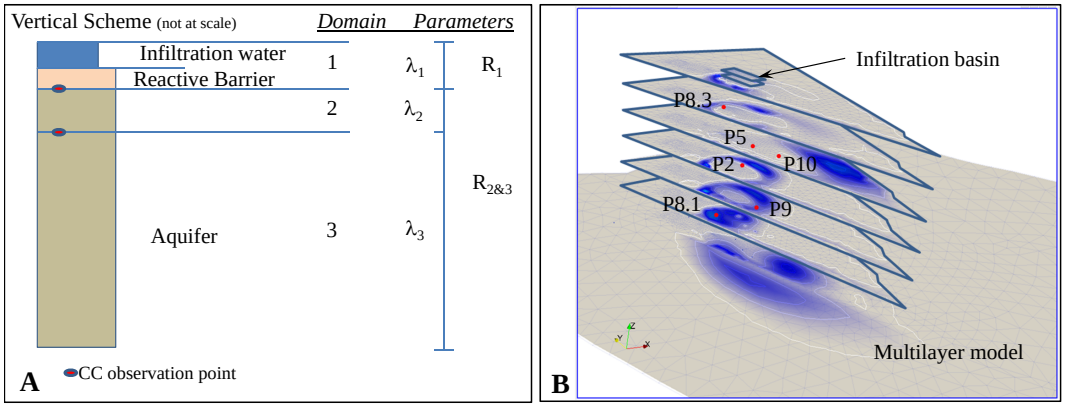

Figure 5.3: Vertical scheme of the parameterization of λ and R (A), and numerical model mesh and layers (B)

representing the mean of the degradation parameters for each contaminant. Regnery *et al.,* (2015), however, concluded that it is more suitable to include different rate constants to reproduce the attenuation of redox-dependent EOCs over time and distance during artificial recharge of aquifers (*Regnery et al.*, 2015). Therefore, we estimated λ values for three different zones based on the redox conditions and R values for two zones based on the solid organic matter content (Table 5.3). The standard deviation assigned to each contaminant concentration measured at each monitoring point was the maximum between the detection limit of such contaminant and the 10% of the highest concentration measured at that monitoring point. Estimated R and λ fit was evaluated by the root mean square-weighted error (RMSWE).

Table 5.1: Limits of quantification and physico-chemical properties of the selected emerging organic compounds

Compound	Acronym	Predominant Charge (pH 7)	Use	MQL [ng/L]	log Kow	pKa
Carbamazepine	CBZ	Neutral	Anticonvulsant	2.2	1.90±0.6	-
Gemfibrozil	GFZ	Anionic	Lipid regulator	2	4.3±0.32	4.75±0.45(A)
Ibuprofen	IBU	Anionic	Analgesic	3.6	3.5±0.23	4.41±0.10(A)
Paracetamol (Acetaminophen)	PRM	Neutral	Analgesic	3.7	0.46	
Sulfamethoxazole	SMX	Anionic	Antibiotic	2.6	0.66±0.41	5.81±0.5(A)
Tolyltriazole	TTR	Neutral	Corrosion inhibitor	4.9	1.8±0.25	8.74±0.40(A)
Iohexol	IOHx	Neutral	Contrast medium	21	-4.16±0.85	
Iomeprol	IOMe	Neutral	Contrast medium	18	-3.08±0.86	
Iopamidol	IOPa	Neutral	Contrast medium	19	-2.09±1	
Iopromide	IOPr	Neutral	Contrast medium	18	-2.95±0.91	

Table 5.2: Mean values of DOC (mg/L), SUVA, NO_3^- (mg/L), and dissolved Fe (μg/L) and Mn (μg/L) measured at suction cups, monitoring piezometers and water from the infiltration basin (INF)

Monitoring Point	Depth (m)	Model Domain	DOC (mg/L)	SUVA n.u.	NO3- (mg/L)	Fe (μg/L)	Mn (μg/L)
INF	0	-	3.11	2	5.8	7.02	8.52
CC1	1	Dom-1	7.30	4.08	0.61	1436.13	589.13
CC2	3	Dom-2	4.6	4.39	0.5	847.17	575.5
P8.3	8	Dom-3	2.6	2.44	0.76	4.40	67.2
P5	10	Dom-3	2.6	2.48	1.68	6.25	30.33
P8.2	12	Dom-3	1.9	1.37	1.24	3.5	2.5
P2	12	Dom-3	2.1	1.93	5.18	3.5	9.67
P9	14	Dom-3	1.9	1.84	1.83	4.67	4.5
P8.1	16	Dom-3	1.4	0.69	6.38	5.6	2.5
P10	10	Dom-3	1.7	2.13	3.86	3.5	3.45
P1	18	Dom-3	1.4	1.15	15.05	4.5	4.13

5.3 Results and Discussion

Results are summarized in terms of model fits in Figures 5.4 to 5.13, and in terms of estimated parameters in Table 5.3. Table 5.3, shows that the first-order rates estimated in the reactive barrier were similar or higher than previous values obtained in column experiments, which used are similar or higher than the values obtained from field experiments.

Figure 5.4 displays the fit of the conservative and reactive models to the measured carbamazepine concentrations at the monitoring points. The highest first-order decay for carbamazepine was estimated in the reactive barrier, 1.006 d^{-1} (Table 5.3, Figure 5.4), where the most reducing redox conditions were found (Table 5.2). This value implies a half-life of 0.69 d, far lower than those reported in the literature in the field (≥60 d (*Laws et al.*, 2011); 66 d (*Henzler et al.*, 2014); 35-54 d (*Wiese et al.*, 2011)), or in column experiments (no degradation was observed by Bertelkamp *et al.,* (2014), Schaffer *et al.,* (2015), and Regnery *et al.,* (2015)) (*Bertelkamp et al.*, 2014; *Schaffer et al.*, 2015; *Regnery et al.*, 2015). The fact that a higher decay rate was estimated for the reactive barrier supports Wiese *et al.,* (2011) who reported better degradation under more reducing conditions (*Wiese et al.*, 2011).

Due to the neutral character of carbamazepine a higher sorption on the organic matter of the reactive barrier was expected compared to the rest of the model domain. However, we estimate a value of 1 for R in the reactive barrier. The Llobregat River source water affected by treatment plants effluents could be the reason for the low R estimated. Indeed, Chefetz *et al.,* (2008) found a decreasing R in secondary treatment water with high dissolved organic mater, which might facilitates the transport of neutral compounds (*Chefetz et al.*, 2008). A similar behavior was described by Bertelkamp *et al.,* (2014) who found R in columns fed with demineralized water higher than in columns fed with treatment plants outflow (*Bertelkamp et al.*, 2014). The retardation for carbamazepine in the rest of the domain was also low (R=1.14) and similar to those reported by Yu *et al.,* (2009), Bertelkamp *et al.,* (2014), and Nham *et al.,* (2015) (*Yu et al.*, 2009; *Bertelkamp et al.*,

2014; *Nham et al.*, 2015).

Figure 5.5 displays the model fit of ibuprofen. A decay rate of 10.15 d^{-1} was estimated in the reactive barrier, which yields a half-life of 1.68 h (Table 5.3). Bertelkamp *et al.,* (2014) reported a similar degradation rate in a column experiment (λ=15.8 d^{-1}). This rate, however, was higher than those found by Schaffer *et al.,* (2015) in columns filled with the compost used in our reactive barrier, who estimated a half-life of 40.11-61.71 d (*Schaffer et al.*, 2015). The λ value estimated for the rest of the domain, Dom-3, yielded half-life of 13.86 d, that was similar to those estimated by Nham *et al.,* (2015) in an infiltration site from Greece (*Nham et al.*, 2015). Maeng *et al.,* (2011) proposed that higher concentrations of biodegradable DOC might favor the co-metabolism of ibuprofen (*Maeng et al.*, 2011a), which would be supported by the variations in our estimations, higher λ in the reactive barrier than in the rest of the model domain where DOC concentration was lower (Table 5.2). Laws *et al.,* (2011) reported poor degradation (≤10%) of ibuprofen during artificial recharge water through the unsaturated zone, but the degradation increased up to 84% with the recharge water flowing through the aquifer (*Laws et al.*, 2011). Drewes *et al.,* (2003) and Amy and Drewes (2007) observed a complete elimination of ibuprofen in an artificial recharge system using reclaimed water after travel times longer than t2 weeks (*Drewes et al.*, 2003a; *Amy and Drewes*, 2007), which is consistent with our estimation of λ in Dom-3, and indicating that the reactive barrier improves the elimination of ibuprofen. We estimated a retardation factor of 6.22 for the reactive barrier and no retardation for the rest of the domain. Bertelkamp *et al.,* (2014) and Nham *et al.,* (2015) observed no retardation in column and field experiments, respectively (*Bertelkamp et al.*, 2014; *Nham et al.*, 2015).

Figure 5.6 displays the fit of the conservative and reactive models to the measured gemfibrozil concentrations at the monitoring points. The estimated degradation rate was higher in Dom-2 (the layer below the reactive barrier) than in Dom-1 (reactive barrier). Both rates were within the range measured in column experiments, and higher than rates obtained in the field (Table 5.3). The degradation rate in the rest of the system (Dom-3) was low, in accordance with

Table 5.3: Estimated values of first-order decay (d^{-1}) in the reactive barrier (Dom-1), the 2 m-thick layer below the reactive barrier (Dom-2), and the rest of the model domain (Dom-3), and reported values from previous studies from column (values in red) and field (values in blue) experiments, estimated retardation factors in the reactive barrier (Dom-1) and the rest of the model domain (Dom-2 & -3), and reported values from previous studies for the 10 selected EOCs and the fit of the model (RMSWE) for both the reactive and the conservative (R=1 and λ=0) hypotheses

EOCs	First order decay				Retardation			RMSWE	RMSWE
	Dom-1	Dom-2	Dom-3	Literature	Dom-1	Dom-2 & -3	Literature	reactive	conservative
Carbamazepine	1.006	0.013	0.0	0.0[a,c], 0.001–0.02[b]	1.0	1.14	1.1[a],1[b]	295.2	367.4
				0.0105[e]			1.43–1.89 [c], 1.7[e]		
				0.099–0.198[g]			1.04[g], 1.4[j]		
Gemfibrozil	2.13	5.15	0.04	0–12.7[a]	4.30	1.0	1.1[a]	513	14670
				0.015–1.49[b]			1[b]		
				0.046–1.73[g]			1.15–1.54[c]		
Ibuprofen	10.15	2.78	0.05	15.8[a], 0[c]	6.22	1.0	1.3–1.51[c]	99.83	9825
				0.578–0.99[g]					
Paracetamol	20.0	5.0	0.0	0–17.1[a]	5.36	2.9	1.1[a], 1[b]	555.7	511300
				0.068–0.134[g]					
Sulfamethoxazole	3.83	0.5	0.003	0[a], 0.009–0.5[b]	1.03	1.0	1[a,b], 1–1.27[c]	456.3	1219
				0[g], 0.002–0.012[d]			1[e], 1.05[j]		
				0.32[e]					
Tolyltriazole	0.092	0.004	0.00025	0[c]	12.02	1.0	1.74–2.43[c]	224.3	695.5
Iohexol	0.44	0.36	0.10	0.277–0.495[g]	3.64	2.20		245.5	2196
Iomeprol	0.897	0.404	0.035	0.347–0.462[g]	3.31	1.68		70.54	475.8
				0.0013–0.066[d]					
Iopamidol	0.286	0.3	0.026	0.198–0.385[g]	1.55	1.0		300.6	412.7
Iopromide	1.087	0.44	0.044	0.16–0.82[b]	1.69	7.20	1[b]	119.2	1289
				0.347–0.533[g]			1.1[j]		

Values obtained in field experiments and Values obtained in column experiments [a] Bertelkamp *et al.,* (2014), [b] Regnery *et al.,* (2015), [c] Schaffer *et al.,* (2015), [d] Grünheid *et al.,* (2005), [e] Henzler *et al.,* (2014), [f] Law *et al.,* (2011), [g] Nham *et al.,* (2015), [h] Ranieri *et al.,* (2014), [i] Regnery *et al.,* 2015a, [j] Wiese *et al.,* (2011)

those observed in the lower range of field and column experiments. Several authors reported that the redox-dependent biotransformation of gemfibrozil (*Rauch-Williams et al.*, 2010; *Nham et al.*, 2015; *Schaffer et al.*, 2015; *Regnery et al.*, 2015) improves with more oxic conditions. This is unlikely here as no prevailing aerobic conditions were found in Dom-2, whereas Dom-3 with slower rates had more oxidizing conditions (Table 5.2). Laws *et al.,* (2011) found an attenuation of 90% in the first 3 days after artificial recharge through an infiltration basin (*Laws et al.*, 2011), which is similar to our findings. Estimated sorption was important in the reactive barrier (R=4.3) whereas no sorption was observed for the rest of the domain (R=1).

Among the selected EOCs, paracetamol was the most highly attenuated in the reactive barrier, λ=20 d^{-1} (Table 5.3). Its concentration dropped from several hundred of nanograms per liter measured at the infiltration basin entrance to less than 100 ng/L at all monitoring points (Figure 5.7). Modeling the behavior of 14 organic micro pollutants in column experiments, Bertelkamp *et al.,* (2014) reported a λ=17.1 d^{-1} for paracetamol, which is similar to the value estimated here (*Bertelkamp et al.*, 2014). In fact, the estimated λ for paracetamol in the reactive barrier was the highest of all the selected EOCs, and it had a half-life of 45 min, which was much shorter than that estimated by Ranieri *et al.,* (2011), who reported half-life between 5.16 and 10.2 h in subsurface flow constructed wetlands (*Ranieri et al.*, 2011). The fact that photolysis might represent an important transformation process of paracetamol in the surface water leading to half-life between 0.7–1.1 d according to Lam *et al.,* (2004) (*Lam et al.*, 2004) and between 1.5–2.3 d according to Yamamoto *et al.,* (2009) (*Yamamoto et al.*, 2009) should be taken into account. We measured the EOC concentrations in the recharge water at the entrance of the infiltration basin, and the residence time in the basin was approximately 24 h; therefore, some photolysis might have occurred before the recharge water infiltrated the basin. The estimated retardation factor for paracetamol in the reactive barrier was practically twice that estimated for the rest of the domain (5.36 and 2.9). Due to its neutral character, paracetamol was expected to adsorb onto the organic matter of the reactive barrier.

Figure 5.8 displays the fit of the conservative and reactive models for the measured sulfamethoxazole concentrations at the monitoring points. The estimated λ for Dom-1, Dom-2, and Dom-3 yielded a half-life of 0.18, 1.39, and 321 d, for each of these domains, respectively. The rate obtained for the reactive barrier (Dom-1) was higher than those reported in the column and field experiments. Several authors have reported higher degradation under more reductive redox conditions (*Grünheid et al.*, 2005; *Wiese et al.*, 2011; *Henzler et al.*, 2014). Banzhaf *et al.,* (2012) reported a strong dependency of sulfamethoxazole degradation on nitrate-reducing conditions, which were established for Dom-1 and Dom-2 (Table 5.2), and Gruenheid *et al.,* (2008) reported that degradation is temperature-dependent (*Grünheid et al.*, 2008). Schaffer *et al.,* (2015) estimated the half-life to be 4.58–5.73 d and R=1.20–1.27 for sand columns with pre-columns filled with compost, and observed no degradation and no retardation in the systems without the compost (*Schaffer et al.*, 2015). Consistently, similar retardation factors of 1.03 and 1.0 were estimated for the reactive barrier and Dom-2 & -3. In laboratory experiments using biosolids, Wu *et al.,* (2009) concluded that the sorption of sulfamethoxazole was too weak to estimate the distribution coefficients (*Wu et al.*, 2009). Henzler *et al.,* (2014) also observed no retardation during river bank filtration (*Henzler et al.*, 2014). Wiese *et al.,* (2011) hypothesized that sulfamethoxazole might be retarded by surface complexation (*Wiese et al.*, 2011). In that case the sorption could be very variable because it is affected by pH, redox conditions, and availability of hydroxides and oxides sorption surfaces. If that was the case, Wiese *et al.,* (2011) postulated that complexation might be followed by biodegradation due to higher local EOC concentrations and better adaptation of microorganisms (*Wiese et al.*, 2011).

Figure 5.9 displays the fit of the conservative and reactive models to the measured tolyltriazole concentrations at the monitoring points. Among the selected EOCs, tolyltriazole had the lowest estimated λ in Dom-1, Dom-2, and Dom-3 (0.092, 0.004, and 0.00025, respectively, Table 5.3). Schaffer *et al.,* (2015) observed no degradation in sand columns with pre-columns containing compost (*Schaffer et al.*, 2015). Liu *et al.,* (2010) observed better removal of sulfamethoxazole in soils under aerobic conditions (half-life = 2 d) than under anoxic conditions (half-life = 7 d) (*Liu*

et al., 2010). This last value is comparable to the estimated λ for the reactive barrier (Table 5.3). The retardation factor of Dom-1 was 12.02, the highest among the selected EOCs, whereas no retardation was obtained for Dom-2&-3. Schaffer *et al.,* (2015) also reported a retardation factor of 2.4 for columns filled with compost and sand (*Schaffer et al.*, 2015).

Figures 5.10, 5.11, 5.12, and 5.13 display the fit of the conservative and reactive models for the measured contrast media iohexol, iomeprol, iopamidol, and iopromide concentrations at the monitoring points. The estimated degradation rates were similar to the estimates described in Nham *et al.,* (2015) during artificial recharge through an infiltration basin using water from a wastewater treatment plant (*Nham et al.*, 2015), and the λ values yielded half-lives comparable to those reported by Grünheid *et al.,* (2005) and Laws *et al.,* (2011) (*Grünheid et al.*, 2005; *Laws et al.*, 2011). Iomeprol and iopromide exhibited better degradation in the reactive barrier than iohexol and iopamidol. Estimated retardation factors varied from 1.0 (iopamidol in Dom-3) to 7.2 (iopromide in Dom-3). The estimated retardation factors differed from those estimated by Nham *et al.,* (2015) who observed no retardation for these four contrast media (*Nham et al.*, 2015).

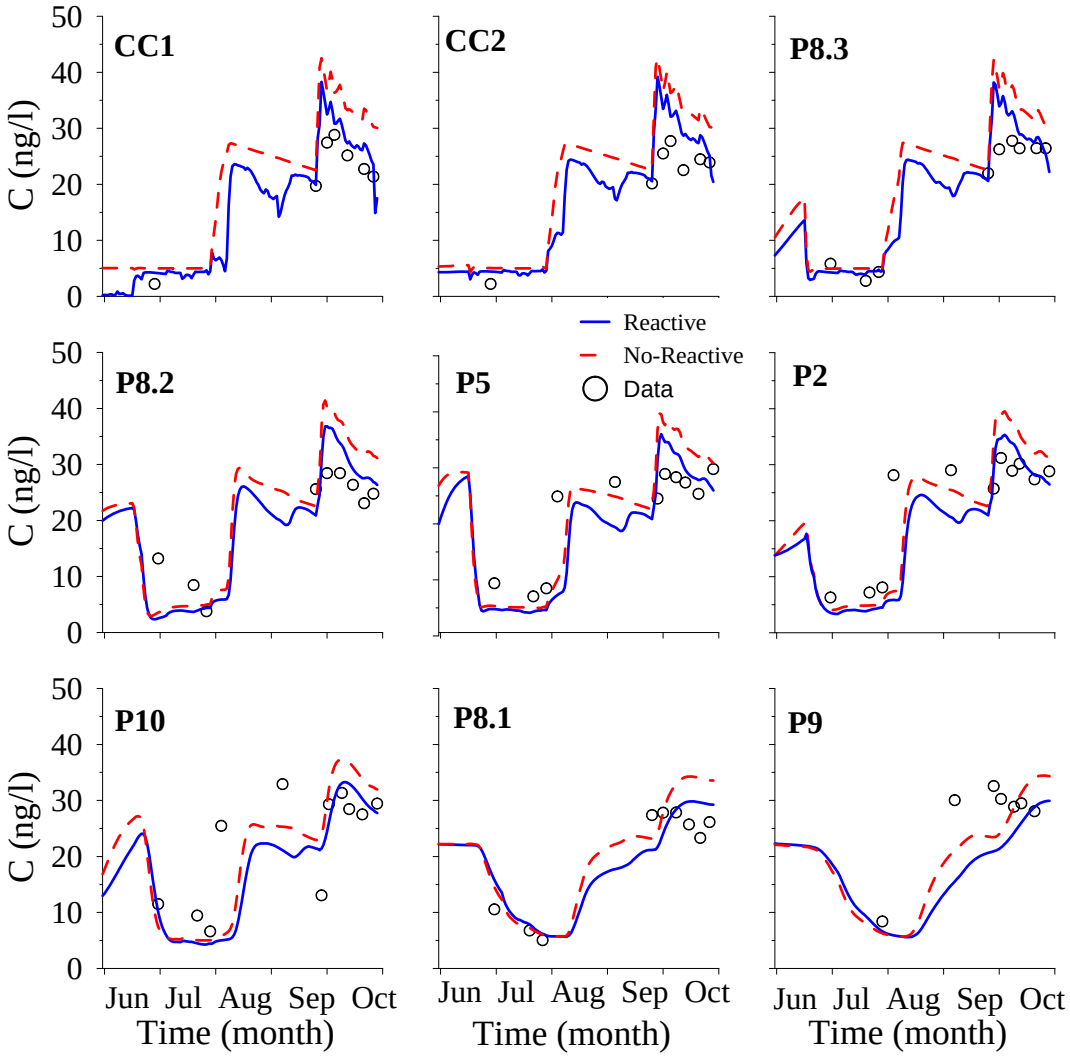

Figure 5.4: Measured carbamazepine concentration (blue circles) and calculated carbamazepine concentration considering conservative behavior (R=1 and λ=0) (dashed red line), and reactive transport (R=1 and λ=0) (blue line) at the monitoring point.

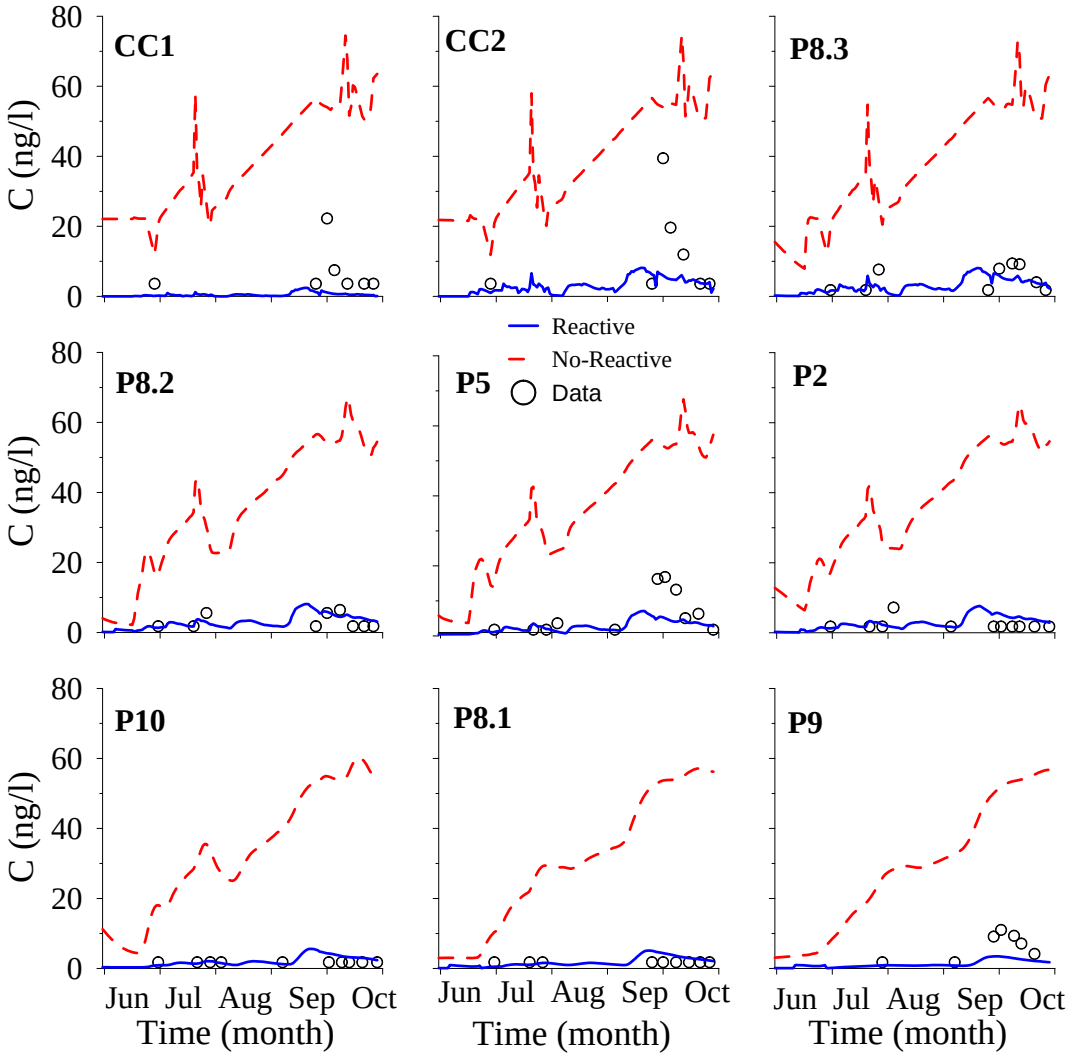

Figure 5.5: Measured ibuprofen concentration (blue circles) and calculated ibuprofen concentration considering non-reactive transport (dashed red line), and reactive transport (blue line) at the monitoring point.

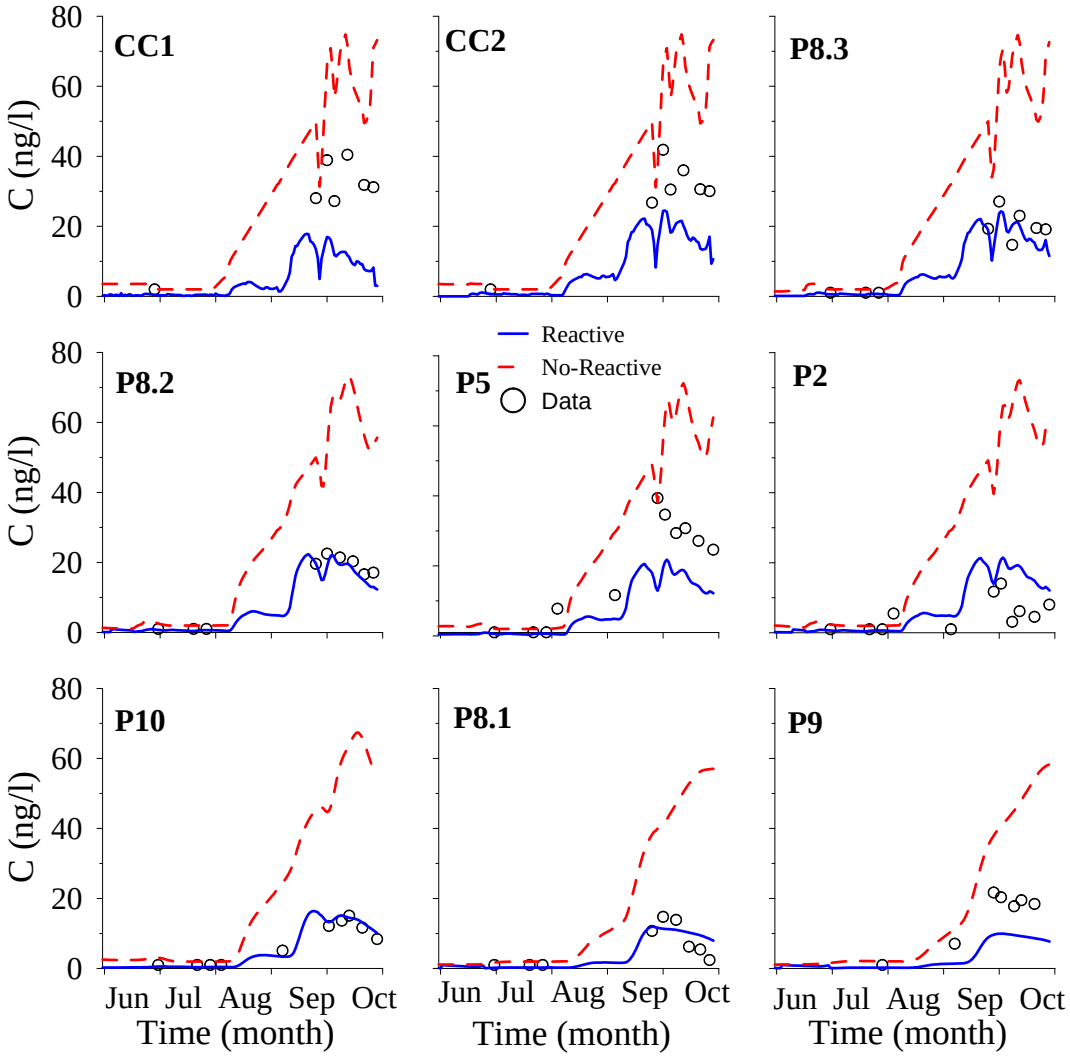

Figure 5.6: Measured gemfibrozil concentration (blue circles) and calculated gemfibrozil concentration considering non-reactive transport (dashed red line), and reactive transport (blue line) at the monitoring point.

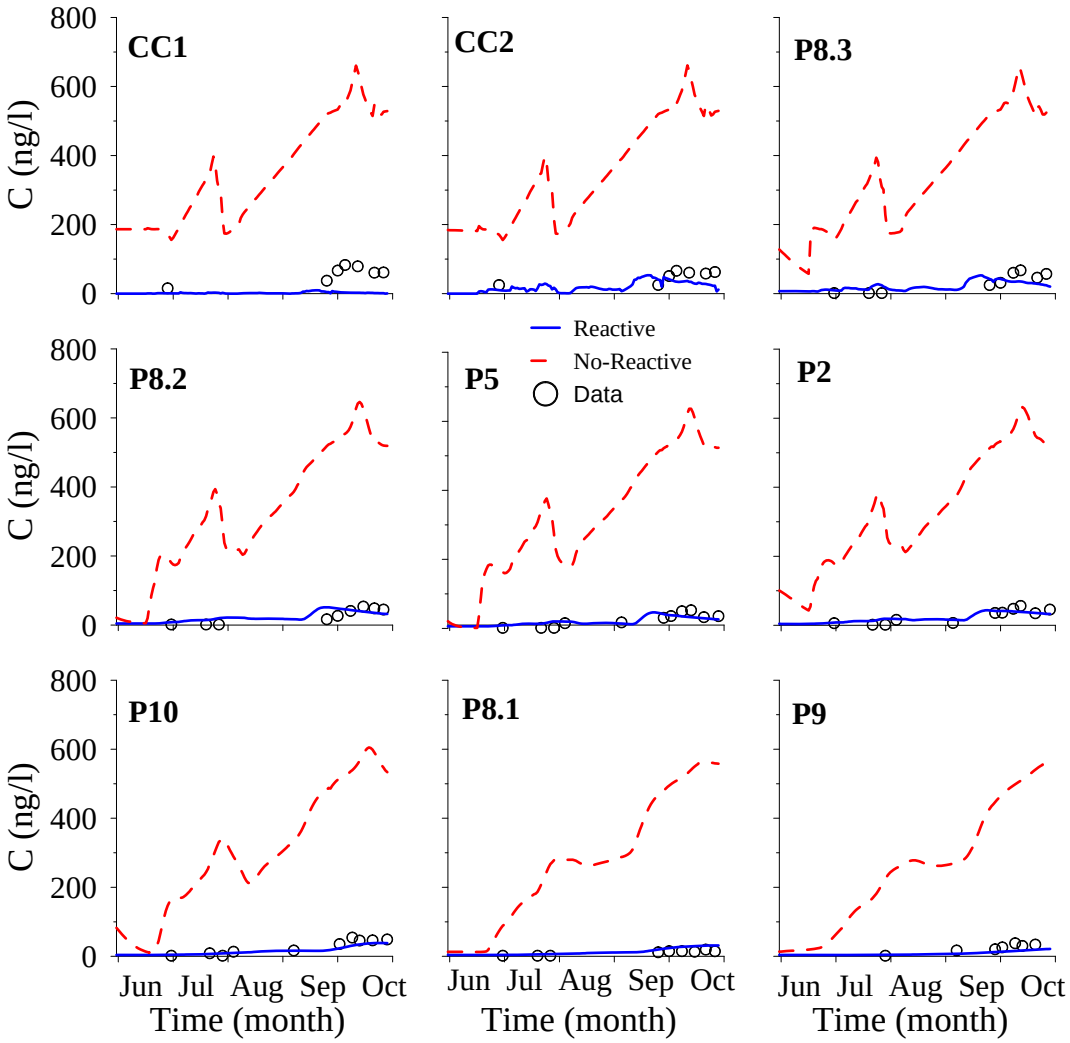

Figure 5.7: Measured paracetamol concentration (blue circles) and calculated paracetamol concentration considering non-reactive transport (dashed red line), and reactive transport (blue line) at the monitoring point.

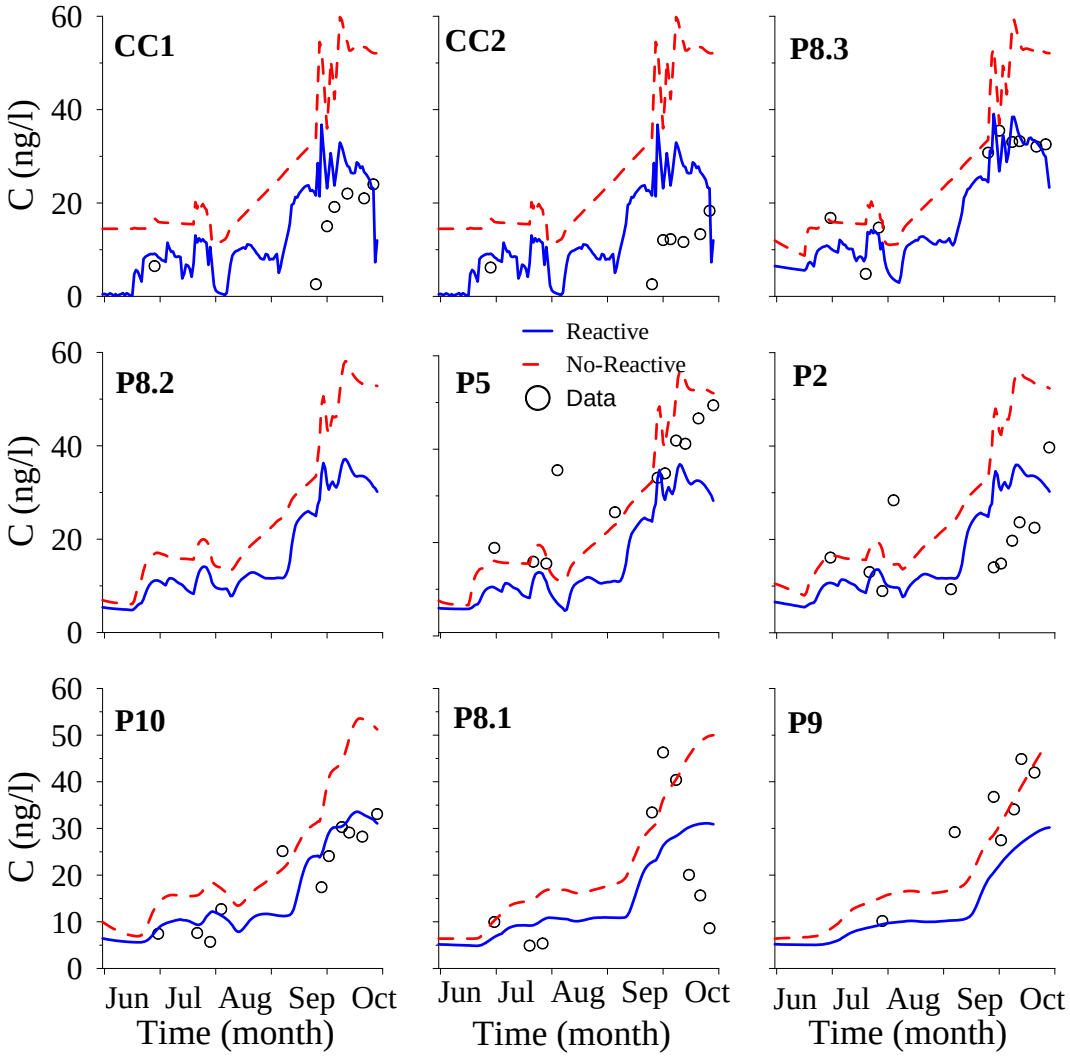

Figure 5.8: Measured sulfamethoxazole concentration (blue circles) and calculated sulfamethoxazole concentration considering non-reactive transport (dashed red line), and reactive transport (blue line) at the monitoring point.

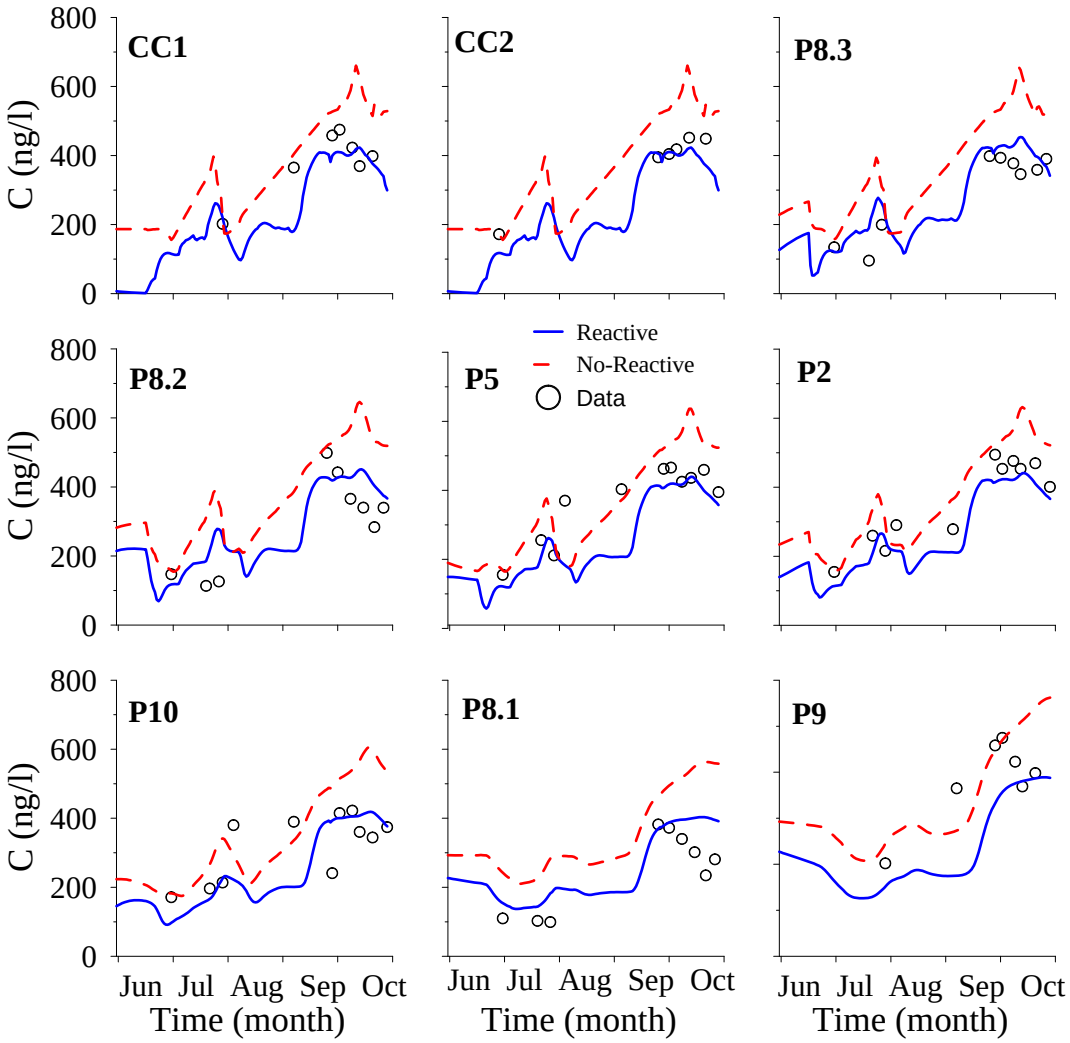

Figure 5.9: Measured tolyltriazole concentration (blue circles) and calculated tolyltriazole concentration considering non-reactive transport (dashed red line), and reactive transport (blue line) at the monitoring point.

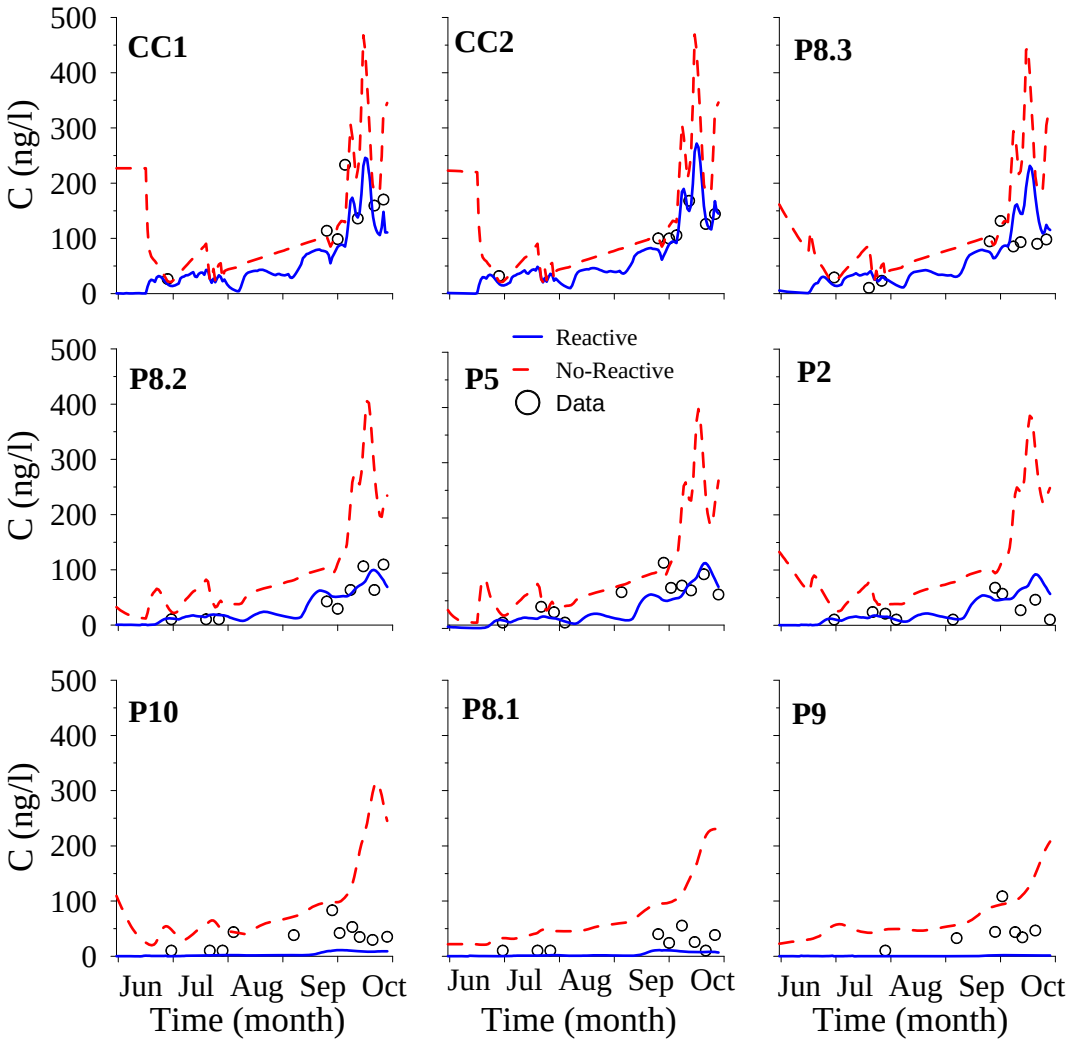

Figure 5.10: Measured iohexol concentration (Blue circles) and calculated iohexol concentration considering non reactive transport (dashed red line), and reactive transport (blue line) at the monitoring point.

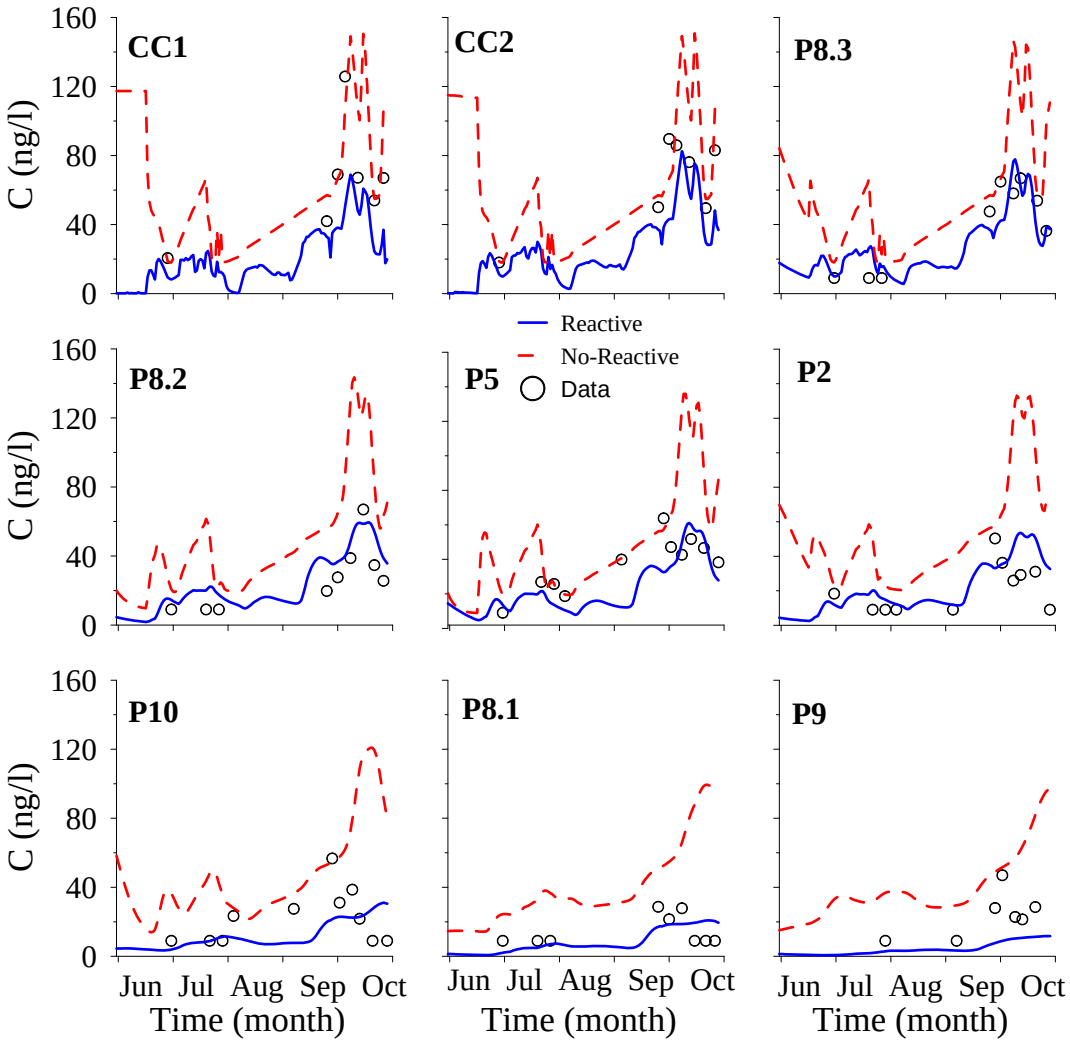

Figure 5.11: Measured iomeprol concentration (blue circles) and calculated iomeprol concentration considering non-reactive transport (dashed red line), and reactive transport (blue line) at the monitoring point.

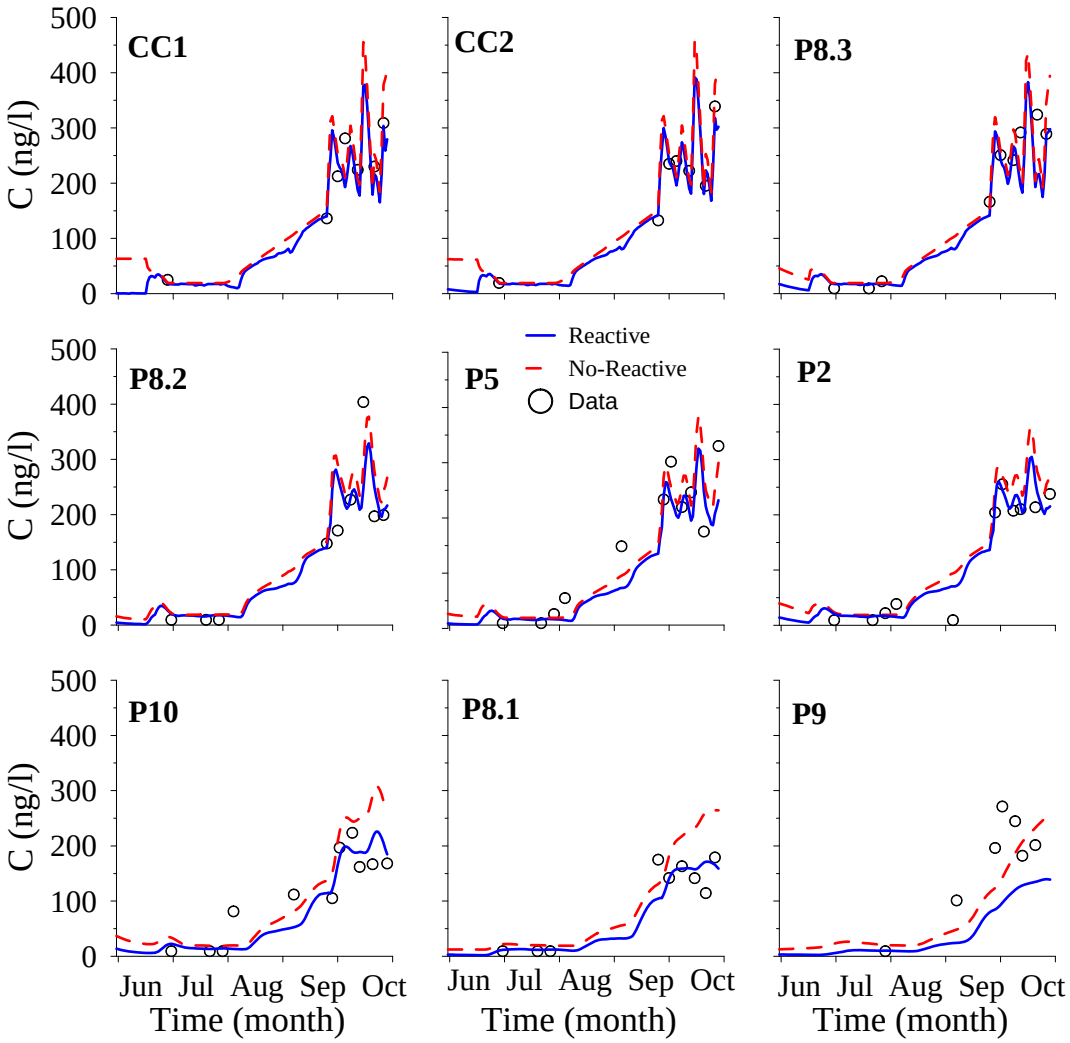

Figure 5.12: Measured iopamidol concentration (blue circles) and calculated iopamidol concentration considering non-reactive transport (dashed red line), and reactive transport (blue line) at the monitoring point.

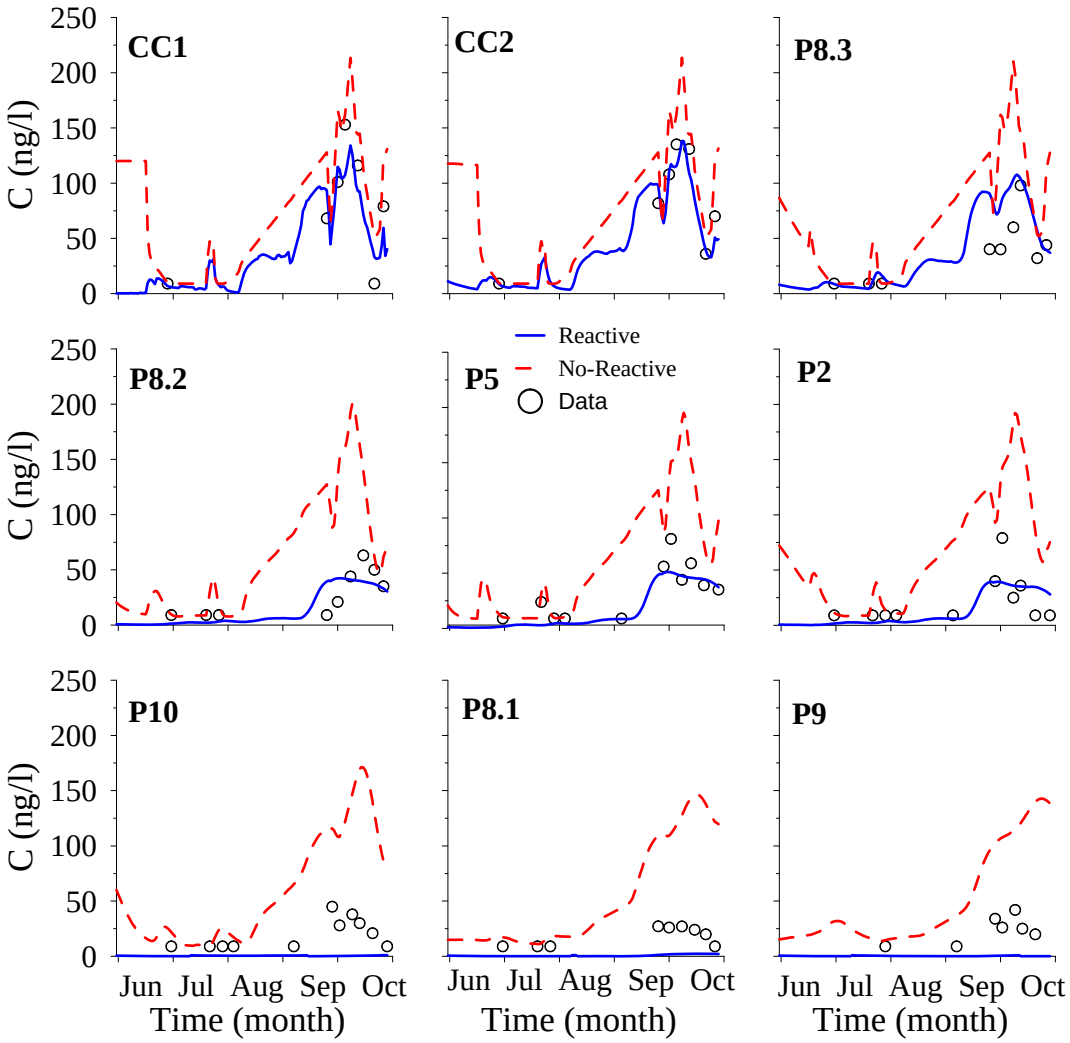

Figure 5.13: Measured iopromide concentration (blue circles) and calculated iopromide concentration considering non-reactive transport (dashed red line), and reactive transport (blue line) at the monitoring point.

5.4 Conclusions

Reactive transport modeling is required to evaluate biotransformation and retardation parameters in real-scale systems, where flow and transport are usually transient and often complex. Addressing this complexity demands a numerical model that, to be reliable, can be calibrated against head values and, possibly, tracer test data. Such a model can then be used to derive reactive transport parameters calibrated against concentration data from several sampling points while acknowledging the broad residence time distributions associated with complex flow regimes. Therefore, the resulting degradation and retardation values are more robust than those obtained from differences in time and concentration between two individual points.

The most relevant result from the calibration of our experiments was that degradation rates found for the reactive barrier were one order of magnitude faster than those of the aquifer downstream, and either faster or within the higher range of values obtained in other column and field experiments. Most of the EOCs exhibited fast degradation rates, with half-lives of a few hours in the barrier and weeks to months in the rest of the aquifer. Carbamazepine is one of the most resilient pharmaceuticals, with a half-life of 17 h in the barrier and approximately 50 d downstream. Although slow, carbamazepine degraded faster than described in the literature. The corrosion inhibitor tolyltriazole was the slowest reacting EOC tested, with a half-life of several days in the barrier and practically not degraded at all in the aquifer downstream. The contrast media behaved consistently and also degraded faster than reported in the literature. They exhibited half-lives of a few days in the reactive barrier and a month downstream. The degradation pattern described for all the studied EOCs emphasizes the role of organic matter as the provider of the DOC necessary to sustain the microbial communities required for biodegradation.

Regarding retardation, it is clear that the coefficients obtained for the barrier were distinctly higher than those downstream, where the organic carbon content was low. With the exception of the contrast media, there was no retardation of the EOCs downstream of the barrier. It must be

noted, however, that retardation is difficult to estimate downstream of the barrier when degradation in the barrier is intense, because of the resulting low downstream concentrations. Retardation coefficients in the barrier were higher than those reported for column and field experiments. With the exception of carbamazepine, retardation in the barrier was equally efficient for neutral and anionic EOCs. This suggests that, in addition to the role of organic matter, the iron oxide added to the barrier filling may have an active role in the sorption of gemfibrozil, ibuprofen, and sulfamethoxazole.

In summary, both biodegradation and sorption were clearly more active in the barrier than downstream. The relationship between these two processes, however, is not clear. Our results suggest that the increased residence time for the EOCs in the barrier enhances biodegradation efficiency.

Chapter 6

Conclusions

A correct characterization of the artificial recharge sites (AR) is essential for the appropriate interpretation and/or prediction of pollutants fate in aquifers. The heterogeneity of the natural media together with the complex flux generated beneath the infiltration basin define the residence time distribution (RTDs) of the recharge water and the mixing betwee recharged waters of different ages and the regional groundwater. Knowing the RTDs from a pulse tracer tests provides a simple method to estimate flow and conservative transport parameters with a numerical model. In our specific recharge system, RTDs were quite narrow at points immediately adjacent to the basin and very broad at points slightly away. The broad RTDs imply significant mixing of recently recharged water with water recharged some time before. Moreover, preferential flow, estimated with the tracer breakthrough curves, ensured mixing of recharged water affected by the reactive barrier with that less modified flowing through the preferential paths.

The reactive barrier was effective in releasing DOC into the recharge water. This extra source of DOC was required to achieve diverse redox conditions below the infiltration basin and the aquifer, because the amount of dissolved organic carbon (DOC) in the infiltration water was barely enough to consume the dissolved oxygen. The most reductive conditions (manganese- and iron-

reducing) were observed in the unsaturated zone immediately beneath the infiltration basin. The mixing of the water traveling through preferential flow paths with the most reducing water through the barrier caused diverse redox conditions downstream (nitrate-, manganese-, and iron-reducing conditions), promoting diverse metabolic paths for a wide range of EOCs present in the water source.

The reactive barrier was successful in enhancing removal of several of the studied EOCs during AR. In a first instance one could think that the reducing conditions achieved beneath the barrier would slow down the removal of those EOCs preferentially removed under aerobic conditions, such as ibuprofen or paracetamol, which did fully degrade before the reactive barrier installation. Nevertheless, according to the estimated λ values, the degradation of such EOCs during passage through the reactive barrier was similar or faster than the degradation reported in the literature. A key factor might be the observed broad RTDs which indicate mixing of waters recharged at diverse times (more than twenty days in the monitoring points more distant).

The qualitative analysis indicates that the removal rates of the studied EOCs were either unaffected (H-benzotriazole, tolyltriazole, carbamazepine) or significantly increased (atenolol, gemfibrozil, cetirizine, sulfamethoxazole, caffeine, benzoylecgonine) with the reactive barrier.

A reactive transport modeling was required for more thorough analysis of the reactive barrier performance and for the quantitative estimation of reactive transport parameters. The estimation of these parameters from a numerical model takes into accounts the complexity of the flow and the broad RTDs. Therefore, the degradation rates obtained were more robust than those obtained from differences in time and concentration between two individual points and allowed a more realistic comparison with values reported by others. The estimated rates indicate that the removal of the studied EOCs in our AR site were fast, with half-lives of a few hours in the reactive barrier and some 50 d downstream. In general degradation rates are faster in the reactive barrier than in the aquifer, where less bioavailable DOC was present and less reducing conditions prevailed. The estimated rates were similar or faster than those reported in the literature. Furthermore, retardation

factors estimated from the reactive transport model were in most cases only relevant in the reactive barrier, where organic mater surfaces predominated. the estimated retardation factor was relevant in the rest of the aquifer only for paracetamol (acetominofen) and contrast media.

Briefly the performance of the artificial recharge through infiltration a basin can be efficiently enhanced regarding to the EOCs removal by the installation of the proposed reactive barrier. Other than this improvement in the EOCs removal, no undesirable effects were observed. In fact, the clogging of the basin was probably delayed due to the vegetation growth favored by the compost, which we will analyze in the future. In any case, it is clear that the addition of the reactive barrier contributes to the renaturalization of reclaimed water.

Bibliography

Abarca, E., E. Vázquez-Suñé, J. Carrera, B. Capino, D. Gámez, and F. Batlle (2006), Optimal design of measures to correct seawater intrusion, *Water Resources Research*, *42*(9), doi:10.1029/2005WR004524, w09415.

Alewell, C., S. Paul, G. Lischeid, and F. Storck (2008), Co-regulation of redox processes in freshwater wetlands as a function of organic matter availability?, *Science of The Total Environment*, *404*(2–3), 335–342, doi:10.1016/j.scitotenv.2007.11.001.

Alidina, M., D. Li, and J. E. Drewes (2014a), Investigating the role for adaptation of the microbial community to transform trace organic chemicals during managed aquifer recharge, *Water Research*, *56*(0), 172 – 180, doi:10.1016/j.watres.2014.02.046.

Alidina, M., D. Li, M. Ouf, and J. E. Drewes (2014b), Role of primary substrate composition and concentration on attenuation of trace organic chemicals in managed aquifer recharge systems, *Journal of Environmental Management*, *144*(0), 58 – 66, doi:10.1016/j.jenvman.2014.04.032.

Amy, G., and J. E. Drewes (2007), Soil aquifer treatment (sat) as a natural and sustainable wastewater reclamation/reuse technology: Fate of wastewater effluent organic matter (efom) and trace organic compounds, *Environmental Monitoring & Assessment*, *129*.

Anonymous (2016), Interactive comment on "tracer test modeling for local scale residence time distribution characterization in an artificial recharge site" by c. valhondo et al., *Hydrol. Earth Syst. Sci. Discuss.*, doi:10.5194/hess-2016-197-RC3.

Arye, G., I. Dror, and B. Berkowitz (2011), Fate and transport of carbamazepine in soil aquifer treatment (sat) infiltration basin soils, *Chemosphere*, *82*(2), 244–252, doi:10.1016/j.chemosphere.2010.09.062.

Bahlmann, A., J. J. Carvalho, M. G. Weller, U. Panne, and R. J. Schneider (2012), Immunoassays as high-throughput tools: Monitoring spatial and temporal variations of carbamazepine, caffeine and cetirizine in surface and wastewaters, *Chemosphere*, *89*(11), 1278–1286, doi:10.1016/j.chemosphere.2012.05.020.

Banzhaf, S., K. Nödler, T. Licha, A. Krein, and T. Scheytt (2012), Redox-sensitivity and mobility of selected pharmaceutical compounds in a low flow column experiment, *Science of The Total Environment*, *438*(0), 113 – 121, doi:10.1016/j.scitotenv.2012.08.041.

Barbieri, M., et al. (2011), Microcosm experiments to control anaerobic redox conditions when studying the fate of organic micropollutants in aquifer material, *Journal of Contaminant Hydrology*, *126*(3–4), 330–345, doi:10.1016/j.jconhyd.2011.09.003.

Barbieri, M., et al. (2012), Formation of diclofenac and sulfamethoxazole reversible transformation products in aquifer material under denitrifying conditions: Batch experiments, *Science of The Total Environment*, *426*(0), 256–263, doi:10.1016/j.scitotenv.2012.02.058.

Bear, J., and Y. Bachmat (1984), *Transport Phenomena in Porous Media — Basic Equations*, pp. 3–61, Springer Netherlands, Dordrecht, doi:10.1007/978-94-009-6175-3_1.

Becker, T. E., J. F. Clark, and T. A. Johnson (2014), Heat, ^{10}b-enriched boric acid, and bromide as recycled groundwater tracers for managed aquifer recharge: Case study, *Journal of Hydrological Engineering, ASCE*, *20*, doi:10.1061/(ASCE)HE.1943-5584.

Bekele, E., S. Toze, B. Patterson, and S. Higginson (2011), Managed aquifer recharge of treated wastewater: Water quality changes resulting from infiltration through the vadose zone, *Water Research*, *45*(17), 5764 – 5772, doi:10.1016/j.watres.2011.08.058.

Bekele, E., B. Patterson, S. Toze, A. Furness, S. Higginson, and M. Shackleton (2014), Aquifer residence times for recycled water estimated using chemical tracers and the propagation of temperature signals at a managed aquifer recharge site in australia, *Hydrogeology Journal*, *22*(6), 1383–1401, doi:10.1007/s10040-014-1142-0.

Bertelkamp, C., J. Reungoat, E. Cornelissen, N. Singhal, J. Reynisson, A. Cabo, J. van der Hoek, and A. Verliefde (2014), Sorption and biodegradation of organic micropollutants during river bank filtration: A laboratory column study, *Water Research*, *52*(0), 231 – 241, doi:10.1016/j.watres.2013.10.068.

Borisover, M., M. Sela, and B. Chefetz (2011), Enhancement effect of water associated with natural organic matter (nom) on organic compound–nom interactions: A case study with carbamazepine, *Chemosphere*, *82*(10), 1454–1460, doi:10.1016/j.chemosphere.2010.11.035.

Bound, J., and N. Voulvoulis (2004), Pharmaceuticals in the aquatic environment–a comparison of risk assessment strategies, *Chemosphere*, *56*(11), 1143 – 1155, doi:10.1016/j.chemosphere.2004.05.010.

Bouwer, H. (2002), Artificial recharge of groundwater: hydrogeology and engineering, *Hydrogeology Journal*, *10*, 121–142, doi:10.1007/s10040-001-0182-4, 10.1007/s10040-001-0182-4.

Burke, V., S. Treumann, U. Duennbier, J. Greskowiak, and G. Massmann (2013), Sorption behavior of 20 wastewater originated micropollutants in groundwater – column experiments with pharmaceutical residues and industrial agents, *Journal of Contaminant Hydrology*, (0), –, doi:http://dx.doi.org/10.1016/j.jconhyd.2013.08.001.

Butler, J. J., J. M. Healey, G. W. McCall, E. J. Garnett, and S. P. Loheide (2002), Hydraulic tests with direct-push equipment, *Ground Water*, *40*(1), 25–36, doi:10.1111/j.1745-6584.2002.tb02488.x.

Carballa, M., F. Omil, J. M. Lema, M. Llompart, C. García-Jares, I. Rodríguez, M. Gómez, and

T. Ternes (2004), Behavior of pharmaceuticals, cosmetics and hormones in a sewage treatment plant, *Water Research*, *38*(12), 2918 – 2926, doi:10.1016/j.watres.2004.03.029.

Carrera, J., A. Alcolea, A. Medina, J. Hidalgo, and L. J. Slooten (2005), Inverse problem in hydrogeology, *Hydrogeology Journal*, *13*(1), 206–222, doi:10.1007/s10040-004-0404-7.

Chefetz, B., T. Mualem, and J. Ben-Ari (2008), Sorption and mobility of pharmaceutical compounds in soil irrigated with reclaimed wastewater, *Chemosphere*, *73*(8), 1335–1343, doi:10.1016/j.chemosphere.2008.06.070.

Clara, M., B. Strenn, and N. Kreuzinger (2004), Carbamazepine as a possible anthropogenic marker in the aquatic environment: investigations on the behaviour of carbamazepine in wastewater treatment and during groundwater infiltration, *Water Research*, *38*(4), 947–954, doi:10.1016/j.watres.2003.10.058.

Clark, J. F. (2016), Interactive comment on "tracer test modeling for local scale residence time distribution characterization in an artificial recharge site" by c. valhondo et al., *Hydrol. Earth Syst. Sci. Discuss.*, doi:10.5194/hess-2016-197-RC1.

Clark, J. F., G. Hudson, a. W. G. Davisson, M. L., and R. Herndon (2004), Geochemical imaging of flow near an artificial recharge facility, orange county, california, *Grownd Water*, *42*(2), 167–174, doi:10.1111/j.1745-6584.2004.tb02665.x.

Clark, J. F., S. Morrissey, J. Dadakis, A. Hutchinson, and R. Herndon (2014), Investigation of groundwater flow variations near a recharge pond with repeat deliberate tracer experiments, *Water*, *6*, 1826–1839, doi:10.3390/w6061826.

Cueto-Felgueroso, L., and R. Juanes (2008), Nonlocal interface dynamics and pattern formation in gravity-driven unsaturated flow through porous media, *Phys. Rev. Lett.*, *101*, 244,504, doi:10.1103/PhysRevLett.101.244504.

D'Agnese, F. A., C. C. Faunt, M. C. Hill, and A. K. Turner (1999), Death valley regional

ground-water flow model calibration using optimal parameter estimation methods and geo-scientific information systems, *Advances in Water Resources*, *22*(8), 777–790, doi:10.1016/S0309-1708(98)00053-0.

de Dreuzy, J.-R., J. Carrera, M. Dentz, and T. Le Borgne (2012), Asymptotic dispersion for two-dimensional highly heterogeneous permeability fields under temporally fluctuating flow, *Water Resources Research*, *48*(1), doi:10.1029/2011WR011129, w01532.

Dean, R. A., E. T. Harper, N. Dumaual, D. A. Stoeckel, and W. F. Bosron (1992), Effects of ethanol on cocaine metabolism: Formation of cocaethylene and norcocaethylene, *Toxicology and Applied Pharmacology*, *117*(1), 1 – 8, doi:http://dx.doi.org/10.1016/0041-008X(92)90210-J.

Dentz, M., T. L. Borgne, A. Englert, and B. BijeljicD (2011), Mixing, spreading and reaction in heterogeneous media: A brief review, *Journal of Contaminant Hydrology*, *120–121*, 1–17, doi:10.1016/j.jconhyd.2010.05.002, reactive Transport in the Subsurface: Mixing, Spreading and Reaction in Heterogeneous Media.

Díaz-Cruz, M. S., and D. Barceló (2008), Trace organic chemicals contamination in ground water recharge, *Chemosphere*, *72*(3), 333–342, doi:10.1016/j.chemosphere.2008.02.031.

Dickenson, E. R., S. A. Snyder, D. L. Sedlak, and J. E. Drewes (2011), Indicator compounds for assessment of wastewater effluent contributions to flow and water quality, *Water Research*, *45*(3), 1199–1212, doi:10.1016/j.watres.2010.11.012.

Dietrich, P., J. J. Butler, and K. Faiß (2008), A rapid method for hydraulic profiling in unconsolidated formations, *Ground Water*, *46*(2), 323–328, doi:10.1111/j.1745-6584.2007.00377.x.

Dillon, P., P. Pavelic, S. Toze, S. Rinck-Pfeiffer, R. Martin, A. Knapton, and D. Pidsley (2006), Role of aquifer storage in water reuse, *Desalination*, *188*(1–3), 123 – 134, doi:10.1016/j.desal.2005.04.109.

Drewes, J. E. (2009), Ground water replenishment with recycled water–water quality improvements during managed aquifer recharge, *Ground Water*, *47*(4), 502–505, doi:10.1111/j.1745-6584.2009.00587_5.x.

Drewes, J. E., T. Heberer, T. Rauch, and K. Reddersen (2003a), Fate of pharmaceuticals during ground water recharge, *Ground Water Monitoring & Remediation*, *23*(3), 64–72, doi:10.1111/j.1745-6592.2003.tb00684.x.

Drewes, J. E., M. Reinhard, and P. Fox (2003b), Comparing microfiltration-reverse osmosis and soil-aquifer treatment for indirect potable reuse of water, *Water Research*, *37*(15), 3612 – 3621, doi:10.1016/S0043-1354(03)00230-6.

Du, B., A. E. Price, W. C. Scott, L. A. Kristofco, A. J. Ramirez, C. K. Chambliss, J. C. Yelderman, and B. W. Brooks (2014), Comparison of contaminants of emerging concern removal, discharge, and water quality hazards among centralized and on-site wastewater treatment system effluents receiving common wastewater influent, *Science of The Total Environment*, *466âĂŞ467*(0), 976 – 984, doi:10.1016/j.scitotenv.2013.07.126.

Farnsworth, C. E., and J. G. Hering (2011), Inorganic geochemistry and redox dynamics in bank filtration settings, *Environmental Science & Technology*, *45*(12), 5079–5087, doi:10.1021/es2001612.

Flury, M., and N. N. Wai (2003), Dyes as tracers for vadose zone hydrology, *Reviews of Geophysics*, *41*, doi:doi:10.1029/2001RG000109.

Fogg, G. E. (1986), Groundwater flow and sand body interconnectedness in a thick, multiple-aquifer system, *Water Resources Research*, *22*(5), 679–694, doi:10.1029/WR022i005p00679.

Gámez, D., J. Simó, F. Lobo, A. Barnolas, J. Carrera, and E. Vázquez-Suñé (2009), Onshore–offshore correlation of the llobregat deltaic system, spain: Development of deltaic geometries under different relative sea-level and growth fault influences, *Sedimentary Geology*, *217*(1–4), 65–84, doi:10.1016/j.sedgeo.2009.03.007.

Göbel, A., C. S. McArdell, M. J.-F. Suter, and W. Giger (2004), Trace determination of macrolide and sulfonamide antimicrobials, a human sulfonamide metabolite, and trimethoprim in wastewater using liquid chromatography coupled to electrospray tandem mass spectrometry, *Analytical Chemistry*, *76*(16), 4756–4764, doi:10.1021/ac0496603, pMID: 15307787.

Grenni, P., L. Patrolecco, N. Ademollo, A. Tolomei, and A. Barra Caracciolo (2013), Degradation of gemfibrozil and naproxen in a river water ecosystem, *Microchemical Journal*, *107*(0), 158–164, doi:10.1016/j.microc.2012.06.008.

Greskowiak, J., H. Prommer, G. Massmann, C. D. Johnston, G. Nützmann, and A. Pekdeger (2005), The impact of variably saturated conditions on hydrogeochemical changes during artificial recharge of groundwater, *Applied Geochemistry*, *20*(7), 1409 – 1426, doi:10.1016/j.apgeochem.2005.03.002.

Greskowiak, J., H. Prommer, G. Massmann, , and G. Nützmann (2006), Modeling seasonal redox dynamics and the corresponding fate of the pharmaceutical residue phenazone during artificial recharge of groundwater, *Environmental Science & Technology*, *40*(21), 6615–6621, doi:10.1021/es052506t, pMID: 17144286.

Grünheid, S., G. Amy, and M. Jekel (2005), Removal of bulk dissolved organic carbon (doc) and trace organic compounds by bank filtration and artificial recharge, *Water Research*, *39*(14), 3219–3228, doi:10.1016/j.watres.2005.05.030.

Grünheid, S., U. Huebner, and M. Jekel (2008), Impact of temperature on biodegradation of bulk and trace organics during soil passage in an indirect reuse system., *Water Science & Technology*, *57*(7), 987–994, doi:10.2166/wst.2008.207.

Haggerty, R., and S. M. Gorelick (1995), Multiple-rate mass transfer for modeling diffusion and surface reactions in media with pore-scale heterogeneity, *Water Resources Research*, *31*(10), 2383–2400, doi:10.1029/95WR10583.

Hart, D., L. Davis, L. Erickson, and T. Callender (2004), Sorption and partitioning parameters of benzotriazole compounds, *Microchemical Journal*, *77*(1), 9 – 17, doi:10.1016/j.microc.2003.08.005.

Heberer, T. (2002), Occurrence, fate, and removal of pharmaceutical residues in the aquatic environment: a review of recent research data, *Toxicology Letters*, *131*(1-2), 5–17, doi:10.1016/S0378-4274(02)00041-3.

Heberer, T., A. Mechlinski, B. Fanck, A. Knappe, G. Massmann, A. Pekdeger, and B. Fritz (2004), Field studies on the fate and transport of pharmaceutical residues in bank filtration, *Ground Water Monitoring & Remediation*, *24*(2), 70–77, doi:10.1111/j.1745-6592.2004.tb00714.x.

Henzler, A. F., J. Greskowiak, and G. Massmann (2014), Modeling the fate of organic micropollutants during river bank filtration (berlin, germany), *Journal of Contaminant Hydrology*, *156*(0), 78 – 92, doi:10.1016/j.jconhyd.2013.10.005.

Hidalgo, J. J., L. Slooten, A. Medina, and J. Carrera (2004), A newton-raphson based code for seawater intrusion modelling and parameter estimation, in *Groundwater and Saline Intrusion Selected Papers from the 18th Salt Water Intrusion Meeting, 18th SWIM*, edited by S. Hidrogeologia y Aguas Subterraneas IGME, Madrid, 15, pp. 111–120, IGME, doi:84-7840-588-7.

Hill, D. E., and J. Y. Parlange (1972), Wetting front instability in layered soils, *Soil Science Society of America Journal*, *36*, 697–702, doi:10.2136/sssaj1972.03615995003600050010x.

Hillebrand, O., K. Nödler, T. Licha, M. Sauter, and T. Geyer (2012), Identification of the attenuation potential of a karst aquifer by an artificial dualtracer experiment with caffeine, *Water Research*, *46*(16), 5381 – 5388, doi:10.1016/j.watres.2012.07.032.

Hillebrand, O., S. Musallam, L. Scherer, K. Nödler, and T. Licha (2013), The challenge of sample-stabilisation in the era of multi-residue analytical methods: A practical guideline for the stabilisation of 46 organic micropollutants in aqueous samples, *Science of The Total Environment*, *454–455*(0), 289–298, doi:10.1016/j.scitotenv.2013.03.028.

Hoppe-Jones, C., G. Oldham, and J. E. Drewes (2010), Attenuation of total organic carbon and unregulated trace organic chemicals in u.s. riverbank filtration systems, *Water Research*, *44*(15), 4643–4659, doi:10.1016/j.watres.2010.06.022.

Iribar, V., J. Carrera, E. Custodio, and A. Medina (1997), Inverse modelling of seawater intrusion in the llobregat delta deep aquifer, *Journal of Hydrology*, *198*, 226 – 244, doi: 10.1016/S0022-1694(96)03290-8.

Jelic, A., F. Fatone, S. Di Fabio, M. Petrovic, F. Cecchi, and D. Barcelo (2012), Tracing pharmaceuticals in a municipal plant for integrated wastewater and organic solid waste treatment, *Science of The Total Environment*, *433*(0), 352–361, doi:10.1016/j.scitotenv.2012.06.059.

Jones, O., N. Voulvoulis, and J. Lester (2004), Potential ecological and human health risks associated with the presence of pharmaceutically active compounds in the aquatic environment, *Critical reviews in toxicology*, *34*, 335–350, doi:10.1080/10408440490464697.

Karnjanapiboonwong, A., A. N. Morse, J. D. Maul, and T. A. Anderson (2010), Sorption of estrogens, triclosan, and caffeine in a sandy loam and a silt loam soil, *Journal of Soils and Sediments*, *10*(7), 1300–1307, doi:10.1007/s11368-010-0223-5.

Kasprzyk-Hordern, B., R. M. Dinsdale, and A. J. Guwy (2008), The occurrence of pharmaceuticals, personal care products, endocrine disruptors and illicit drugs in surface water in south wales, uk, *Water Research*, *42*(13), 3498–3518, doi:10.1016/j.watres.2008.04.026.

Köck-Schulmeyer, M., et al. (2011), Wastewater reuse in mediterranean semi-arid areas: The impact of discharges of tertiary treated sewage on the load of polar micro pollutants in the llobregat river (ne spain), *Chemosphere*, *82*(5), 670–678, doi:10.1016/j.chemosphere.2010.11.005.

Konikow, L. F., and E. Kendy (2005), Groundwater depletion: A global problem, *Hydrogeology Journal*, *13*, 317–320, doi:10.1007/s10040-004-0411-8, 10.1007/s10040-004-0411-8.

Kosonen, J., and L. Kronberg (2009), The occurrence of antihistamines in sewage waters and in recipient rivers., *Environ Sci Pollut Res Int*, *16*(5), 555–564, doi:10.1007/s11356-009-0144-2.

Kröger, K. F. (2014), Behavior of selected organic micro pollutants during alternative wastewater treatment, Master's thesis, M.Sc. Course hydrogeology and environmental geociences. University of Göttingen, doi:21167136.

Lam, M. W., C. J. Young, R. A. Brain, D. J. Johnson, M. A. Hanson, C. J. Wilson, S. M. Richards, K. R. Solomon, and S. A. Mabury (2004), Aquatic persistence of eight pharmaceuticals in a microcosm study, *Environmental Toxicology and Chemistry*, *23*(6), 1431–1440, doi:10.1897/03-421.

Lapworth, D., N. Baran, M. Stuart, and R. Ward (2012), Emerging organic contaminants in groundwater: A review of sources, fate and occurrence, *Environmental Pollution*, *163*(0), 287–303, doi:10.1016/j.envpol.2011.12.034.

Laws, B. V., E. R. Dickenson, T. A. Johnson, S. A. Snyder, and J. E. Drewes (2011), Attenuation of contaminants of emerging concern during surface-spreading aquifer recharge, *Science of The Total Environment*, *409*(6), 1087–1094, doi:10.1016/j.scitotenv.2010.11.021.

Le Borgne, T., M. Dentz, D. Bolster, J. Carrera, J.-R. de Dreuzy, and P. Davy (2010), Non-fickian mixing: Temporal evolution of the scalar dissipation rate in heterogeneous porous media, *Advances in Water Resources*, *33*(12), 1468–1475, doi:10.1016/j.advwatres.2010.08.006.

Levine, A. D., and T. Asano (2004), Peer reviewed: Recovering sustainable water from wastewater, *Environmental Science & Technology*, *38*(11), 201A–208A, doi:10.1021/es040504n.

Li, D., M. Alidina, M. Ouf, J. O. Sharp, P. Saikaly, and J. E. Drewes (2013), Microbial community evolution during simulated managed aquifer recharge in response to different biodegradable dissolved organic carbon (bdoc) concentrations, *Water Research*, *47*(7), 2421 – 2430, doi:10.1016/j.watres.2013.02.012.

Lim, M.-H., S. A. Snyder, and D. L. Sedlak (2008), Use of biodegradable dissolved organic carbon (bdoc) to assess the potential for transformation of wastewater-derived contaminants in surface waters, *Water Research*, *42*(12), 2943–2952, doi:10.1016/j.watres.2008.03.008.

Lin, K., and J. Gan (2011), Sorption and degradation of wastewater-associated non-steroidal anti-inflammatory drugs and antibiotics in soils, *Chemosphere*, *83*(3), 240 – 246, doi:10.1016/j.chemosphere.2010.12.083.

Liu, F., G. Ying, J. Yang, L. Zhou, R. Tao, L. Wang, L. Zhang, and P. Peng (2010), Dissipation of sulfamethoxazole, trimethoprim and tylosin in a soil under aerobic and anoxic conditions, *Environ. Chem.*, *7*(4), 370–376, doi:10.1071/EN09160.

Liu, Y.-S., G.-G. Ying, A. Shareef, and R. S. Kookana (2013), Biodegradation of three selected benzotriazoles in aquifer materials under aerobic and anaerobic conditions, *Journal of Contaminant Hydrology*, *151*(0), 131 – 139, doi:10.1016/j.jconhyd.2013.05.006.

Maeng, S. K., E. Ameda, S. K. Sharma, G. Grützmacher, and G. L. Amy (2010), Organic micropollutant removal from wastewater effluent-impacted drinking water sources during bank filtration and artificial recharge, *Water Research*, *44*(14), 4003–4014, doi:10.1016/j.watres.2010.03.035.

Maeng, S. K., S. K. Sharma, C. D. Abel, A. Magic-Knezev, and G. L. Amy (2011a), Role of biodegradation in the removal of pharmaceutically active compounds with different bulk organic matter characteristics through managed aquifer recharge: Batch and column studies, *Water Research*, *45*(16), 4722–4736, doi:10.1016/j.watres.2011.05.043.

Maeng, S. K., S. K. Sharma, K. Lekkerkerker-Teunissen, and G. L. Amy (2011b), Occurrence and fate of bulk organic matter and pharmaceutically active compounds in managed aquifer recharge: A review, *Water Research*, *45*(10), 3015–3033, doi:10.1016/j.watres.2011.02.017.

Maeng, S. K., S. K. Sharma, C. D. Abel, A. Magic-Knezev, K.-G. Song, and G. L. Amy (2012), Effects of effluent organic matter characteristics on the removal of bulk organic matter and

selected pharmaceutically active compounds during managed aquifer recharge: Column study, *Journal of Contaminant Hydrology*, *140–141*(0), 139 – 149, doi:10.1016/j.jconhyd.2012.08.005.

Maoz, A., and B. Chefetz (2010), Sorption of the pharmaceuticals carbamazepine and naproxen to dissolved organic matter: Role of structural fractions, *Water Research*, *44*(3), 981–989, doi:10.1016/j.watres.2009.10.019.

Martin, P., and E. Frind (1998), Modeling a complex multi-aquifer system: The waterloo moraine, *Ground Water*, *36*(4), 679–690, doi:10.1111/j.1745-6584.1998.tb02843.x.

Massmann, G., J. Greskowiak, U. Dünnbier, S. Zuehlke, A. Knappe, and A. Pekdeger (2006), The impact of variable temperatures on the redox conditions and the behaviour of pharmaceutical residues during artificial recharge, *Journal of Hydrology*, *328*(1-2), 141–156, doi:10.1016/j.jhydrol.2005.12.009.

Massmann, G., U. Dünnbier, T. Heberer, and T. Taute (2008a), Behaviour and redox sensitivity of pharmaceutical residues during bank filtration - investigation of residues of phenazone-type analgesics, *Chemosphere*, *71*(8), 1476–1485, doi:10.1016/j.chemosphere.2007.12.017.

Massmann, G., J. Sültenfuß, U. Dünnbier, A. Knappe, T. Taute, and A. Pekdeger (2008b), Investigation of groundwater residence times during bank filtration in berlin: a multi-tracer approach, *Hydrological Processes*, *22*, 788–801, doi:10.1002/hyp.6649.

McMahon, P. B., and F. H. Chapelle (2008), Redox processes and water quality of selected principal aquifer systems, *Ground Water*, *46*(2), 259–271, doi:10.1111/j.1745-6584.2007.00385.x.

Medina, A., and J. Carrera (1996), Coupled estimation of flow and solute transport parameters, *Water Resources Research*, *32*(10), 3063–3076, doi:10.1029/96WR00754.

Medina, A., and J. Carrera (2003), Geostatistical inversion of coupled problems: dealing with computational burden and different types of data, *Journal of Hydrology*, *281*(4), 251–264, doi:10.1016/S0022-1694(03)00190-2.

Mohatt, J. L., L. Hu, K. T. Finneran, and T. J. Strathmann (2011), Microbially mediated abiotic transformation of the antimicrobial agent sulfamethoxazole under iron-reducing soil conditions, *Environmental Science & Technology*, *45*(11), 4793–4801, doi:10.1021/es200413g.

Moore, J., P. C. Lichtner, A. F. White, and S. L. Brantley (2012), Using a reactive transport model to elucidate differences between laboratory and field dissolution rates in regolith, *Geochimica et Cosmochimica Acta*, *93*, 235 – 261, doi:10.1016/j.gca.2012.03.021.

Nödler, K., T. Licha, K. Bester, and M. Sauter (2010), Development of a multi-residue analytical method, based on liquid chromatography-tandem mass spectrometry, for the simultaneous determination of 46 micro-contaminants in aqueous samples, *Journal of Chromatography A*, *1217*(42), 6511–6521, doi:10.1016/j.chroma.2010.08.048.

Nödler, K., T. Licha, M. Barbieri, and S. PÃľrez (2012), Evidence for the microbially mediated abiotic formation of reversible and non-reversible sulfamethoxazole transformation products during denitrification, *Water Research*, *46*(7), 2131 – 2139, doi:http://dx.doi.org/10.1016/j.watres.2012.01.028.

Nödler, K., O. Hillebrand, K. Idzik, M. Strathmann, F. Schiperski, J. Zirlewagen, and T. Licha (2013), Occurrence and fate of the angiotensin {II} receptor antagonist transformation product valsartan acid in the water cycle âĂŞ a comparative study with selected Îš-blockers and the persistent anthropogenic wastewater indicators carbamazepine and acesulfame, *Water Research*, *47*(0), 6650–6659, doi:10.1016/j.watres.2013.08.034.

Nham, H. T. T., J. Greskowiak, K. Nödler, M. A. Rahman, T. Spachos, B. Rusteberg, G. Massmann, M. Sauter, and T. Licha (2015), Modeling the transport behavior of 16 emerging organic contaminants during soil aquifer treatment, *Science of The Total Environment*, *514*, 450 – 458, doi:10.1016/j.scitotenv.2015.01.096.

Onesios, K. M., J. T. Yu, and E. J. Bouwer (2009), Biodegradation and removal of pharmaceuticals

and personal care products in treatment systems: a review, *Biodegradation*, *20*, 441–466, doi: 10.1007/s10532-008-9237-8.

Park, H., D. Cha, and P. Fox (2006), Uncertainty analysis of mound monitoring for recharged water from surface spreading basins, *Journal of Environmental Engineering*, *132*(12), 1527–1579, doi:10.1061/(ASCE)0733-9372(2006)132:12(1572).

Patterson, B., M. Shackleton, A. Furness, E. Bekele, J. Pearce, K. Linge, F. Busetti, T. Spadek, and S. Toze (2011), Behaviour and fate of nine recycled water trace organics during managed aquifer recharge in an aerobic aquifer, *Journal of Contaminant Hydrology*, *122*(1–4), 53–62, doi:10.1016/j.jconhyd.2010.11.003.

Pedersen, J. A., M. Soliman, and I. H. M. Suffet (2005), Human pharmaceuticals, hormones, and personal care product ingredients in runoff from agricultural fields irrigated with treated wastewater, *Journal of Agricultural and Food Chemistry*, *53*(5), 1625–1632, doi:10.1021/jf049228m, pMID: 15740050.

Poeter, E. P., and M. C. Hill (1997), Inverse models: A necessary next step in ground-water modeling, *Ground Water*, *35*(2), 250–260, doi:10.1111/j.1745-6584.1997.tb00082.x.

Radjenović, J., S. Pérez, M. Petrović, and D. Barceló (2008), Identification and structural characterization of biodegradation products of atenolol and glibenclamide by liquid chromatography coupled to hybrid quadrupole time-of-flight and quadrupole ion trap mass spectrometry, *Journal of Chromatography A*, *1210*(2), 142–153, doi:10.1016/j.chroma.2008.09.060.

Radke, M., C. Lauwigi, G. Heinkele, T. E. MuÌĹrdter, and M. Letzel (2009), Fate of the antibiotic sulfamethoxazole and its two major human metabolites in a water sediment test, *Environmental Science & Technology*, *43*(9), 3135–3141, doi:10.1021/es900300u.

Ranieri, E., P. Verlicchi, and T. M. Young (2011), Paracetamol removal in subsurface flow constructed wetlands, *Journal of Hydrology*, *404*(3âĂŞ4), 130 – 135, doi:10.1016/j.jhydrol.2011.03.015.

Rauch-Williams, T., C. Hoppe-Jones, and J. Drewes (2010), The role of organic matter in the removal of emerging trace organic chemicals during managed aquifer recharge, *Water Research*, *44*(2), 449–460, doi:10.1016/j.watres.2009.08.027.

Reemtsma, T., U. Miehe, U. Duennbier, and M. Jekel (2010), Polar pollutants in municipal wastewater and the water cycle: Occurrence and removal of benzotriazoles, *Water Research*, *44*(2), 596 – 604, doi:http://dx.doi.org/10.1016/j.watres.2009.07.016, <ce:title>Emerging Contaminants in water: Occurrence, fate, removal and assessment in the water cycle (from wastewater to drinking water)</ce:title> ratios of either BTri or 5-TTri to the most persistent 4-TTri.

Regnery, J., A. Wing, M. Alidina, and J. Drewes (2015), Biotransformation of trace organic chemicals during groundwater recharge: How useful are first-order rate constants?, *Journal of Contaminant Hydrology*, *179*(0), 65 – 75, doi:10.1016/j.jconhyd.2015.05.008.

Rivera-Utrilla, J., M. Sánchez-Polo, M. A. Ferro-García, G. Prados-Joya, and R. Ocampo-Pérez (2013), Pharmaceuticals as emerging contaminants and their removal from water. a review, *Chemosphere*, *93*(0), 1268–1287, doi:http://dx.doi.org/10.1016/j.chemosphere.2013.07.059.

Samper, J., A. Sahuquillo, J. E. Capilla, and J. J. Gomez Hernández (1999), *La contaminación de las aguas subterraneas: un pproblem pendiente*, Ministerio de medio ambiente, doi:I.S.B.N.: 84-7840-364-7.

Schaffer, M., H. Börnick, K. Nödler, T. Licha, and E. Worch (2012a), Role of cation exchange processes on the sorption influenced transport of cationic beta-blockers in aquifer sediments, *Water Research*, *46*(17), 5472–5482, doi:10.1016/j.watres.2012.07.013.

Schaffer, M., N. Boxberger, H. Börnick, T. Licha, and E. Worch (2012b), Sorption influenced transport of ionizable pharmaceuticals onto a natural sandy aquifer sediment at different ph, *Chemosphere*, *87*(5), 513 – 520, doi:10.1016/j.chemosphere.2011.12.053.

Schaffer, M., K. F. Kröger, K. Nödler, C. Ayora, J. Carrera, M. Hernández, and T. Licha (2015), Influence of a compost layer on the attenuation of 28 selected organic micropollutants under

realistic soil aquifer treatment conditions: Insights from a large scale column experiment, *Water Research*, *74*, 110 – 121, doi:10.1016/j.watres.2015.02.010.

Schwarzenbach, R. P., B. I. Escher, K. Fenner, T. B. Hofstetter, C. A. Johnson, U. von Gunten, and B. Wehrli (2006), The challenge of micropollutants in aquatic systems, *Science*, *313*(5790), 1072–1077, doi:10.1126/science.1127291.

Selker, J. S., T. S. Steenhuis, and J.-Y. Parlange (1996), An engineering approach to fingered vadose pollutant transport, *Geoderma*, *70*(2–4), 197 – 206, doi:10.1016/0016-7061(95)00085-2.

Shamrukh, M., and A. Abdel-Wahab (2008), Riverbank filtration for sustainable water supply: application to a large-scale facility on the nile river, *Clean Technologies and Environmental Policy*, *10*(4), 351–358, doi:10.1007/s10098-007-0143-2.

Silva, L. J., C. M. Lino, L. M. Meisel, and A. Pena (2012), Selective serotonin re-uptake inhibitors (ssris) in the aquatic environment: An ecopharmacovigilance approach, *Science of The Total Environment*, *437*(0), 185 – 195, doi:10.1016/j.scitotenv.2012.08.021.

Silva, O., J. Carrera, M. Dentz, S. Kumar, A. Alcolea, and M. Willmann (2009), A general real-time formulation for multi-rate mass transfer problems, *Hydrol. Earth Syst. Sci.*, *13*(8), 1399–1411, doi:10.5194/hess-13-1399-2009.

Smart, P., and D. Smith (1976), Water tracing in tropical regions, the use of fluorometric techniques in jamaica, *Journal of Hydrology*, *30*(1–2), 179–195, doi:10.1016/0022-1694(76)90097-4.

Srinivasan, P., A. K. Sarmah, and M. Manley-Harris (2014), Sorption of selected veterinary antibiotics onto dairy farming soils of contrasting nature, *Science of The Total Environment*, *472*(0), 695 – 703, doi:10.1016/j.scitotenv.2013.11.104.

Storck, F. R., C. K. Schmidt, F. Lange, J. Henson, and K. Hahn (2012), Factors controlling micropollutant removal during riverbank filtration, *American water works association*, *104*(12), E643–E652, doi:10.5942/jawwa.2012.104.0147.

Tompson, A. F. B., S. F. Carle, N. D. Rosenberg, and R. M. Maxwell (1999), Analysis of groundwater migration from artificial recharge in a large urban aquifer: A simulation perspective, *Water Resources Research*, *35*(10), 2981–2998, doi:10.1029/1999WR900175.

Torres, E., R. Couture, B. Shafei, A. Nardi, C. Ayora, and P. V. Cappellen (2015), Reactive transport modeling of early diagenesis in a reservoir lake affected by acid mine drainage: Trace metals, lake overturn, benthic fluxes and remediation, *Chemical Geology*, *419*, 75 – 91, doi:10.1016/j.chemgeo.2015.10.023.

Tran, N. H., T. Urase, H. H. Ngo, J. Hu, and S. L. Ong (2013), Insight into metabolic and cometabolic activities of autotrophic and heterotrophic microorganisms in the biodegradation of emerging trace organic contaminants, *Bioresource Technology*, *146*(0), 721 – 731, doi:10.1016/j.biortech.2013.07.083.

Trudgill, S. T. (1987), Soil water dye tracing, with special reference to the use of rhodamine wt, lissamine ff and amino g acid, *Hydrological Processes*, *1*(2), 149–170, doi:10.1002/hyp.3360010204.

Valhondo, C., J. Carrera, C. Ayora, M. Barbieri, K. Nödler, T. Licha, and M. Huerta (2014), Behavior of nine selected emerging trace organic contaminants in an artificial recharge system supplemented with a reactive barrier, *Environmental Science and Pollution Research*, pp. 1–12, doi:10.1007/s11356-014-2834-7.

Valhondo, C., J. Carrera, C. Ayora, I. Tubau, L. Martinez-Landa, K. Nödler, and T. Licha (2015), Characterizing redox conditions and monitoring attenuation of selected pharmaceuticals during artificial recharge through a reactive layer, *Science of The Total Environment*, *512âĂŞ513*(0), 240 – 250, doi:10.1016/j.scitotenv.2015.01.030.

Valhondo, C., L. Martínez-Landa, J. Carrera, J. J. Hidalgo, I. Tubau, K. De Pourcq, A. Grau-Martínez, and C. Ayora (2016a), Interactive comment on "tracer test modeling for local scale

residence time distribution characterization in an artificial recharge site" by c. valhondo et al., *Hydrol. Earth Syst. Sci. Discuss.*, doi:10.5194/hess-2016-197-AC2.

Valhondo, C., L. Martínez-Landa, J. Carrera, J. J. Hidalgo, I. Tubau, K. De Pourcq, A. Grau-Martínez, and C. Ayora (2016b), Interactive comment on "tracer test modeling for local scale residence time distribution characterization in an artificial recharge site" by c. valhondo et al., *Hydrol. Earth Syst. Sci. Discuss.*, doi:10.5194/hess-2016-197-AC3.

Valhondo, C., L. Martinez-Landa, J. Hidalgo, I. Tubau, K. De Pourcq, A. Grau-Martinez, and C. Ayora (2016c), Tracer test modeling for local scale residence time distribution characterization in an artificial recharge site, doi:10.5194/hess-2016-197.

Vanderzalm, J., C. L. G. L. Salle, and P. Dillon (2006), Fate of organic matter during aquifer storage and recovery (asr) of reclaimed water in a carbonate aquifer, *Applied Geochemistry*, *21*(7), 1204 – 1215, doi:10.1016/j.apgeochem.2006.02.022.

Vázquez-Suñé, E., et al. (2006), Groundwater modelling as a tool for the european water framework directive (wfd) application: The llobregat case, *Physics and Chemistry of the Earth, Parts A/B/C*, *31*(17), 1015–1029, doi:10.1016/j.pce.2006.07.008.

Wada, Y., L. P. H. van Beek, C. M. van Kempen, J. W. T. M. Reckman, S. Vasak, and M. F. P. Bierkens (2010), Global depletion of groundwater resources, *Geophys. Res. Lett.*, *37*(20), L20,402, doi:10.1029/2010GL044571.

Walther, M. (2016), Interactive comment on "tracer test modeling for local scale residence time distribution characterization in an artificial recharge site" by c. valhondo et al., *Hydrol. Earth Syst. Sci. Discuss.*, doi:10.5194/hess-2016-197-RC2.

White, A. F., and S. L. Brantley (2003), The effect of time on the weathering of silicate minerals: why do weathering rates differ in the laboratory and field?, *Chemical Geology*, *202*(3âĂŞ4), 479 – 506, doi:10.1016/j.chemgeo.2003.03.001, controls on Chemical Weathering.

Wiese, B., G. Massmann, M. Jekel, T. Heberer, U. Dünnbier, D. Orlikowski, and G. Grützmacher (2011), Removal kinetics of organic compounds and sum parameters under field conditions for managed aquifer recharge, *Water Research*, *45*(16), 4939 – 4950, doi:10.1016/j.watres.2011.06.040.

Wu, C., A. L. Spongberg, and J. D. Witter (2009), Sorption and biodegradation of selected antibiotics in biosolids, *Journal of Environmental Science and Health, Part A: Toxic/Hazardous Substances and Environmental Engineering*, *44*, 454–461, doi:10.1080/10934520902719779.

Yamamoto, H., Y. Nakamura, S. Moriguchi, Y. Nakamura, Y. Honda, I. Tamura, Y. Hirata, A. Hayashi, and J. Sekizawa (2009), Persistence and partitioning of eight selected pharmaceuticals in the aquatic environment: Laboratory photolysis, biodegradation, and sorption experiments, *Water Research*, *43*(2), 351 – 362, doi:10.1016/j.watres.2008.10.039.

Yu, L., G. Fink, T. Wintgens, T. Melin, and T. A. Ternes (2009), Sorption behavior of potential organic wastewater indicators with soils, *Water Research*, *43*(4), 951–960, doi:10.1016/j.watres.2008.11.032.

Zhang, X., X. Zhao, M. Zhang, and Q. yuan Wu (2011), Safety evaluation of an artificial groundwater recharge system for reclaimed water reuse based on bioassays, *Desalination*, *281*(0), 185 – 189, doi:10.1016/j.desal.2011.07.060.